2011

An analysis and simulation of launch vehicle separation dynamics including thrust transients

Charles David Capps

AN ANALYSIS AND SIMULATION OF LAUNCH VEHICLE SEPARATION DYNAMICS INCLUDING THRUST TRANSIENTS

by

CHARLES DAVID CAPPS

A THESIS

Submitted in partial fulfillment of the requirements
for the degree of Master of Science in Engineering
in
The Department of Mechanical and Aerospace Engineering
to
The School of Graduate Studies
of
The University of Alabama in Huntsville

HUNTSVILLE, ALABAMA

2011

In presenting this thesis in partial fulfillment of the requirements for a master's degree from The University of Alabama in Huntsville, I agree that the Library of this University shall make it freely available for inspection. I further agree that permission for extensive copying for scholarly purposes may be granted by my advisor or, in his/her absence, by the Chair of the Department or the Dean of the School of Graduate Studies. It is also understood that due recognition shall be given to me and to The University of Alabama in Huntsville in any scholarly use which may be made of any material in this thesis.

Charles D. Cagle 10-13-11

(Student signature) (Date)

THESIS APPROVAL FORM

Submitted by Charles David Capps in partial fulfillment of the requirements for the degree of Master of Science in Engineering in Mechanical Engineering and accepted on behalf of the Faculty of the School of Graduate Studies by the thesis committee.

We, the undersigned members of the Graduate Faculty of The University of Alabama in Huntsville, certify that we have advised and/or supervised the candidate on the work described in this thesis. We further certify that we have reviewed the thesis manuscript and approve it in partial fulfillment of the requirements for the degree of Master of Science in Engineering in Mechanical Engineering.

10/13/2011 Committee Chair
(Date)

10/13/11

Robert A Frederick 10/13/11

Department Chair

College Dean

Rhonda Kay Gaede 12/2/11 Graduate Dean

ABSTRACT

The School of Graduate Studies
The University of Alabama in Huntsville

Degree Master of Science in Engineering College/Dept. Engineering/Mechanical and Aerospace Engineering

Name of Candidate Charles David Capps

Title An Analysis and Simulation of Launch Vehicle Separation Dynamics Including Thrust Transients

An analysis of the stage separation of a launch vehicle and potential for re-contact is conducted. The launch vehicle with thrust transient and mass offset in the spent stage is assumed; the engine lies recessed at the time of separation within the spent-stage's forward skirt. The potential for and effects of re-contact during separation are investigated. Coordinate systems and the equations of motion are developed. Closed-form analyses are performed for simplified cases. Furthermore, simulations are performed to verify the closed-form solutions, and the differences between simulation results and analytical solutions are discussed.

Abstract Approval: Committee Chair

Department Chair

Graduate Dean

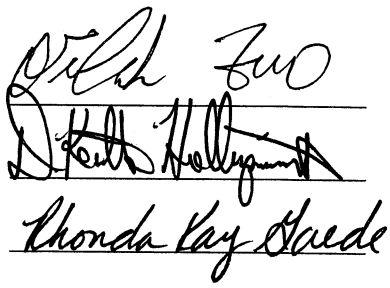

ACKNOWLEDGMENTS

I wish to express many thanks to Dr. Ken Zuo, my thesis advisor, for directing my research, for editorial guidance, recommending many improvements, and for having patience with me during this long process. I also would thank the members of my committee, Dr. John Gilbert and Dr. Robert Frederick, for their time and attention in reviewing the thesis. Lastly, many thanks to my wife and children for the time taken from them devoted to the preparation of this work.

TABLE OF CONTENTS

LIST OF FIGURES

LIST OF SYMBOLS

Symbol		Page
$\boldsymbol{C}_a^b$	Direction cosine matrix from frame a to frame b on post-multiplication	6
$\vec{r}_{fs}^{\,s}$	Position vector of station frame origin relative to fixed frame in station coordinates	6
$\vec{r}_{sb}^{\,b}$	Position vector of body frame origin relative to station frame in body coordinates	8
$\boldsymbol{I}^p$	Component matrix of the inertia tensor in principal coordinates	10
$\boldsymbol{I}^b$	Component matrix of the inertia tensor in body coordinates	10
$\boldsymbol{A}(\delta_y, \delta_z)$	Gimbal angle rotation function	12
$\vec{F}$	Force vector	14
m	Mass	14
$\vec{V}_0$	Velocity in the moving frame	14
$\vec{\omega}_{m\backslash f}$	Angular velocity with respect to a fixed frame	14
$\vec{r}_c$	Position vector of center of mass relative to origin of the moving frame	14
$\vec{V}$	Velocity in the fixed frame	15
$\vec{M}^m$	Moment applied in the moving frame	15
M	Moment in the plane	16
I	Moment of inertia in the plane	16
T	Thrust	18
T_0	Initial thrust of transient	18
t_0	Start-time of thrust transient	18
α	Inverse of time constant of thrust transient	18
t	Time	18
$\bar{\boldsymbol{I}}$	Identity matrix	19

$\vec{T}^{s}$	Thrust vector in station coordinates	19
$\vec{M}^{s}_{thrust}$	Moment vector due to thrust in station coordinates	19
$\vec{F}^{s}_{sep}$	Force vector due to separation motors in station coordinates	21
$\vec{M}^{s}_{sep}$	Moment vector due to separation motors in station coordinates	21
$\vec{r}^{\,s_1}_{u_j}$	Position of j^{th} pusher in spent stage station coordinates	23
$\vec{r}^{\,s_2}_{w_j}$	Position of center of j^{th} pusher patch in ongoing stage station coordinates	23
$\vec{\mathrm{r}}^{\,s_2}_{v_j}$	Position of intersection of j^{th} pusher's intersection with ongoing stage base plane	23
$\vec{\mathrm{r}}^{\,f}_{uv_j}$	Position vector of points of application of force on both stages	23
L_{pusher}	Length of pushers	24
r_{patch}	Radius of pusher patch on ongoing stage	24
$\boldsymbol{Q}$	Point of intersection of line and plane in the plane-line intersection test	26
$\boldsymbol{A}$	Starting point of line segment in the plane-line intersection test	26
$\boldsymbol{B}$	End point of line segment in the plane-line intersection test	26
$\boldsymbol{n}$	Plane normal vector in the plane-line intersection test	26
d	Scalar constant of the plane in the plane-line intersection test	26
$\boldsymbol{X}$	Trial intersection point in the plane-line intersection test	26
m_j	Boolean multiplier for j^{th} pusher maximum length	28
n_j	Boolean multiplier for j^{th} pusher within patch radius	28
$\vec{\mathrm{F}}^{\,s_1}_{u_j}$	Force vector in spent stage frame exerted by j^{th} pusher on spent stage	28
$\vec{r}^{\,s_1}_{cm_1}$	Position vector of spent stage C.M. in spent stage station coordinates	29
$\vec{M}^{p_1}_{u_j}$	Moment vector exerted by j^{th} pusher on spent stage in spent stage principal frame	29
$\vec{F}^{f}_{v_j}$	Force vector exerted by j^{th} pusher on ongoing stage in fixed frame	29
$\vec{M}^{p_2}_{v_j}$	Moment vector exerted by j^{th} pusher on ongoing stage in principal frame	29

$\vec{F}_{pneu_1}^{f}$	Total pusher force vector exerted on spent stage in fixed frame	30
$\vec{M}_{pneu_1}^{p_1}$	Total pusher moment vector exerted on spent stage in spent stage principal frame	30
$\vec{F}_{pneu_2}^{f}$	Total pusher force vector exerted on ongoing stage in fixed frame	30
$\vec{M}_{pneu_2}^{p_2}$	Total pusher moment vector exerted on ongoing stage in ongoing stage principal frame	30
$\vec{r}_e^{\,s}$	Position of engine C.M. in station coordinates	32
$\vec{r}_g^{\,s}$	Position of engine gimbal in station coordinates	32
l	Distance from gimbal to engine C.M.	32
m_1	Total mass of spent stage	32
m_t	Mass of spent-stage tankage	32
m_e	Mass of spent-stage engine	32
$\boldsymbol{I}_e^{s_1}$	Component matrix of inertia tensor of engine in spent stage station frame	32
$\vec{r}_{(e\|cm)}^{\,s_1}$	Position vector of engine C.M. relative to stage C.M. in spent stage station frame	32
$\vec{r}_{(t\|cm)}^{\,s_1}$	Position vector of tankage C.M. relative to stage C.M. in spent stage station frame	33
$\boldsymbol{I}_{(e\|cm)}^{s_1}$	Inertia matrix of engine referred to stage C.M. in spent stage station frame	33
P	Total impulse from engine thrust transient	37
P_{before}	Impulse from engine thrust transient before t_0	37
P_{after}	Impulse from engine thrust transient after t_0	37
$T_{impulse}$	Equivalent thrust for equivalent impulse model of transient	38
$t_{applied}$	Time of application of thrust for equivalent impulse model of transient	38
n	Number of separation motors or pushers	39
F_c	Average force of each separation motor	39
h	Radius from stage centerline of each separation motor or pusher	39
dF	Gradient in separation motor force per unit length radially	39

F_p	Force of each pusher	39
l_0	Distance along centerline of pusher ring from stage C.M.	40
γ	Angle between spent and ongoing stage centerlines in the plane	40
F_{base}	Average force of each pusher	41
δ	Gimbal angle in the plane for the engine mass offset problem	41
$\vec{M}_{sep}$	Moment vector induced by nominal separation devices with engine mass offset	41

CHAPTER I

INTRODUCTION

The rocket equation, combined with the significant mass fraction of booster structure and the limited specific impulse of available rocket engines, dictate that a multi-stage approach be taken to achieve long range, for a ballistic missile, or orbit, for a space launch vehicle. As each successive stage completes its burn, having depleted its propellants, it separates from the rest of the vehicle and falls away, in a process called "staging." Other items are discarded as soon as practical to reduce the penalty of carrying unneeded mass; interstages are dropped soon after ongoing stage engine ignition, and payload fairings are jettisoned as soon as the payload is safe from the atmosphere's heating effects at hypersonic velocities. If the spent stage or discarded fairing makes contact with the vehicle after separation, this is called "re-contact," and it is highly undesirable because of the potential for damage or disturbance to the ongoing vehicle.

From the earliest days of multi-stage launch vehicles, problems with separation and re-contact have recurred. The designers of the Atlas, the United States' first Intercontinental Ballistic Missile (ICBM) and one of the earliest multi-stage vehicles, were so concerned about the unknowns of staging, especially within the lower atmosphere, that the booster stage separated from the ongoing stage (with sustainer engine and all the tankage) on a set of rails. The rails prevented the booster stage from re-contacting the sustainer engine, which was completely surrounded by the entire length of the booster stage, even protruding from the booster stage's stern [21]. The first Atlas-Agena A flight (vehicle serial number 29D, February 26, 1960) ended in failure when the Agena stage failed to separate properly [4].

Even today, re-contact after separation is of great concern and remains a relevant engineering problem, especially for development flights. The newer upper stage rocket engines have very high expansion ratios (greater than 1:64). The diameter of the nozzle rim approaches the inner diameter of the skirt or interstage in which it is contained, the space between them is much tighter than previously, and so the margin for unexpected dynamics during separation is greatly reduced.

The concern is greater for development flights. During first stage separation for SpaceX Falcon 1 flight 2, launched on March 20, 2007, the nozzle of the second stage re-contacted the interstage attached to the first stage, exciting the slosh modes of the propellant of the second stage, eventually resulting in failure to reach orbit [2]. On Falcon1's next test flight, flight 3, on August 2, 2008, a first-stage thrust transient during staging provided enough force to overcome the pneumatic pusher separation mechanisms. As a result, the stages did not achieve any separation distance until after the second stage engine ignited, still recessed within the forward skirt of the first stage. The perturbation to the second stage was enough to again cause flight failure [3].

This thesis studies the dynamics of separation and re-contact. It examines the role of asymmetric mass properties, cut-off thrust transients of the spent-stage main engine, solid rocket separation motors, and simple pressure-based separation devices in the staging problem.

The specific problem posited is that of a booster above the tenable atmosphere undergoing staging. Since re-contact is being examined, motion of one stage relative to another, not absolute motion, is the desired object. The spent and ongoing stages achieve separation distance by either small solid rocket motors or pneumatic pusher mechanisms located circumferentially and near the separation plane. The spent stage may have significant mass offset from the centerline, primarily due to the final gimbal position of the main engine, as well as residual thrust tail-off of the main engine following the thrust-termination command.

The goal of this work is to analyze the separation dynamics of the booster, including the potential for re-contact, and to verify the analysis with numerical simulations.

Chapter II details the coordinate systems needed for the current work and the transformations between them. Chapter III develops the translational and rotational equations of motion and the forces and moments that are significant to exo-atmospheric staging. Chapter IV describes the simplified geometry of separation and re-contact used for analysis. In Chapter V, various aspects of the staging problem are studied using a simplified closed-form approach. In Chapter VI, comprehensive numerical simulations are developed to verify the earlier analysis and to model more complex problems that cannot be easily subjected to closed-form analysis, such as three-dimensional problems, and results of simulation are

presented. Chapter VII gives conclusions of the thesis with a summary of results. Chapter VIII offers suggestions for further lines of inquiry in separation and re-contact.

CHAPTER II

COORDINATE SYSTEMS

In order to establish the kinetics and kinematics of the separation problem, coordinate systems must be constructed that conveniently describe the relevant vectors. All of these coordinate systems are right-handed systems, that is, systems where, if $\vec{\imath}_1$, $\vec{\imath}_2$, and $\vec{\imath}_3$ are the unit vectors corresponding to the X, Y, and Z axes, respectively, of the system, then $\vec{\imath}_1 \times \vec{\imath}_2 = \vec{\imath}_3$ is always true.

2.1 Fixed Frame

Since the separation problem is primarily one of relative motion, an inertial frame referred to a distant, well-known location, such as the center of the earth or the launch site, is unnecessary. It is sufficient to have a local coordinate system in which to perform the inertial calculations.

The fixed frame in this thesis refers to a non-accelerating frame whose axes and origin are determined at the instant of separation. This thesis does not consider behavior prior to separation. Using Regan's [1] superscripted notation, the X^f axis points along the centerline of the joined vehicle, which for most boosters is an axis of rotational symmetry, the Z^f axis is directed toward a well-known location on the body's separation plane (such as an interstage umbilical connection) at that very instant, and the Y^f axis completes the system. At that same moment, the origin O_f lies in the separation plane and along the centerline of the joined vehicle. While the frame is referred to as a fixed frame, its origin continues to move during separation at the same linear velocity as the whole vehicle did at the initiation of separation. This is sufficient for the fixed frame to be inertial, since the frame moves at a constant velocity, hence is non-accelerating.

At the instant of separation, the axes of the fixed frame are parallel to those of the station frames or systems introduced in the following sections. After separation, the fixed frame serves as the common frame to which locations on both stages are transformed, so that re-contact may be detected.

Figure 2.1 shows the fixed frame just prior to separation, and Figure 2.2 depicts the same frame some time afterward.

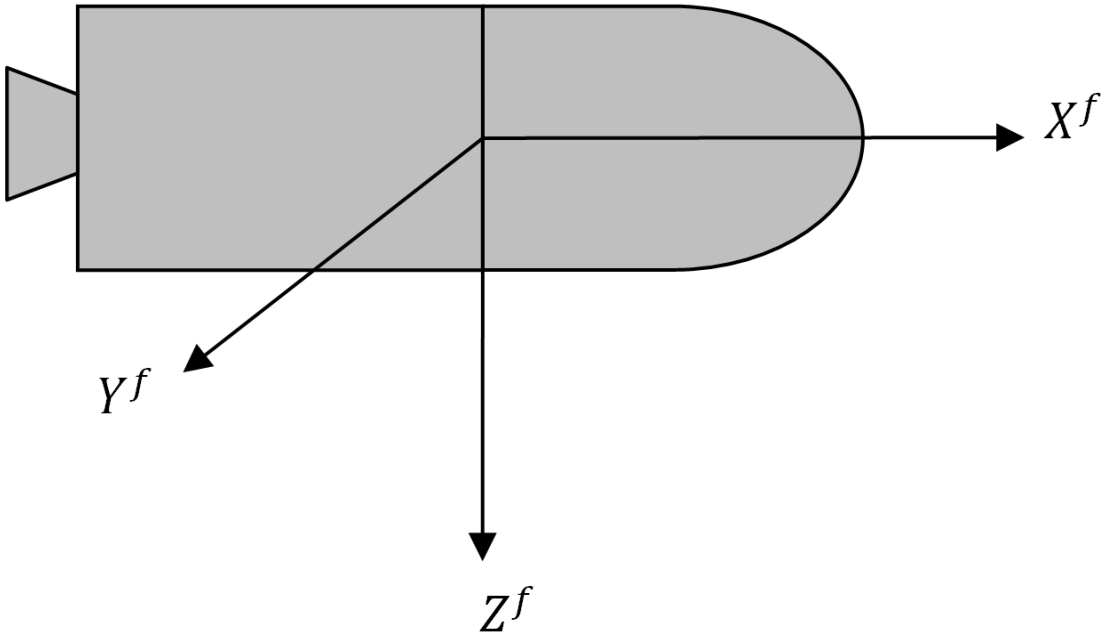

Figure 2.1: Fixed Frame at Instant of Separation

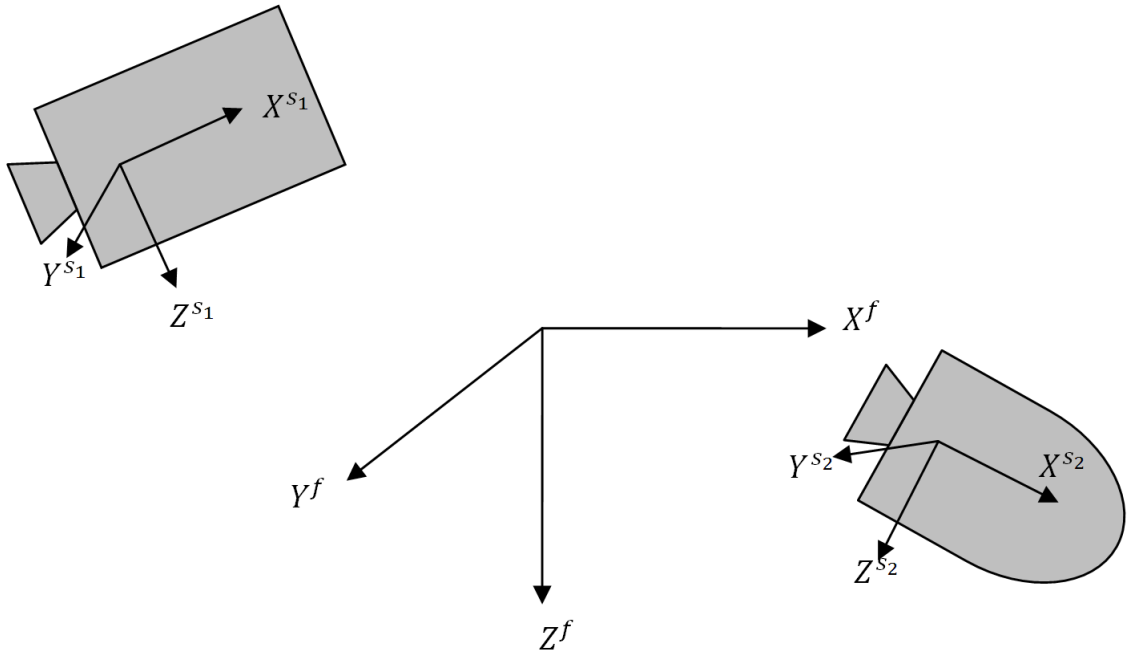

Figure 2.2: Fixed Frame after Separation

2.2 Station Coordinate System

The station coordinate system is a body-fixed system whose origin is fixed to a particular location on the body. Station coordinates are necessary to describe the location of the various parts of the body, such as the gimbal position, separation plane, separation mechanisms, and current center of mass. During design and construction, station coordinates describe the mechanical layout of all components. For an entire intact launch vehicle, one might refer to "vehicle station coordinates," which describe the location of any point on the vehicle relative to an origin, usually near the tail. When referring to a stage, it is not uncommon to talk of "stage station coordinates" relative to a fixed point on the stage. This distinction is important during separation, where one vehicle becomes two, and the previously authoritative "vehicle station coordinates" cease to have meaning for at least one of the stages.

When the coordinate system origin is in the tail, the X^s coordinate axis (the "roll" axis) runs along the body longitudinal axis, the launch vehicle "centerline," toward the nose. The Z^s axis (the "yaw" axis)

points from the origin radially toward some known reference on the surface of the vehicle, and the Y^s axis (the "pitch" axis) completes the system. For planar (that is, two-dimensional) analysis about the pitch axis, X^s is forward, Z^s is down, and Y^s is out of the page.

As will be developed more in Chapter III, the station coordinates are difficult to use for dynamics calculations, because they are not centered at the instantaneous center of mass (C.M.). It is more convenient to do the attitude dynamics calculations in some body axes frame, keeping track of the center of mass as a matter of bookkeeping.

$$\vec{g}^s = \boldsymbol{C}_f^s \vec{g}^f + \vec{r}_{fs}^s \,, \tag{2.1}$$

where $\vec{g}^s$ is a position vector in the station frame, $\vec{g}^f$ is a position vector of the same point described in the fixed frame, $\boldsymbol{C}_f^s$ is the direction cosine matrix (D.C.M.) transforming vectors in fixed coordinate system to those in the station coordinates, and $\vec{r}_{fs}^s$ is the position vector of the origin of the fixed coordinate frame relative to the station frame in the coordinates of the station frame. The direction cosine matrix, described in Appendix A, is an orthonormal (rotation) matrix describing the angular relationship of two frames. The notation used here is that of Britting [17], where the subscript is the source frame and the superscript is the destination frame, so that premultiplying by the D.C.M. transforms the components of the vector from the subscript frame to the superscript frame.

Figure 2.3 shows vehicle and stage station coordinates and their relationships.

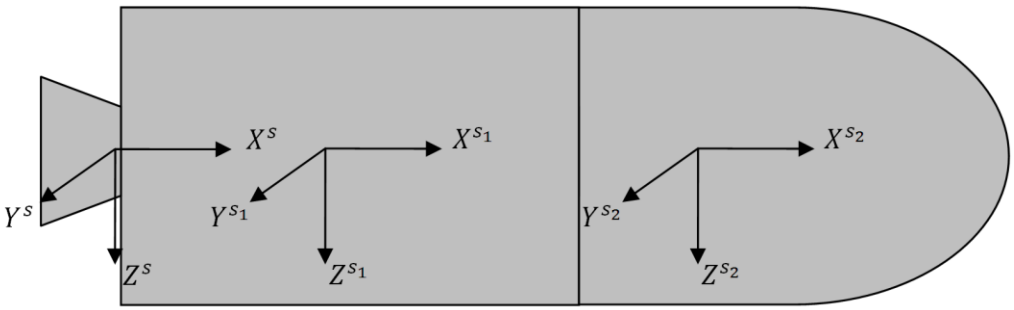

Figure 2.3: Vehicle and Stage Station Frames

2.3 Body Coordinates

The origin of the body coordinate system is set at the instantaneous mass center of a body, and the coordinate axes rotate with that body. That is, the frame is fixed to the body. The body frame is useful for attitude dynamics calculations, because, as shown in Chapter III, the main equations for attitude dynamics have simpler forms when the origin is taken to be the center of mass and when the angular velocity is described in body coordinates.

The orientations of body axes are fixed relative to the body but otherwise arbitrary, in this thesis, they are assumed to be parallel to the station coordinate axes. That is, the X^b axis (roll) is along the longitudinal axis, Z^b (yaw) some reference direction, usually down, and Y^b (pitch) completing the triad. In general, these axes will not coincide with the principal body axes introduced in the next section. Figure 2.4 illustrates the body axes and their relationship to the station coordinates.

$$\vec{g}^b = \vec{g}^s + \vec{r}_{sb}^b \,, \tag{2.2}$$

where $\vec{g}^b$ is a position vector of a point expressed in the body frame, $\vec{g}^s$ describes the same position vector in the station frame, and $\vec{r}_{sb}^b$ is the position vector of the station frame origin (i.e., the stage C.M.) relative to the body frame in the body frame.

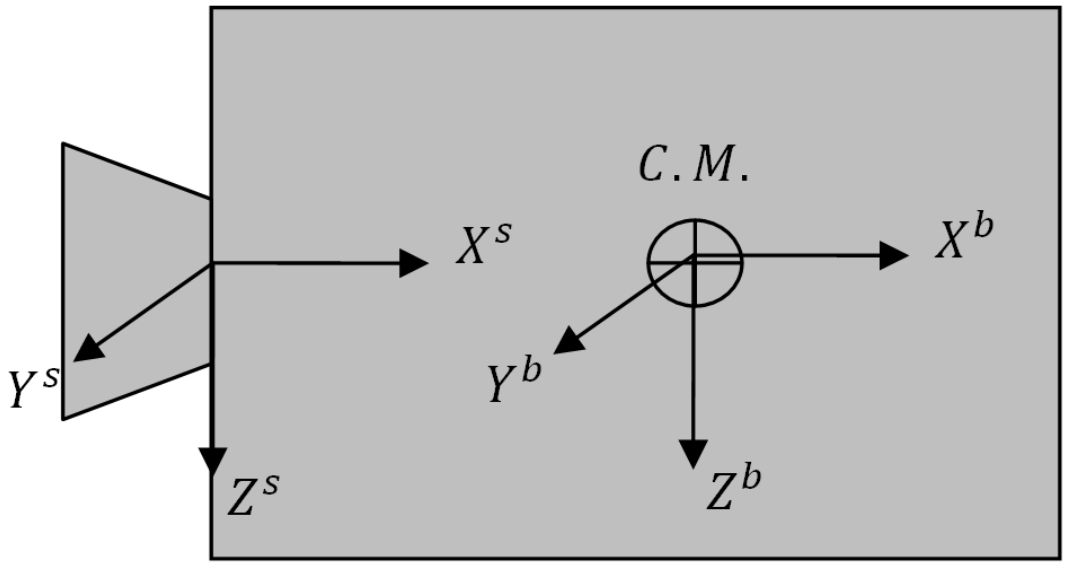

Figure 2.4: Body and Station Frames

2.4 Principal Body Coordinates

Principal body coordinates are, as the name suggests, a special type of body coordinates where the axes are aligned with the principal axes of the body. Consequently, the component matrix of the inertia tensor in the principal body coordinates becomes diagonal; all the products of inertia are zero, and only the moments of inertia remain.

The principal body coordinates are very convenient for calculating the attitude of a rigid body when the rigid body configuration is not time-varying, because the equations of motion are simplified even more than using the body frame (the equations become decoupled). However, if the rigid body configuration is changing, as it is for a rocket in powered flight, the inertia tensor is quickly changing as the rocket is losing mass at a high rate. It then becomes necessary to re-diagonalize the inertia matrix on every change of the configuration, that is, every simulation interval. The diagonalization involves solving the eigenvalue problem for the inertia matrix, a 3 by 3 symmetric matrix. This can be computationally

expensive, although significant simplifications are available. Consequently, it is often more efficient to just use the body frame despite the fully-populated, non-diagonal component matrix of the inertia tensor.

Though the station coordinates and the body coordinates are both body-fixed, the origins and axes of them can be different. As the center of mass shifts within the body, the station coordinate's origin is always at the same location on the body, whereas the origin of the body coordinates is moving with the center of mass. The X^s axis of the station frame is always directed down the longitudinal (roll) axis, while the axes of the principal body frame are always the principal axes of the inertia matrix derived from mass distribution. The relationship between the components of a position vector in the body frame and those of the same vector expressed in the principal frame is as usual [1]:

$$\vec{g}^p = \boldsymbol{C}_b^p \, \vec{g}^b \,, \tag{2.3}$$

where $\vec{g}^p$ is a position vector expressed in the principal body axes system, $\vec{g}^b$ is the same vector with components expressed in the body axes, and $\boldsymbol{C}_b^p$ is the direction cosine matrix transforming components of vectors in the body frame to these in the principal-body frame. This is the same matrix that, through pre- and post-multiplication transforms the component matrix of the inertia tensor in the body frame (nondiagonal) to that in the principal body frame, which is diagonal [1]:

$$\boldsymbol{I}^p = \boldsymbol{C}_p^b \boldsymbol{I}^b \boldsymbol{C}_b^p = \begin{bmatrix} I_{xx}^p & 0 & 0 \\ 0 & I_{yy}^p & 0 \\ 0 & 0 & I_{zz}^p \end{bmatrix}. \tag{2.4}$$

Since the D.C.M. is orthonormal, its inverse is simply its transpose, and the inverse of a coordinate transformation simply reverses the direction of the transformation:

$$\boldsymbol{C}_m^n = (\boldsymbol{C}_n^m)^T = (\boldsymbol{C}_n^m)^{-1} \tag{2.5}$$

for all frames m and n. The inertia tensor is a second order tensor, so that pre-multiplication by the inverse of a rotation matrix and post-multiplication by the same rotation matrix performs the transformation of the inertia matrix. When the D.C.M. is filled with the eigenvectors of the inertia matrix in body coordinates, which are each the directions of the principal axes in the body frame, pre- and post-multiplication result in the inertia matrix being transformed to the principal axes, resulting in the above diagonalized form.

Figure 2.5 depicts the principal body coordinate system of a booster along with some station-parallel body axes for comparison.

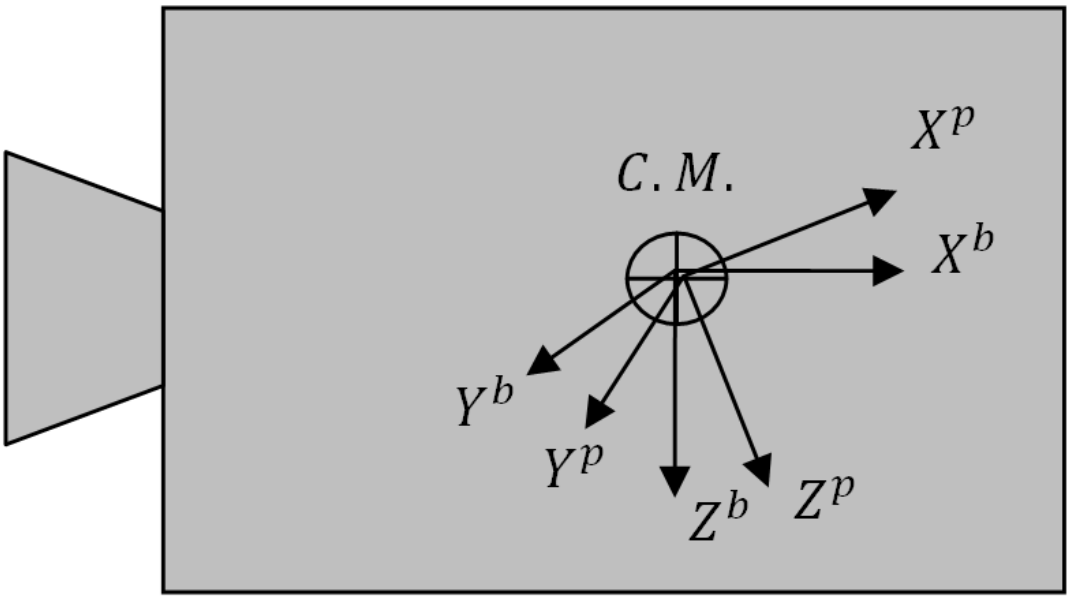

Figure 2.5: Relationship between Body and Principal Body Axes

2.5 Engine Gimbal Coordinates

For the case where an engine's mass offset from centerline is suspected of leading to re-contact, the engine gimbal coordinate system is most convenient to express the inertia matrix of the engine and the position of the C.M. of the engine. The engine gimbal coordinate system is centered at the engine gimbal. The X^g axis of the system runs forward coincident with the longitudinal axis of the engine, the centerline about which the nozzle is shaped. The nozzle itself extends in the $-X^g$ direction. The Z^g axis is parallel to the stage station coordinates at zero gimbal angles, and the Y^g axis completes the system.

This frame is anchored to the station coordinates at the gimbal. The gimbal lies some distance from the spent stage's station coordinate origin on the negative X^saxis. The engine C.M. lies a distance l from the gimbal. For the single main engine boosters considered in this thesis, the gimbal location (the origin) always lies on the centerline of the spent stage. Two gimbal angles, δ_y and δ_z, relate the orientation of the axes of the engine gimbal coordinates to the coordinate axes of the stage-station frame.

$$\vec{g}^{\,g} = \boldsymbol{C}_s^g \vec{g}^{\,s} + \vec{r}_{sg}^{\,g}\,, \tag{2.6}$$

where $\vec{g}^{\,g}$is the components of a position vector in the gimbal frame, $\boldsymbol{C}_s^g$ is the rotation matrix taking vectors in the station coordinates to the gimbal frame, $\vec{g}^{\,s}$ is the components of the position vector in the station frame, and $\vec{r}_{sg}^{\,g}$ is the position vector of the gimbal relative to the station coordinates origin, expressed in the gimbal system. The direction cosine matrix $\boldsymbol{C}_g^s$ is given as

$$\boldsymbol{C}_g^{\boldsymbol{s}} = \boldsymbol{A}(\delta_y, \delta_z) = \begin{bmatrix} \cos\delta_z & \sin\delta_z & 0 \\ -\sin\delta_z & \cos\delta_z & 0 \\ 0 & 0 & 1 \end{bmatrix} \begin{bmatrix} \cos\delta_y & 0 & -\sin\delta_y \\ 0 & 1 & 0 \\ \sin\delta_y & 0 & \cos\delta_y \end{bmatrix}. \tag{2.7}$$

There are only two degrees of freedom, angles δ_y and δ_z; a roll angle about the X^g axis would be meaningless. The Y axis rotation is performed first, followed by that about the new Z axis. Figure 2.6 illustrates the relationship between the gimbal axes and the station axes, and the angles of rotation between them.

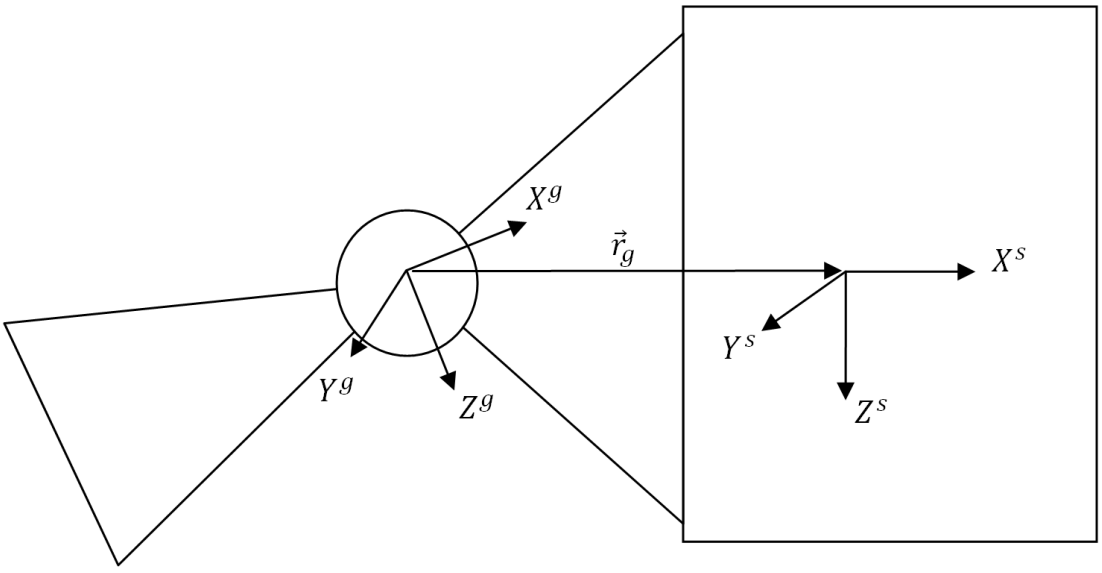

Figure 2.6: Engine Gimbal Frame

CHAPTER III

EQUATIONS OF MOTION

In this chapter, the relevant equations of motion for the stage separation problem are developed. First, the equations of motion for translation and rotation are presented. Thereafter the main forces and moments that occur during the staging event are given.

3.1 Translation: Newton's Equations

Regan [1] derives the translational equations of motion (Newton's Equations), relating acceleration to force, for a rigid body where the origin of the coordinate system is general, and not taken to be co-located with the center of mass. In a frame moving with the body (i.e., the body frame), the components of the force vector on the body and the velocity vector are related by

$$\vec{F} = m\left[\frac{d\vec{V}_0}{dt} + \vec{\omega}_{m\backslash f} \times \vec{V}_0 + \frac{d^2\vec{r}_c}{dt^2} + \frac{d\vec{\omega}_{m\backslash f}}{dt} \times \vec{r}_c + 2\vec{\omega}_{m\backslash f} \times \frac{d\vec{r}_c}{dt} + \vec{\omega}_{m\backslash f} \times \left(\vec{\omega}_{m\backslash f} \times \vec{r}_c\right)\right], \tag{3.1}$$

where $\vec{F}$ is the force acting on the rigid body, m is the mass of the body, $\vec{\omega}_{m\backslash f}$ is the angular velocity of the body with respect to a fixed frame in fixed-frame coordinates, $\vec{r}_c$ is the position vector of the center of mass relative to the origin of the moving frame, and $\vec{V}_0$ is the velocity of the origin of the moving (body) frame, given in the moving frame. If instead the origin of moving frame is taken to be at the mass center of the body, so that $\vec{r}_c$ and its derivatives are zero, then the force equation is much simpler:

$$\vec{F} = m\left[\frac{d\vec{V}_0}{dt} + \vec{\omega}_{m\backslash f} \times \vec{V}_0\right]. \tag{3.2}$$

This is Regan's Equation 5.23a [1]. If the dynamics of staging are analyzed or simulated with the body frame, which has its origin at the stage center-of-mass, then the much simpler Equation 3.2 can be used. However, if stage station coordinates are used as the moving frame coordinates, then $\vec{r}_c$ is in general non-zero, and the more complex Equation 3.1 must be used. For most analysis and simulation, the distance between stage station coordinates origin and the stage center of mass has to be known anyway. Calculations can be performed in a body-centered frame (where the center of mass is potentially changing) and a simple coordinate transformation, a translation, performed to get the results in stage station coordinates. Something similar can be done for external forces and moments, as well as their points of application, and for mass offsets: these are known in station coordinates, but are moved to the body-centered frame for calculations; the results are moved back to station coordinates for output.

If, however, a fixed frame is used to analyze or simulate the translational dynamics of staging, Newton's equation reduces to the familiar

$$\vec{F} = m\,\frac{d\vec{V}}{dt}, \tag{3.3}$$

where $\vec{V}$ is the velocity of the mass center. This simple form is very common in simulation of dynamics.

3.2 Rotation: Euler's Equations

The rotational equations of motion relate the moments acting on the body to the angular velocities and accelerations it experiences. If the origin of the moving frame is at the center of mass and the body is rigid, then the moments equation is ([1], Equation 5.56), again, in the body frame,

$$\vec{M}^m = \boldsymbol{I}\frac{d\vec{\omega}^m_{m\backslash f}}{dt} + \vec{\omega}^m_{m\backslash f} \times \boldsymbol{I}\vec{\omega}^m_{m\backslash f} \tag{3.4}$$

where $\vec{M}^m$ is the moment applied to the body in the moving frame, and $\boldsymbol{I}$ is the component matrix of the inertia tensor in the body frame, called the inertia matrix. The complexity of the equations is much greater if taken about an arbitrary point instead of the center of mass; as with the forces, it is easier to keep track of the moving C.M. relative to station coordinates than to analyze or simulate the equations for a moving frame situated at an arbitrary point. If principal axes are used, the inertia matrix $\boldsymbol{I}$ is diagonal, and the 3 equations reduce to

$$\begin{aligned} M_x^m &= I_{xx}\dot{\omega}_x + \omega_y\omega_z(I_{zz} - I_{yy}) \\ M_y^m &= I_{yy}\dot{\omega}_y + \omega_x\omega_z(I_{xx} - I_{zz}) \\ M_z^m &= I_{zz}\dot{\omega}_z + \omega_x\omega_y(I_{yy} - I_{xx}) \end{aligned} . \tag{3.5}$$

These equations are usually referred to as Euler's Equations in the context of attitude dynamics.

Note that in two dimensions (say the $X - Y$ plane), the Euler equations simplify to

$$M_z^m = I_z\dot{\omega}_z , \tag{3.6}$$

where $\dot{\omega}_z$ is the angular acceleration. This is the familiar equation from introductory dynamics.

The use of the non-principal body axes form (Equation 3.3) requires the inversion of the inertia matrix on every change in mass distribution. This arises because that equation must be solved for the angular accelerations in order for them to be integrated over time to find the angular rates. On the other hand, the principal axes form (Equation 3.4) demands the diagonalization of the inertia matrix, i.e., a solution of the 3×3 eigenvalue / eigenvector problem, with each change in that matrix, because that equation only applies to principal body axes. For the mass offset case, the engine is gimbaled, and so the inertia tensor has a component of arbitrary mass offset, which will almost certainly not result in principal axes along the axis of rotational symmetry. But in this case, the engine is at a static gimbal position throughout separation, so the principal axes can be determined before analysis and simulation begin, and the simpler Equations 3.4 utilized. For most other cases considered in this thesis, the principal body axes coincide with the body axes, making it easier to use Equations. 3.4 always.

Note, then, that for simulating rotation, the principle body axes are preferred, whereas for translation, the fixed axes are preferred.

3.3 Principle Forces

Almost all separation events are confined to times below 10 seconds (s), and often below 1 s, from initial separation to achieving enough distance and relative velocity between the bodies that re-contact is no longer a concern. The separations being considered in this thesis are those between upper stages and those between upper stage and payload. Many of the last stage separations for common launch vehicles happen above the tenable atmosphere, and, of course, all payload separations happen in space [5], [6], [7]. The main forces acting on the bodies during separation could be aerodynamic, gravitational, thrust, or arising

from separation devices like thrusters or pushers. An understanding of the relative magnitude of these forces will show which forces can be safely ignored in a relative motion problem, resulting in important simplifications.

3.3.1 Aerodynamic and Gravitational Forces

Appendix B gives several examples showing why aerodynamic and gravitational forces can be neglected for the problems considered in this thesis. The altitudes considered (above the "tenable atmosphere", above 100 km), are so high that there is little aerodynamic force even near orbital velocity, especially for the short duration of the separation event, usually about 1 s and always less than 10 s. Since the separation problem is primarily one of relative motion, gravity, affecting both stages mostly equally, can also be neglected.

3.3.2 Thrust

After the initiation of separation, the ongoing stage and spent stage are separate bodies, and so any thrust, whether from separation motors, ullage motors, main engine cutoff thrust transient, or propellant venting, will accelerate primarily one stage. Any thrust will affect stage relative motion and should be examined. One aspect of this thesis is to study the thrust transient from main engine cutoff and the consequences of non-uniform separation motors.

Rocket exhaust plume impingement on the other body may be significant, but it is beyond the scope of this thesis and is neglected.

3.4 Main Engine Thrust Transient

On Falcon 1 flight 3, a new regeneratively-cooled kerosene-LOX first stage engine produced an unexpected thrust transient after cutoff, resulting in failure of the stages to achieve separation distance. Ignition of the second stage engine occurred while still within the interstage, and was a contributing factor

to eventual loss of mission. The thrust transient arose out of residual propellants still in the engine after thrust termination. The presence of this 10psi transient in ground engine test data was obscured by the 15psi atmospheric pressure at sea level in which the tests were conducted [3].

A thrust transient can be modeled as a declining exponential of the form

$$T(t) = \begin{cases} T_0 e^{-\alpha(t-t_0)}, & t \geq t_0 \\ T_0, & t < t_0 \end{cases}, \tag{3.8}$$

where T_0 is the initial thrust of the transient, that is, the steady state thrust just prior to and at the instant of thrust termination, t_0 (units of seconds) is the start-time of the transient, which is the instant of thrust termination, and α (units of Hz) is the inverse of the time constant associated with the transient. T_0 is equal to the steady state thrust at thrust termination, and thus can be in the hundreds of kilonewtons. Time t is measured in seconds. If the thrust transient is of the same order of magnitude of duration as the separation event, that is, 0.1 s to 10 s, then time constant α would be in the range 0.1 Hz to 10 Hz as well. In the case of a liquid propellant rocket engine, the transient is due to residual propellant in the engine continuing the combustion. The transient in a solid rocket motor is due to the tail-off in pressure in the motor case after propellant is exhausted as the remaining combustion products discharge through the nozzle.

The thrust transient exerts itself where main engine thrust is always applied, that is, at the gimbal in the opposite direction of the engine nozzle. $\vec{T}^s$ is the thrust vector for the main engine transient in spent-stage station coordinates (see Figure 2.6). Since thrust is along the longitudinal axis of the engine (the X^g axis of the engine coordinate system), and the gimbal angles δ_y and δ_z control the direction of that thrust relative to station coordinates, the thrust vector is

$$\vec{T}^s = T(t)\ \mathbf{A}^{\mathbf{T}}(\delta_y, \delta_z)\vec{\imath}_1^g = T(t)\ \mathbf{A}^{\mathbf{T}}(\delta_y, \delta_z)\begin{bmatrix}1\\0\\0\end{bmatrix}, \tag{3.9}$$

where $\mathbf{A}^{\mathbf{T}}(\delta_y, \delta_z) = C_g^s$ is the rotation matrix introduced in Chapter II and a function only of the engine gimbal angles, transforming a vector in the components of the engine coordinate system to stage coordinates.

Newton's equations are easiest to integrate and apply when the forces are expressed in a fixed frame.

$$\vec{T}^f = \boldsymbol{C}_{s_1}^f \vec{T}^s\,, \tag{3.10}$$

where the subscript 1 in s_1 indicates the first stage station frame. The above D.C.M., $\boldsymbol{C}_{s_1}^{f}$, is not directly available. When the Euler equations are integrated to obtain angular velocity and position, the angular position produced describes the orientation of the principal axes relative to the fixed axes, expressed in D.C.M. form as $\boldsymbol{C}_{f}^{p}$. The matrix relating the orientation of the stage coordinates to the principal frame is $\boldsymbol{C}_{p}^{s_1} = \boldsymbol{C}_{b}^{s_1}\boldsymbol{C}_{p}^{b}$. Since the axes of the body frame and the stage station frame are parallel, differing only in their origin locations, the rotation matrix between them is the identity matrix: $\boldsymbol{C}_{b}^{s_1} = \bar{\boldsymbol{I}}$. The $\boldsymbol{C}_{p}^{b}$ matrix is part of the solution to the 3×3 eigenvalue problem, whose input is the mass properties. Since the mass properties of the stages are assumed to be constant throughout the separation event, the relationship between the stage coordinates and principal frame is constant:

$$\boldsymbol{C}_{p}^{s_1} = \boldsymbol{C}_{b}^{s_1}\boldsymbol{C}_{p}^{b} = \bar{\boldsymbol{I}}\boldsymbol{C}_{p}^{b} = \boldsymbol{C}_{p}^{b}\,. \tag{3.11}$$

So the thrust in the fixed frame is usually calculated using the two available D.C.M.s:

$$\vec{T}^{f} = \boldsymbol{C}_{p}^{f}\boldsymbol{C}_{b}^{p}\vec{T}^{s}\,. \tag{3.12}$$

The thrust will induce a moment on the spent stage if the thrust is not directed through the spent stage's C.M.

$$\vec{M}_{thrust}^{s} = \left(\vec{r}_{gs}^{\,s} - \vec{r}_{cm}^{\,s}\right) \times \vec{T}^{s}\,, \tag{3.13}$$

where $\vec{M}_{thrust}^{s}$ is the moment caused by the thrust vector, $\vec{r}_{gs}^{\,s}$ is the position of the gimbal, and $\vec{r}_{cm}^{\,s}$ is the position of the spent stage C.M., all in spent-stage station coordinates. Since Euler's equations will be integrated in the principal body axes of each stage, the moment needs to be transformed from spent stage station coordinates to the principal frame.

$$\vec{M}_{thrust}^{p} = \boldsymbol{C}_{b}^{p}\boldsymbol{C}_{s_1}^{b}\vec{M}_{thrust}^{s} = \boldsymbol{C}_{b}^{p}\vec{M}_{thrust}^{s} \tag{3.14}$$

Again $\left(\boldsymbol{C}_{b}^{s_1}\right)^{-1} = \boldsymbol{C}_{s_1}^{b} = \bar{\boldsymbol{I}}$. In the above, the change in mass due to the thrust transient is considered negligible.

3.5 Separation Motors

Retro-mounted solid rocket motors located circumferentially about the forward skirt or interstage of the spent stage, as well as forward-pushing motors placed round about the aft skirt of the ongoing stage,

are often used to achieve separation, especially on larger launch vehicles. Often, the thrust from these separation motors is canted slightly outward (10-30 degrees) from parallel to the main axis of symmetry.

Although solid rocket motors can be modeled with startup and shutdown transients, the short burn duration of such motors (on the order of one second) indicates that a simple constant thrust model may be accurate enough. For closed form analysis, it may be sufficient even to model all the motors as one force and one moment.

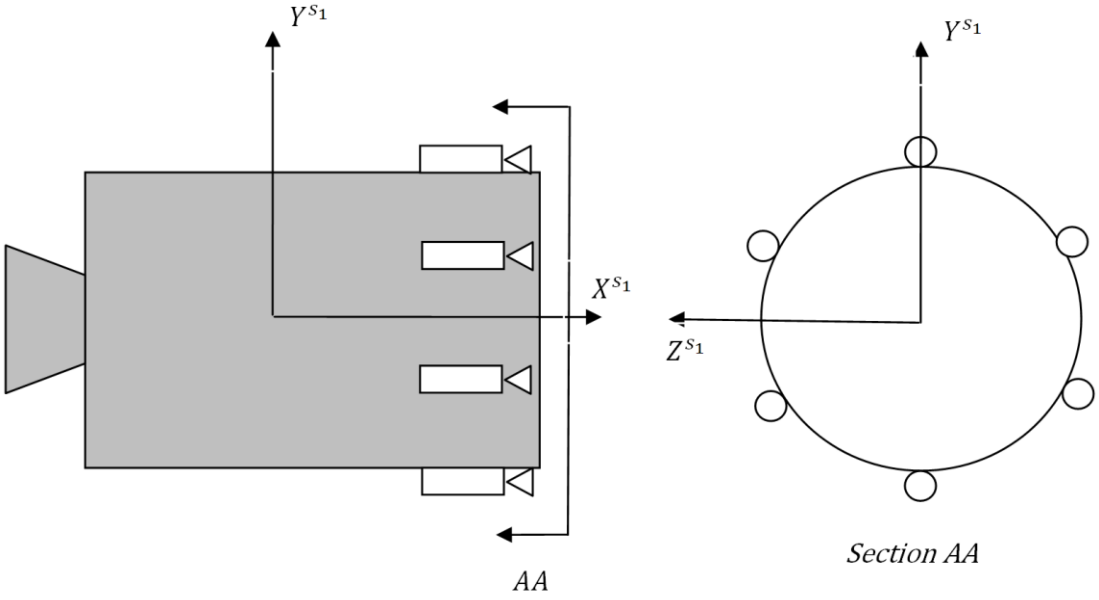

Figure 3.1: Separation Motors Placement

It is assumed that (1) each motor is situated and pointed ideally, (2) the mass change due to the burn of the separation motors is negligible compared to the total stage mass, and (3) the stage C.M. is also ideally situated on the centerline. If the stage C.M. were not on the centerline, then a moment in the yaw or pitch planes would arise even with perfectly matched separation motors. The primary case considered is that of unmatched separation motors.

The total force and moment exerted are simply the sum of all the forces and moments caused by the individual separation motors.

$$\vec{F}_{sep}^{s} = \sum_{i=0}^{n-1} \vec{F}_{i}^{s} \tag{3.15}$$

$$\vec{M}_{sep}^{s} = \sum_{i=0}^{n-1} (\vec{r}_i^{s} - \vec{r}_{cm}^{s}) \times \vec{F}_i^{s} \,. \tag{3.16}$$

In the above equations, $\vec{F}_i^{s}$ is the force of the i[th] motor in station coordinates, $\vec{r}_i^{s}$ is the position of the i[th] motor in station coordinates, and n the number of separation motors. As in the previous section, the forces need to be in a non-rotating frame and the moments in the principal body. The same rotations apply here.

$$\vec{F}_{sep}^{f} = \boldsymbol{C}_{s_1}^{f} \vec{F}_{sep}^{s} = \boldsymbol{C}_{p}^{f} \boldsymbol{C}_{b}^{p} \vec{F}_{sep}^{s} = \boldsymbol{C}_{p}^{f} \boldsymbol{C}_{b}^{p} \sum_{i=0}^{n-1} \vec{F}_i^{s} \tag{3.17}$$

$$\vec{M}_{sep}^{p} = \boldsymbol{C}_{b}^{p} \vec{M}_{sep}^{s} = \boldsymbol{C}_{b}^{p} \sum_{i=0}^{n-1} (\vec{r}_i^{s} - \vec{r}_{cm}^{s}) \times \vec{F}_i^{s} \tag{3.18}$$

These equations are equally applicable to whichever stage the motors are mounted to, whether spent or ongoing.

3.6 Mechanical Separation Devices

Devices that act principally by pushing apart the two stages, such as pneumatic pushers or springs, must be included in the modeling of a staging event. Several recent studies [9, 16, 23, 24] examined the behavior of separation springs in this context. Colbaugh [9] developed and analyzed a model for separation springs where the separation force exerted was proportional to the separation distance. This thesis will touch briefly on the behavior of pneumatic pushers. For springs, whose behavior is described by Hooke's Law, the force exerted is linearly proportional to the displacement of the spring from its neutral position. Pneumatic pushers, which were used in the Falcon 1 booster, rely on gas pressure and exert a constant or nearly-constant force all the way out to their maximum extent [16].

3.7 Pneumatic Pushers

The Falcon 1 booster, among others, uses pneumatic devices to push the stages apart, imparting a small velocity to each stage relative to the other.

The assumption that pushers provide a constant force out to their full extent is equivalent to assuming a very large reservoir or a regulated pressure system. This force is always parallel to the spent stage's longitudinal axis. More sophisticated force-distance profiles, beyond the scope of this thesis, are possible.

In normal operation, once a pusher reaches full extent, contact is lost, as the pushers have achieved some relative velocity between the stages; subsequently, it ceases to apply any force (it cannot carry any tension, and it is unlikely to be correctly aligned on both stages during a subsequent re-contact that might cause compression). After full extension, therefore, a pusher disappears from the simulation.

Each pusher is modeled as a force applied at a fixed point on each stage out to a specified distance, its "full extent". This full extent is always much less than the diameter of the stage, so that even if one pusher is at full extent while its radially-opposite counterpart has not actuated at all, the angle between centerlines of the bodies at that moment is still a small angle, though it may grow quickly if the induced angular velocity is considerable. The direction of the force is always parallel to the longitudinal axis of the spent stage, even at the point of application on the ongoing stages. That the force is applied at a fixed point on the spent stage and that it is parallel to that stage's axis of symmetry is simply a result of the mechanical nature of the pushers: they are built into the forward skirt or interstage of the spent stage and are fixed in direction to push directly forward, parallel to the X^{S_1} axis. On the aft skirt of the ongoing stage, in the separation plane, there is typically a small region against which the pusher pushes, but this region does not extend across the entire separation plane. Outside this region, there is nothing to push against, and so the force becomes zero. That the direction of the force on the ongoing stage should be parallel to the axis of the spent (first) stage is only a consequence of equal force, opposite directions.

The location of each pusher in station coordinates of the spent stage $\vec{r}_{u_j}^{S_1}$ is given, as is the center of the patch in station coordinates of the ongoing stage $\vec{r}_{w_j}^{S_2}$. The pusher force calculation must begin in the station coordinates of the spent stage, because that is where the pushers are mounted.

The position vector $\vec{\mathrm{r}}_{uv_j}^{f}$ between the points of application of pusher force on the spent and ongoing stages is

$$\vec{\mathrm{r}}_{uv_j}^{f} = \vec{\mathrm{r}}_{u_j}^{f} - \vec{\mathrm{r}}_{v_j}^{f}, \tag{3.19}$$

where $\vec{r}_{u_j}^{f}$ is the position of the j^{th} pusher on the spent stage in inertial coordinates, and $\vec{r}_{v_j}^{f}$ is the position of the j^{th} pusher's applied force on the ongoing stage in inertial coordinates, if contact is actually made. Since the pusher is of finite length L_{pusher}, no force is exerted if $\vec{\mathrm{r}}_{uv_j}^{f}$ is longer than that. The u end is the end fixed to the spent stage. The v end is toward the opposite end of the pusher, which is either in contact with the contact patch on the ongoing stage, or has lost contact. The far end $\vec{\mathrm{r}}_{v_j}^{f}$ is the intersection of the pointing vector of the pusher (perpendicular to the base plane of the spent stage) with the base plane of the ongoing stage.

The region against which a pusher may exert force against the ongoing stage does not extend across the entire separation plane of that stage. Instead, the zone where a force may be applied is limited to a small region centered about where the pusher is initially in contact. Point w is the center of the pusher contact region on the ongoing stage. The location of this point is a given of the stage construction and is designated by the position vector $\vec{\mathrm{r}}_{w_j}^{s_2}$ in ongoing stage station coordinates. The radius of the patch about point w where force can be exerted is r_{patch}.

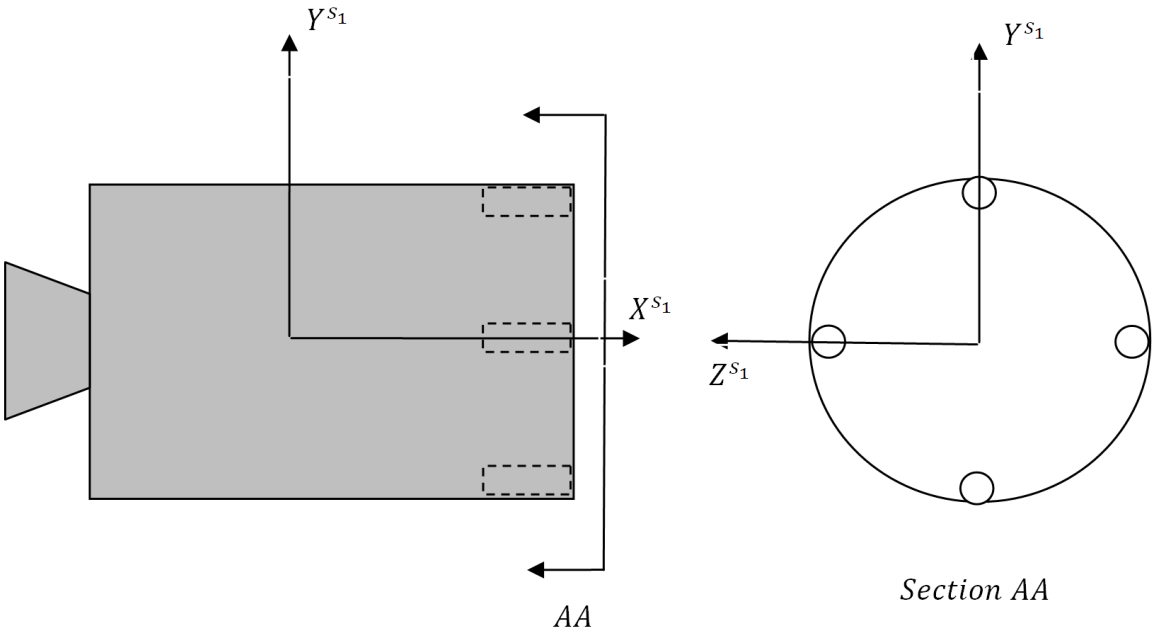

Figure 3.2: Pneumatic Pusher Placement

The base plane of the ongoing stage is defined vectorially as the plane with normal i_1^{s2} (the ongoing stage centerline) passing through the point w.

Calculating the location of point v involves finding the point of intersection between the line defined by the location and direction of the pusher with the plane normal to the X^{S_2} axis passing through point w. Although methods for finding this point derived from college Calculus exist (see Appendix C), the simpler and geometrically more intuitive line-plane intersection test of Ericson, pp. 174-176, is utilized here. The benefit of this method is computation can be performed in any frame. For the pusher problem, fixed frame $X^f Y^f Z^f$ is selected to reduce the number of required coordinate transformations.

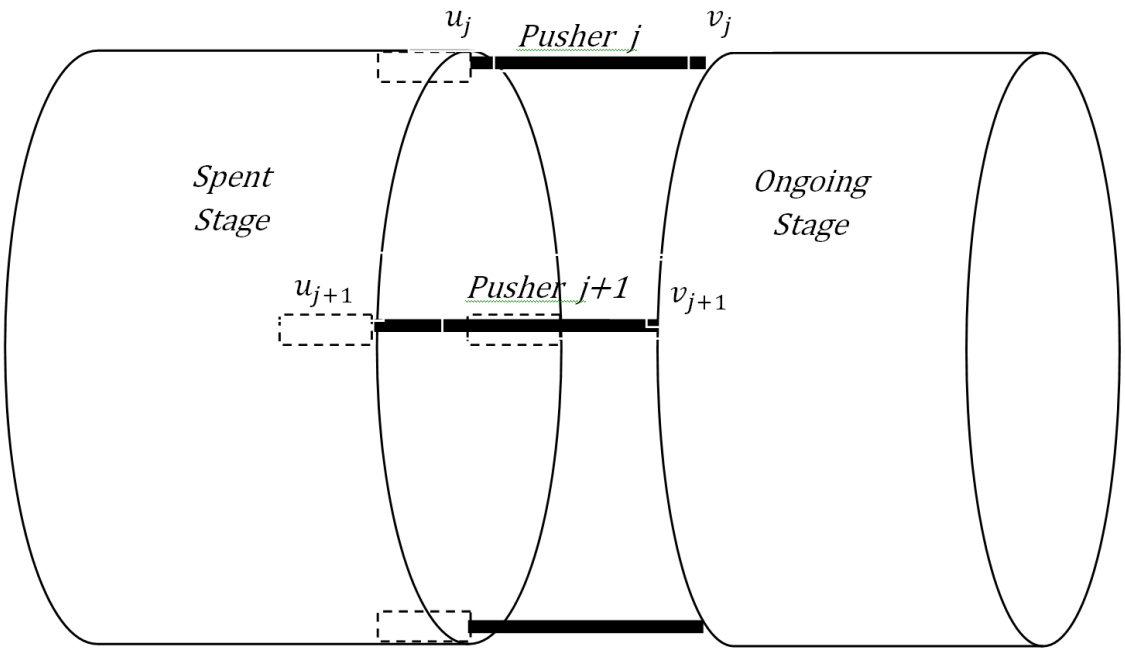

Figure 3.3: Pusher End Point Variables

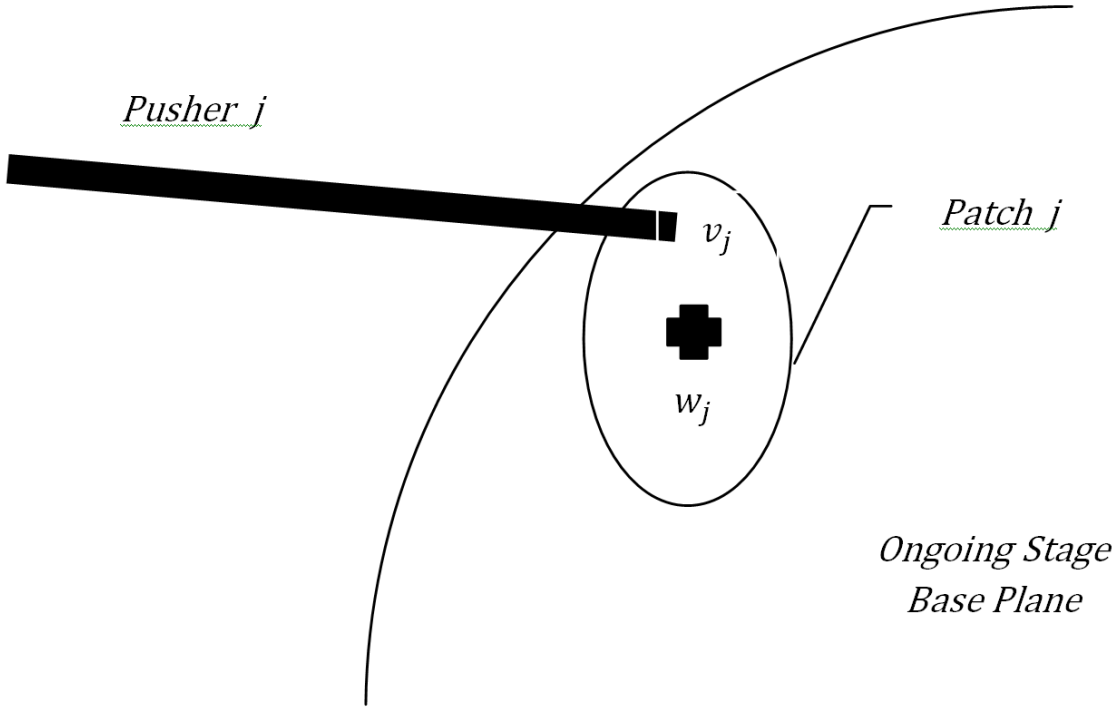

Figure 3.4: Pusher Contact Geometry

All calculations can be performed in the fixed frame, since the definition of the plane to be penetrated is sufficiently general (it does not have to be a coordinate plane), and since all that is needed is a common coordinate system for all points and vectors.

From Section 5.3.1 of Ericson [26], a simple result from projective geometry, using that text's notation:

$$\boldsymbol{Q} = \boldsymbol{A} + \left[\frac{d - \boldsymbol{n} \cdot \boldsymbol{A}}{\boldsymbol{n} \cdot (\boldsymbol{B} - \boldsymbol{A})}\right](\boldsymbol{B} - \boldsymbol{A}), \tag{3.20}$$

where $\boldsymbol{A}$ and $\boldsymbol{B}$ are two points at the end of a line segment, the plane is defined by the linear equation $(\boldsymbol{n} \cdot \boldsymbol{X}) = d$, where $\boldsymbol{n}$ is the normal to the plane; and $\boldsymbol{Q}$ is the point of intersection of the line and the plane.

For our case,

$$\boldsymbol{B} - \boldsymbol{A} = \vec{\mathrm{d}}_j^{\,f} = \boldsymbol{C}_{s_1}^{f}\vec{\mathrm{d}}_j^{\,s_1} = \boldsymbol{C}_{b_1}^{f}\vec{\mathrm{i}}_1^{\,s_1} = \boldsymbol{C}_{b_1}^{f}\begin{bmatrix}1\\0\\0\end{bmatrix} = \boldsymbol{C}_{p_1}^{f}\boldsymbol{C}_{b_1}^{p_1}\begin{bmatrix}1\\0\\0\end{bmatrix} \tag{3.21}$$

and

$$\boldsymbol{A} = \vec{\mathrm{r}}_{u_j}^{\,f} = \vec{\mathrm{r}}_{s_1}^{\,f} + \boldsymbol{C}_{s_1}^{f}\vec{\mathrm{r}}_{u_j}^{\,s_1} = \vec{\mathrm{r}}_{s_1}^{\,f} + \boldsymbol{C}_{p_1}^{f}\boldsymbol{C}_{b_1}^{p_1}\vec{\mathrm{r}}_{u_j}^{\,s_1}\,. \tag{3.22}$$

It is necessary to calculate vector $\vec{\mathrm{r}}_{s_1}^{f}$, which points from the fixed frame origin to the spent stage station coordinates origin. It is not in itself a known quantity. What is given?

$$\vec{\mathrm{r}}_{cm_1}^{f} \equiv position\ of\ spent\ stage\ C.M.\ in\ fixed\ frame$$

$$\boldsymbol{C}_{b_1}^{f} \equiv rotation\ from\ spent\ body\ to\ fixed\ (2\ DCMs, \boldsymbol{C}_{p_1}^{f}\boldsymbol{C}_{b_1}^{p_1})$$

$$\vec{\mathrm{r}}_{cm_1}^{s_1} \equiv position\ of\ spent\ stage\ C.M.\ in\ station\ frame$$

In the above, $\vec{\mathrm{r}}_{cm_1}^{f}$ is a direct result of integrating Newton's equations twice and is part of the stage's state, $\boldsymbol{C}_{b_1}^{f}$ is an indirect result of integrating Euler's equations twice and is part of the stage's state with a constant rotation applied, and $\vec{\mathrm{r}}_{cm_1}^{s_1}$ is a constant for any particular mass properties condition.

$$\vec{\mathrm{r}}_{s_1}^{b_1} = -\vec{\mathrm{r}}_{cm_1}^{s_1} \tag{3.23}$$

$$\vec{\mathrm{r}}_{s_1}^{f} = \vec{\mathrm{r}}_{cm_1}^{f} + \boldsymbol{C}_{b_1}^{f}\vec{\mathrm{r}}_{s_1}^{b_1} = \vec{\mathrm{r}}_{cm_1}^{f} - \boldsymbol{C}_{b_1}^{f}\vec{\mathrm{r}}_{cm_1}^{s_1} = \vec{\mathrm{r}}_{cm_1}^{f} - \boldsymbol{C}_{p_1}^{f}\boldsymbol{C}_{b_1}^{p_1}\vec{\mathrm{r}}_{cm_1}^{s_1} \tag{3.24}$$

The results for the ongoing stage follow exactly along the same lines.

$$\vec{\mathrm{r}}_{s_2}^{f} = \vec{\mathrm{r}}_{cm_2}^{f} - \boldsymbol{C}_{p_2}^{f}\boldsymbol{C}_{b_2}^{p_2}\vec{\mathrm{r}}_{cm_2}^{s_2}\,. \tag{3.25}$$

Substituting known quantities for $\vec{\mathrm{r}}_{s_1}^{f}$,

$$\boldsymbol{A} = \vec{\mathrm{r}}_{u_j}^{f} = \vec{\mathrm{r}}_{cm_1}^{f} - \boldsymbol{C}_{p_1}^{f}\boldsymbol{C}_{b_1}^{p_1}\vec{\mathrm{r}}_{cm_1}^{s_1} + \boldsymbol{C}_{p_1}^{f}\boldsymbol{C}_{b_1}^{p_1}\vec{\mathrm{r}}_{u_j}^{s_1}\,. \tag{3.26}$$

And factoring

$$\boldsymbol{A} = \vec{\mathrm{r}}_{u_j}^{f} = \vec{\mathrm{r}}_{cm_1}^{f} + \boldsymbol{C}_{p_1}^{f}\boldsymbol{C}_{b_1}^{p_1}\left(\vec{\mathrm{r}}_{u_j}^{s_1} - \vec{\mathrm{r}}_{cm_1}^{s_1}\right). \tag{3.27}$$

The normal $\boldsymbol{n}$ to the plane is

$$\boldsymbol{n} = \boldsymbol{C}_{s_2}^{f}\vec{\mathrm{i}}_1^{s_2} = \boldsymbol{C}_{b_2}^{f}\begin{bmatrix}1\\0\\0\end{bmatrix} = \boldsymbol{C}_{p_2}^{f}\boldsymbol{C}_{b_2}^{p_2}\begin{bmatrix}1\\0\\0\end{bmatrix}. \tag{3.28}$$

The center of the patch on the ongoing stage $\vec{\mathrm{r}}_{w_j}^{f}$ is known to be in the plane, and so satisfies the equation of the plane $(\boldsymbol{n}\cdot\boldsymbol{X}) = d$.

$$\boldsymbol{X} = \vec{\mathrm{r}}_{w_j}^{f} = \vec{\mathrm{r}}_{s_2}^{f} + \boldsymbol{C}_{s_2}^{f}\vec{\mathrm{r}}_{w_j}^{s_2} = \vec{\mathrm{r}}_{s_2}^{f} + \boldsymbol{C}_{p_2}^{f}\boldsymbol{C}_{b_2}^{p_2}\vec{\mathrm{r}}_{w_j}^{s_2}\,. \tag{3.29}$$

Eliminating $\vec{\mathrm{r}}_{s_2}^{f}$ yields

$$\boldsymbol{X} = \vec{\mathrm{r}}_{w_j}^{f} = \vec{\mathrm{r}}_{cm_2}^{f} + \boldsymbol{C}_{p_2}^{f}\boldsymbol{C}_{b_2}^{p_2}\left(\vec{\mathrm{r}}_{w_j}^{s_2} - \vec{\mathrm{r}}_{cm_2}^{s_2}\right). \tag{3.30}$$

Thus d is found simply as

$$d = (\boldsymbol{n} \cdot \boldsymbol{X}) = \left[\boldsymbol{C}_{p_2}^{f}\boldsymbol{C}_{b_2}^{p_2}\begin{bmatrix}1\\0\\0\end{bmatrix}\right] \cdot \left[\vec{\mathrm{r}}_{cm_2}^{f} + \boldsymbol{C}_{p_2}^{f}\boldsymbol{C}_{b_2}^{p_2}\left(\vec{\mathrm{r}}_{w_j}^{s_2} - \vec{\mathrm{r}}_{cm_2}^{s_2}\right)\right]. \tag{3.31}$$

Since the value of d is a constant throughout the plane, it is enough to evaluate the equation of the plane at the one point $\boldsymbol{X} = \vec{\mathrm{r}}_{w_j}^{f}$.

Substituting in the values for $\boldsymbol{A}$, $\boldsymbol{B}$, d, and $\boldsymbol{n}$ into the equation of Ericson above produces $\boldsymbol{Q}$ in the fixed frame.

$$\vec{\mathrm{r}}_{v_j}^{f} = \boldsymbol{Q}\,. \tag{3.32}$$

The distance from the u end of the pusher to the projected intercept point in the ongoing stage's base plane at point v is

$$\vec{\mathrm{r}}_{uv_j}^{f} = \vec{\mathrm{r}}_{v_j}^{f} - \vec{\mathrm{r}}_{u_j}^{f}\,. \tag{3.33}$$

The length of $\vec{\mathrm{r}}_{uv_j}^{f}$ must be less than the maximum extent of the pusher to exert any force. A Boolean multiplier expresses this in a simpler form than a series of conditional statements.

$$m_j = \begin{cases} 0, & \left\|\vec{\mathrm{r}}_{uv_j}^{f}\right\| > L_{pusher} \\ 1, & \left\|\vec{\mathrm{r}}_{uv_j}^{f}\right\| \le L_{pusher} \end{cases}. \tag{3.34}$$

The vector from the projected intercept point to the center of the pusher contact patch on the stern of the ongoing stage is

$$\vec{\mathrm{r}}_{wv_j}^{f} = \vec{\mathrm{r}}_{v_j}^{f} - \vec{\mathrm{r}}_{w_j}^{f}\,. \tag{3.35}$$

Only if the intercept point lies within the circular contact patch of radius r_{patch} can the pusher exert any force.

$$n_j = \begin{cases} 0, & \left\|\vec{\mathrm{r}}_{wv_j}^{f}\right\| > r_{patch} \\ 1, & \left\|\vec{\mathrm{r}}_{wv_j}^{f}\right\| \le r_{patch} \end{cases}. \tag{3.36}$$

Knowing whether and where the pusher contacted the patch allows the force of the j^{th} pusher on the spent stage to be determined:

$$\vec{\mathrm{F}}_{u_j}^{s_1} = -m_j n_j F_{pusher}\vec{\imath}_1^{s_1} = -m_j n_j F_{pusher}\begin{bmatrix}1\\0\\0\end{bmatrix}. \tag{3.37}$$

Note the assumption that pusher force is always parallel to the spent stage centerline X^{s_1}. For simulation, additional constraints should disable the pusher force if the pusher has gone to full extent or otherwise lost contact and then a later re-contact is occurring, and also if it is detected that the pusher extent is in fact negative, indicating stage interpenetration, a physical impossibility but a case that must be handled by software.

To calculate stage moment and attitude with Euler's equations, the moment is calculated in station coordinates about the stage C.M. and then rotated to the principal body axes. The point of application of the pusher forces is also expressed in body coordinates as

$$\vec{r}_{u_j}^{\,b_1} = \vec{r}_{u_j}^{\,s_1} - \vec{r}_{cm_1}^{\,s_1} \tag{3.38}$$

leading directly to the moment

$$\vec{M}_{u_j}^{p_1} = \boldsymbol{C}_{b_1}^{p_1} \vec{M}_{u_j}^{s_1} = \boldsymbol{C}_{b_1}^{p_1} \left(\vec{r}_{u_j}^{\,b_1} \times \vec{F}_{u_j}^{s_1} \right) = \boldsymbol{C}_{b_1}^{p_1} \left[\left(\vec{r}_{u_j}^{\,s_1} - \vec{r}_{cm_1}^{\,s_1} \right) \times \vec{F}_{u_j}^{s_1} \right]. \tag{3.39}$$

Since the calculation of translation for both spent and ongoing stages is done in inertial coordinates with Newton's equations, the pusher force is transformed to those inertial coordinates.

$$\vec{F}_{u_j}^{f} = \boldsymbol{C}_{s_1}^{f} \vec{F}_{u_j}^{s_1} = \boldsymbol{C}_{p_1}^{f} \boldsymbol{C}_{b_1}^{p_1} \vec{F}_{u_j}^{s_1} . \tag{3.40}$$

Both the point of application of the force and its direction are needed, since the moment induced by the pusher on the ongoing stage will vary with the point of application. The force on the ongoing body is of equal magnitude and opposite direction to that on the spent stage.

$$\vec{F}_{v_j}^{f} = -\vec{F}_{u_j}^{f} . \tag{3.41}$$

The position of contact $\vec{r}_{v_j}^{\,f}$ is also available in fixed coordinates, as is the position of the ongoing stage C.M. $\vec{\mathrm{r}}_{cm_2}^{\,f}$. The moment about the ongoing stage C.M. in the fixed coordinate system is then

$$\vec{M}_{v_j}^{f} = \left(\vec{r}_{v_j}^{\,f} - \vec{r}_{cm_2}^{\,f} \right) \times \vec{F}_{v_j}^{f} \tag{3.42}$$

which is readily transformed to principal axes:

$$\vec{M}_{v_j}^{p_2} = \boldsymbol{C}_{f}^{p_2} \left[\left(\vec{r}_{v_j}^{\,f} - \vec{r}_{cm_2}^{\,f} \right) \times \vec{F}_{v_j}^{f} \right]. \tag{3.43}$$

Combining all the forces and moments for each stage allows some factoring to reduce computation. Namely, all the spent stage forces and moments can be summed in station coordinates before transforming just once for translation (forces) and once for rotation (moments).

$$\vec{F}^{f}_{pneu_1} = \sum_{j=0}^{n-1} \vec{F}^{f}_{u_j} = \sum_{j=0}^{n-1} \boldsymbol{C}^{f}_{p_1} \boldsymbol{C}^{p_1}_{b_1} \vec{F}^{s_1}_{u_j} = \boldsymbol{C}^{f}_{p_1} \boldsymbol{C}^{p_1}_{b_1} \sum_{j=0}^{n-1} \vec{F}^{s_1}_{u_j}$$

$$\vec{M}^{s_1}_{pneu_1} = \sum_{j=0}^{n-1} \vec{M}^{s_1}_{u_j} = \sum_{j=0}^{n-1} \left(\vec{r}^{s_1}_{u_j} - \vec{r}^{s_1}_{cm_1} \right) \times \vec{F}^{s_1}_{u_j} \tag{3.44}$$

$$\vec{M}^{p_1}_{pneu_1} = \boldsymbol{C}^{p_1}_{b_1} \vec{M}^{s_1}_{\boldsymbol{1}} = \boldsymbol{C}^{p_1}_{b_1} \sum_{j=0}^{n-1} \left(\vec{r}^{s_1}_{u_j} - \vec{r}^{s_1}_{cm_1} \right) \times \vec{F}^{s_1}_{u_j} \ .$$

For the ongoing stage:

$$\vec{F}^{f}_{pneu_2} = \sum_{j=0}^{n-1} \vec{F}^{f}_{v_j} = -\sum_{j=0}^{n-1} \vec{F}^{f}_{u_j} = -\vec{F}^{f}_{pneu_1}$$

$$\vec{M}^{f}_{pneu_2} = \sum_{j=0}^{n-1} \vec{M}^{f}_{v_j} = \sum_{j=0}^{n-1} \left(\vec{r}^{f}_{v_j} - \vec{r}^{f}_{cm_2} \right) \times \vec{F}^{f}_{v_j} \tag{3.45}$$

$$\vec{M}^{p_2}_{pneu_2} = \boldsymbol{C}^{p_2}_{f} \vec{M}^{f}_{\boldsymbol{2}} = \boldsymbol{C}^{p_2}_{f} \sum_{j=0}^{n-1} \left(\vec{r}^{f}_{v_j} - \vec{r}^{f}_{cm_2} \right) \times \vec{F}^{f}_{v_j} \ .$$

Note the similarities of the forces and moments acting on the spent stage in the cases of separation thrusters and of pneumatic pushers. In the pusher case, there is an equal and opposite force on the ongoing stage, which is not matched in the separation motor case. Motors use stored chemical energy to produce "external forces" so that linear and angular momentum are not preserved; that is, if the momentum of the stages before and after the separation event is compared, they will not match in the separation motors case, but should for pushers.

Unlike the separation motors, the pushers act on each stage with the same force, but in opposite directions.

3.8 Mass Offset

Mass offsets from the launch vehicle centerline can be thought to create "inertial forces" as a result. When the separation devices activate, even though they do so perfectly, a mass offset can create apparent moments causing rotation of the stage. Another aspect of this thesis is to examine the effects of spent stage engine mass offset.

Initial conjecture about the re-contact on Falcon 1 flight 2 had centered on the mass offset caused by the gimbaled first stage main engine. This was not believed to be a "tail-wags-dog" phenomenon [14], in which the inertia of the moving engine would affect vehicle dynamics, but instead was thought to arise simply from the static displacement from centerline of the engine at full gimbal [2].

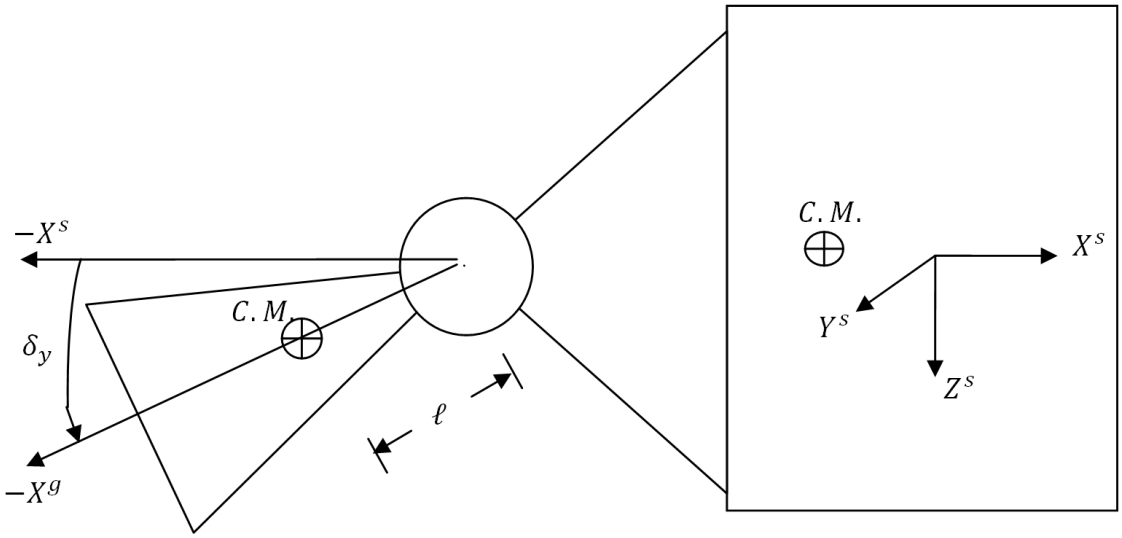

Figure 3.5: Engine Mass Offset Geometry

In order to study the effects of such a mass offset, the new center of mass and the new inertia tensor of the entire stage must be determined. The spent stage is assumed to consist of two rigid bodies, the spent stage proper, consisting of cylindrical tankage with forward and aft skirts, and a single engine, attached to the tankage at the gimbal and pivoted a certain angle δ_y and δ_z from the centerline (the longitudinal axis of symmetry). This configuration is static; active gimbaling, with the gimbal angles $\delta_y$and δ_z changing over time, is not considered here. The origin of the first stage's station coordinates is attached to the tankage. The gimbal is located relative to this origin, as is the instantaneous C.M. of the tankage section. The C.M. of the engine is located a fixed distance l from the gimbal along the gimbal coordinate's negative X^g axis.

To determine the center of mass of the entire stage, the location of the engine and tankage C.M.s must be expressed in the same coordinate system. The most convenient system is the stage station coordinates. Transforming the engine C.M. to station coordinates,

$$\vec{r}_e^{\,s} = \vec{r}_{gs}^{\,s} + l\,\mathbf{A}\left(\delta_y, \delta_z\right)\vec{\imath}_1^{\,g} = \vec{r}_g^{\,s} + \mathbf{A}\left(\delta_y, \delta_z\right)\begin{bmatrix} -l \\ 0 \\ 0 \end{bmatrix}, \tag{3.46}$$

where $\mathbf{A}(\delta_y, \delta_z)$, introduced in Chapter II, is the rotation matrix of the engine relative to the tankage $\boldsymbol{C}_g^s = \boldsymbol{A}(\delta_y, \delta_z)$.

The center of mass of the whole stage is then

$$m_1 = m_t + m_e \tag{3.47}$$

$$\vec{r}_{cm}^{\,s_1} = \frac{m_t\vec{r}_t^{\,s_1} + m_e\vec{r}_e^{\,s_1}}{m_1}. \tag{3.48}$$

To determine the inertia tensor for the whole stage, the inertia tensor of the main engine must be transformed to the same set of coordinates (station coordinates) and referred to the just-calculated instantaneous C.M. To express an inertia tensor given in one coordinate system in a different coordinate systems related only by rotation requires pre- and post-multiplication by the transformation matrix relating those coordinate systems [1].

$$\boldsymbol{I}_e^{s_1} = \boldsymbol{C}_g^{s_1}\boldsymbol{I}_e^g\boldsymbol{C}_{s_1}^g\,, \tag{3.49}$$

where

$$\boldsymbol{C}_{s_1}^g = \mathbf{A}(\delta_y, \delta_z) \tag{3.50}$$

and

$$\boldsymbol{C}_g^{s_1} = \mathbf{A}^{\mathbf{T}}\left(\delta_y, \delta_z\right). \tag{3.51}$$

The inertia tensor $\boldsymbol{I}_e^{s_1}$ is now in a set of axes parallel to the stage coordinates but the new tensor needs to be referred to the instantaneous C.M. through the use of the parallel axis theorem ([10], [11], [12]), also known as the Huygens-Steiner theorem. The position vector of the engine C.M. relative to the whole stage C.M. in station coordinates is

$$\vec{r}_{(e|cm)}^{\,s_1} = \vec{r}_e^{\,s_1} - \vec{r}_{cm}^{\,s_1}\,. \tag{3.52}$$

The inertia tensor of the tankage must also be referred to the instantaneous C.M.

$$\vec{r}_{(t|cm)}^{\,s_1} = \vec{r}_t^{\,s_1} - \vec{r}_{cm}^{\,s_1}\,. \tag{3.53}$$

The parallel axis theorem in matrix form may be expressed [10] as

$$\boldsymbol{I}^{s_1}_{(e|cm)} = \boldsymbol{I}^{s_1}_{e} + m_e \begin{bmatrix} l_2^2 + l_3^2 & -l_1 l_2 & -l_1 l_3 \\ -l_1 l_2 & l_1^2 + l_3^2 & -l_2 l_3 \\ -l_1 l_3 & -l_2 l_3 & l_1^2 + l_2^2 \end{bmatrix}, \tag{3.54}$$

where l_1, l_2, and l_3 arise from $\vec{r}^{\,s_1}_{(e|cm)} = l_1 \vec{i}^{\,s_1}_1 + l_2 \vec{i}^{\,s_1}_2 + l_3 \vec{i}^{\,s_1}_3$, the position vector of the old location about which the inertia tensor was referred. The final inertia tensor of the entire first stage referred to the present C.M. is

$$\boldsymbol{I}^{s_1}_{cm} = \boldsymbol{I}^{s_1}_{(e|cm)} + \boldsymbol{I}^{s_1}_{(t|cm)} . \tag{3.55}$$

Since the inertia matrix for the whole stage together, $\boldsymbol{I}^{s_1}_{cm}$, is already referred to the stage C.M., and since the body axes are parallel to the stage axes but the body axes are rooted at the C.M., the tensor for the body axes is the same:

$$\boldsymbol{I}^{b_1} = \boldsymbol{I}^{s_1}_{cm} . \tag{3.56}$$

The eigenvector / eigenvalue problem is solved once for the matrix $\boldsymbol{I}^{b_1}$ prior to simulation so that the diagonalized principal inertia matrix $\boldsymbol{I}^{p_1}$ and the rotation matrix $\boldsymbol{C}^{p_1}_{b_1}$ are available to integrate Euler's equations.

CHAPTER IV

GEOMETRY OF SEPARATION AND RE-CONTACT

During a nominal separation, the spent body and the ongoing body move apart without any contact. Re-contact occurs when, after separation, the stages come together again or if the separation devices fail to achieve any separation distance. Figure 4.1 depicts the geometry of separation and re-contact. At separation on most launch vehicles, the engine of the ongoing stage lies within a volume made up of the interiors of the spent stage's forward skirt, the ongoing stage's aft skirt, and an optional interstage separating the two stages.

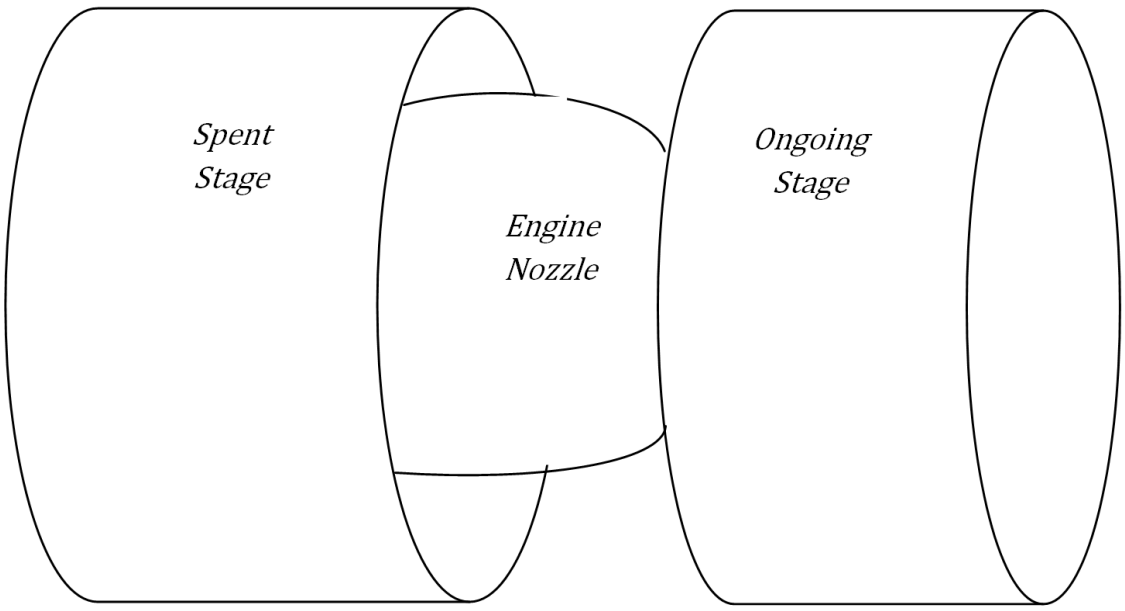

Figure 4.1: Geometry of Separation and Re-contact

For this thesis, the interstage is not modeled except as a lengthened aft skirt of the ongoing stage. The bell of the ongoing stage's single engine is partially recessed within the forward skirt of the spent stage, and this is where the greatest potential for re-contact comes from. With today's upper-stage rocket engines using higher expansion ratios, the volume between the stages is highly utilized [22]. Consequently, the tolerances between skirt and nozzle are much tighter. The greatest potential for re-contact is therefore between the maximum diameter of the rocket engine of the ongoing stage, the rim of the bell, and the inside of the forward skirt of the spent stage. The forward skirt is modeled simply as a hollow cylinder of the diameter of its interior diameter and the same length as the skirt. The engine is modeled as a hollow cylinder of the diameter of the engine at its broadest, at the engine exit plane. The ongoing stage's engine is assumed not to be gimbaled during the separation event: δ_y and δ_z are always zero The aft skirt is modeled as a simple cylinder having the diameter of the ongoing stage. If at any time the shapes intersect, re-contact is considered to have occurred. This is an undesirable outcome, one that nominally should never occur; so analysis stops at re-contact. Modeling behavior after re-contact is not the subject of this thesis. It is, however, important to find out when re-contact is possible and to engineer the vehicle to minimize the probability of such events, subject to all the other constraints under which multi-stage rockets must perform.

If, after time $t = t_{sep} = 0$, the open cylinder representing the spent stage ever intersects the closed cylinder of the engine or the open cylinder of the ongoing stage's aft skirt, re-contact has occurred. Two tests per time interval should be sufficient for this simple geometry: testing for intersection of the forward skirt with the engine, and testing for intersection of the forward skirt with the aft skirt. Since the development of collision detection algorithms is beyond the scope of this thesis, simple *ad hoc* algorithms for detecting re-contact, detailed in Chapter VI, are used. These algorithms basically convert the ongoing stage into a field of points and detect when the points straddle the cylinder describing the forward skirt of the spent stage.

Because of the axial symmetry of each stage, the geometry of each stage can be reduced to two dimensions. With this simplification, the aft skirt and engine become boxes, and the forward skirt becomes an open box, a rectangle with a side missing. This simplified geometry is depicted in Figure 4.2.

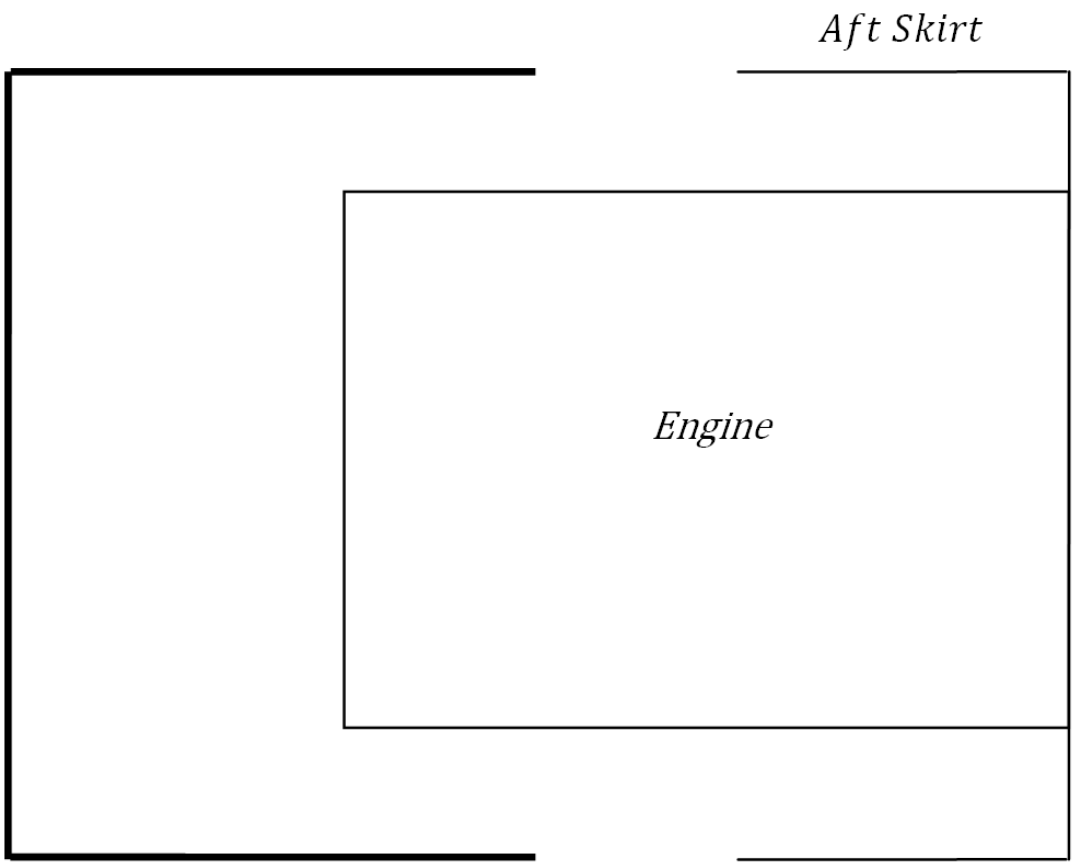

Figure 4.2: Simplified 2D Geometry of Separation and Re-contact

There is some loss of generality with the reduction to two dimensions. This is especially evident when the axes of revolution (the body/station X axes) of the two stages are not coplanar.

Re-contact occurs whenever the open box representing the forward skirt intersects either the aft skirt or engine. Thus the test for intersection is reduced to the 3 line segments of the forward skirt and the 6 line segments of the aft skirt. Testing for intersection of line segments in two dimensions is analytically simple and computationally inexpensive.

CHAPTER V

ANALYSIS

Many of the situations described in Chapter III are difficult to analyze in their complete form and must be simulated. In this chapter, important simplifying assumptions are made which make analysis possible.

5.1 Thrust Transient

In Chapter III, the declining exponential model of a main engine thrust termination transient was introduced.

Any thrust before separation contributes to accelerations of both stages and does not contribute to relative motion; it is totally irrelevant to the separation problem. The portion of the thrust transient after separation may cause re-contact, as it acts on the spent stage only. A transient of short duration may be modeled as a simple impulse by integrating the thrust over its entire period of application and applying one such impulse at time t_0. The impulse after the separation is the portion of the total impulse which is of concern here, not the total impulse, which is much larger.

$$P = \int_{t0}^{\infty} T\, dt \tag{5.1}$$

$$P = \int_{t_0}^{\infty} T_0 e^{-\alpha(t-t_0)}\, dt \tag{5.2}$$

$$P = -\frac{T_0}{\alpha} e^{-\alpha(t-t_0)} \Big|_{t_0}^{\infty} = \frac{T_0}{\alpha}. \tag{5.3}$$

The time t_0 above is the start time of the transient. Let t_1 be the time of separation, some time after the beginning of spent stage thrust termination $= t_1 > t_0$. Then the impulses before and after separation, P_{before} and P_{after}, respectively, are

$$P = P_{before} + P_{after} = -\frac{T_0}{\alpha} e^{-\alpha(t-t_0)} \Big|_{t_0}^{t_1} - \frac{T_0}{\alpha} e^{-\alpha(t-t_0)} \Big|_{t_1}^{\infty} \tag{5.4}$$

$$P_{before} = -\frac{T_0}{\alpha} e^{-\alpha(t_1-t_0)} + \frac{T_0}{\alpha} = \frac{T_0}{\alpha}\left[1 - e^{-\alpha(t_1-t_0)}\right] \tag{5.5}$$

$$P_{after} = \frac{T_0}{\alpha} e^{-\alpha(t_1-t_0)} . \tag{5.6}$$

An impulse may be sufficient for analytical modeling, but is difficult to implement in simulation. To approximate an impulse in simulation, a constant force is spread out over a short time interval, which might be one or a few simulation intervals:

$$T_{impulse} = \frac{P_{after}}{t_{applied}} = \frac{T_0}{\alpha t_{applied}} e^{-\alpha(t_1-t_0)} , \tag{5.7}$$

where $T_{impulse}$ is the constant thrust for this time interval and $t_{applied}$ is the total time over which the constant thrust is applied.

The main engine thrust transient problem is not to be confused with the main engine gimbaling mass offset problem. In the latter case, the engine is gimbaled from its nominal position, and as a result its center of mass is not on the stage centerline. In the thrust transient case, the moment caused by a gimbaled engine's thrust is not the focus of analysis; the thrust transient along centerline is. Therefore, besides the impulsive limit, a further simplifying assumption for the thrust transient problem is that of zero gimbal angles ($\delta_y = 0, \delta_z = 0$). The gimbal D.C.M.s disappear from the thrust equation.

$$\vec{T}^s = T(t)\vec{\imath}_1^s \tag{5.8}$$

Correspondingly for the impulsive limit,

$$\vec{P}^s = P_{after}\vec{\imath}_1^s . \tag{5.9}$$

5.2 Separation Motors

In Appendix E, the specific case of separation thrusters mounted symmetrically around the outer circumference of a stage is analyzed. All thrusters are assumed to fire in a direction parallel to the stage's centerline.

For the case in which all n thrusters ($n > 1$) produce identical force F_c, the resultant force and moment on the stage are

$$\vec{F}_{sep} = nF_c\vec{\imath}_1 \tag{5.10}$$

$$\vec{M}_{sep} = \vec{0}\,. \tag{5.11}$$

This is reasonable, since the force is spread evenly at discrete points about the circumference, so any moment from an individual thruster is balanced out by the thruster located at the diametrically opposite location.

When a uniform gradient in thrust in the $\vec{\imath}_2$ direction dF exists among the n thrusters ($n > 2$), the forces remain the same but a moment is now generated. It is shown in Appendix E that

$$\vec{F}_{sep} = n\,F_c\vec{\imath}_1 \tag{5.12}$$

$$\vec{M}_{sep} = -\frac{1}{2}h^2 dF n\vec{\imath}_3\,, \tag{5.13}$$

where F_c is the nominal (average) thrust; $dF = (F_{max} - F_{min})/h$, and h is the radius of the motors from the centerline. This moment could give rise to motion leading to re-contact.

If the time of burn is considered very brief compared to other time scales, then taking the forces and moments of the separation thrusters to the impulsive limit is reasonable.

$$\vec{P}_{sep} = n\,F_c t_{burn}\vec{\imath}_1 \tag{5.14}$$

$$\vec{Q}_{sep} = -\frac{1}{2}h^2 dF\; t_{burn} n\vec{\imath}_3\,, \tag{5.15}$$

where t_{burn} is the thrust duration of separation motors, $\vec{P}_{sep}$ is the impulse due to all separation motors, and $\vec{Q}_{sep}$ is the impulsive torque from those same motors due to thrust gradient.

5.3 Pneumatic Pushers

An analysis of pneumatic pushers was also performed in Appendix E. For the case in which all pushers exerting equal force, the forces and moments are

$$\vec{F}^s_{pp_s} = nF_p\vec{\imath}^s_1 \tag{5.16}$$

$$\vec{M}_{pp_s} = \vec{0}\,. \tag{5.17}$$

These results for the spent stage are the same as those for separation motors.

Separation motors do not affect the other stage, since plume impingement is assumed negligible. Pushers by definition and design affect both stages. For the case of uniform pushers, this is relatively trivial, since no moment develops. The force and moment on the ongoing stage are

$$\vec{F}^s_{sep_o} = -\vec{F}^s_{sep_s} \tag{5.18}$$

$$\vec{M}_{sep_o} = \vec{0}\,. \tag{5.19}$$

When a gradient in pusher force exists across the stage in the separation plane in the $\vec{\imath}^s_2$ direction, the results for the spent stage are the same as that for separation motors with gradient, but the resultant forces and moments on the ongoing stage are a little different, as shown in Appendix E:

$$\vec{F}^o_i = -\vec{F}^s_i \tag{5.20}$$

$$\vec{M}^o_{sep} = -l_o n\gamma F_{base}\vec{\imath}^o_3 - \frac{1}{2}h^2 dFn\vec{\imath}^o_3\,, \tag{5.21}$$

where h is the radius of the ring of the pushers and $dF = (F_{max} - F_{min})/h$. The second term has been seen before, with a gradient in separation motor force, and arises because of the linear gradient in pusher strength. The first term is due to the angle γ between the axes of the spent and ongoing stages (measured in the plane). The moment that the pushers produce grows with this misalignment. Note that a small angle assumption has been used for the angle γ, and this will introduce some error, especially for conservation of momentum calculations.

When all pushers produce equal force, Appendix E shows that the relative velocity at any point out to maximum extent is

$$v_{rel} = -Ft\frac{m_1 + m_2}{m_1 m_2}. \tag{5.22}$$

For such a case, maximum extent is reached when

$$t_{sep} = \sqrt{2\frac{sm}{F}}, \tag{5.23}$$

where s is the maximum length of the pushers and $m = \frac{m_1 m_2}{m_1 + m_2}$.

When a moment arises due to unequal pushers, the angular velocity is

$$\omega_{rel} = -M_1 t \frac{I_1 + I_2}{I_1 I_2}, \tag{5.24}$$

where M_1 is the moment acting on the spent stage, and I_1 and I_2 are the moments of inertia of the spent and ongoing stages, respectively.

5.4 Mass Offset in Two Dimensions

The mass offset due to engine gimbaling is quite amenable to analysis since the gimbal angle rarely exceeds 5°, especially toward stage burnout, permitting small angle assumptions in the engine-to-station transformation matrix. Furthermore, the distance of the engine C.M.to the gimbal is so much smaller than the distance from the stage C.M. to the gimbal that another round of simplifications can be made. These are detailed in Appendix E in the section on mass offsets.

As shown in that Appendix, when nominally-performing separation devices produce a force F in the reverse direction along the centerline, an engine of mass m_e whose C.M. is a distance l from the gimbal and is vectored an angle δ from the centerline of the stage will produce a moment

$$\vec{M}_{sep} = \frac{Fl\delta m_e}{m_t + m_e}\vec{\imath}_3 \tag{5.25}$$

on the stage. The change in the stage's moments of inertia about the axis perpendicular to the plane, $I_{s_{zz}}$, from engine deflection is primarily caused by the shortening of the distance of the engine C.M. to the stage C.M.. For small angles, this shortening is negligible, so that the equation of motion in the plain is simply

$$M_{sep} = I_{s_{zz}}\dot{\omega} \tag{5.26}$$

or

$$\dot{\omega} = \frac{M_{sep}}{I_{s_{zz}}} = \frac{1}{I_{s_{zz}}} \frac{Fl\delta m_e}{m_t + m_e}. \tag{5.27}$$

5.5 Simplified Separation Trajectories in Two Dimensions

In the Geometry of Separation and Re-contact section of Appendix E, the separation problem is simplified to a two-dimensional problem. If the separation is considered to be initiated impulsively, a velocity $(v^s_{x_{CM_o}}, v^s_{y_{CM_o}})$ and angular velocity ω is given to the ongoing stage relative to the spent stage. If the angle of separation θ between the two stages is still small, the time t_2 when the arbitrary point *A* on the ongoing stage passes the spent stage outer diameter r_B is

$$t_2 = \frac{r_B - y^o_a - y^s_{CM_o}(0) - \theta_0 x^o_a}{v^s_{y_{CM_o}} + \omega x^o_a}, \tag{5.28}$$

where (x^o_a, y^o_a) is the location of point *A* on the ongoing stage, $(x^s_{CM_o}(0), y^s_{CM_o}(0))$ is the initial location of the ongoing stage C.M. relative to the spent stage, and $(v^s_{x_{CM_o}}, v^s_{y_{CM_o}})$ is the velocity of the ongoing stage relative to the spent stage. The location along the line of the forward skirt where point *A* crosses it is

$$h_B = x^o_a + x^s_{CM}(0) - \theta_0 y^o_a + \left(v^s_{x_{CM_o}} - \omega y^o_a\right) t_2 . \tag{5.29}$$

If $h_B \leq x_B$, the extreme tip of the spent stage's forward skirt, then re-contact has occurred.

CHAPTER VI

SIMULATIONS

A simulation program was constructed in MATLAB in order to verify/validate the two-dimensional analysis developed in this thesis and to simulate the situations that are not amenable to analytical simplifications. MATLAB was chosen, because it combined ease of coding for heavily mathematical manipulations with ready visualization of numeric results. An additional tool was written in C++ with the OpenGL graphics library purely to animate the motion of the stages computed during MATLAB simulation, primarily as a debugging tool for the MATLAB simulation.

6.1 Methods and Algorithms

A MATLAB simulation implemented the three-dimensional general equations of motion without significant simplification as presented in Chapter III. The three-dimensional simulation was used both to verify the simpler two-dimensional simulations and to simulate cases which cannot be sufficiently reduced to two-dimensional problems.

The simulation runs from time $t = 0$, the instant of stage separation, until either re-contact is detected or enough separation distance is achieved to guarantee no contact. Since computation is inexpensive, the typical simulation time step is 1msec. Every time step, the state (position, velocity, angular position, and angular velocity) of each stage is computed, and checks for re-contact are performed. The numerical integration routine may use finer time steps internally to achieve a pre-defined level of numerical accuracy.

The origin of the inertial system is the center of the separation plane at the start of staging. Throughout simulation, this origin continues to move with the velocity of the conjoined launch vehicle just

prior to the instant of separation. In the simulation, the inertial frame appears stationary numerically; its position is never updated.

Because a staging event is being simulated, stage mass properties (mass and moments of inertia) are assumed to be constant. If large motors were firing, the mass properties would be changing continuously, and every step of the simulation would require the re-computation of the relationship between stage body axes and the corresponding principal axes. This would require the solution of the three-dimensional eigenvalue problem every simulation time step. Since the mass properties are constant during separation, the relationship between stage body coordinates and principal coordinates only needs to be found once, prior to the start of simulation. Thereafter, $\boldsymbol{C}_{b_1}^{p_1}$ and $\boldsymbol{C}_{b_2}^{p_2}$ are considered constants during separation.

Two bodies, the spent and ongoing stages, are simulated. Since simulation begins at separation, the launch vehicle is never represented as a single rigid body but as two separate rigid bodies. Rectilinear state, positions and velocities, of the stages are maintained in inertial coordinates, the fixed frame described in Chapter II. Angular state is kept in the principal axes of each stage. Attitude is represented in quaternions throughout the core of the 3D simulations, with human-readable inputs and results transformed to DCMs and Euler angles from their original quaternion formats.

Obtaining velocities from forces and moments in three dimensions is carried out through numerical integration of Newton's equations for translation and Euler's equations for rotation in the form of quaternions. The new positions are then calculated through numerical integration of the velocities. Instead of calling the numeric integrator twice, once for each stage, the integrator is called only once each time step to advance the states of both stages at once. The states of the two stages are related in the pusher case through the shared force on either end of each pusher. Also, when pusher contact is lost, the force on either end drops precipitously, so the numerical results need to be of higher quality if the change in force can propagate to all affected components as (numerically) fast as possible. The numerical integrator used throughout is the standard routine ODE45 from MATLAB, which internally uses 4^{th}-5^{th} order Runge-Kutta integration.

Contact is not modeled directly, so the momentum exchange due to collision or contact is not calculated. Instead, the two stages, even in the case of pushers, are treated as two rigid bodies with a possibly interrelated set of forces acting on them.

In three dimensions, the geometry of the two stages is described by cylinders and planes, which are further broken down into hundreds of points. Since collision detection algorithms are not a focus of this thesis, the ongoing stage geometry is modeled simply as a field of points in space describing the aft skirt cylinder and the cylinder that represents the engine. Before the first simulation time step, the field of points is generated from the ongoing stage geometry and then preserved. These points are in the stage coordinates of the ongoing stage. For each simulation time step, the field of points is transformed from the ongoing stage coordinates to the spent stage coordinates. There, each point is tested against a simple set of formulae describing the forward skirt of the spent stage, whose axis of symmetry is the X^{S_1} axis. If a point is outside the forward skirt, that is, if it lies beyond the radius of the cylinder from the X^{S_1} axis, and it also lies below the top lip of the forward skirt, then a re-contact event has occurred.

No control systems are modeled in the simulations. Flight continues without measurement of attitude or acceleration, calculation of error, or corrective response. For some of the simulations which take the equations of motion to the impulsive limit, impulses are modeled explicitly by the user as very short forces, lasting one or a few calculation cycles, not of infinitesimal duration, which is hard to simulate. Some quantities are calculated every simulation cycle even though simulation itself does not need them: linear momentum and angular momentum of each stage, for example, are calculated every cycle to identify any error accruing from possibly incorrect pusher calculations. These are then written to a file for quality control purposes. Main engine thrust transient, separation motors, pneumatic pushers, and main engine mass offset are all modeled in the three-dimensional simulation.

The simulation is detailed enough to handle other situations that would be difficult to evaluate analytically: random pusher and motor variation, failed pushers, large angle between stages, loss of pusher contact on some pushers but not others, and non-zero angular rate at the moment of separation.

A main output of the simulation is the state record file, the state of each stage at every time instance. Another output is the timestamp of any contact and where, both on the spent and ongoing stages, it occurred. To keep from having to write parsing code in the MATLAB programming language, all input

files are simply MATLAB .m files included with an "eval" statement. So each input file to the simulation is actually a MATLAB code file, and that code is executed to initialize the simulation. This requires extensive error checking in the surrounding code to make sure no important variables are left uninitialized. To manage all the separate test cases, each test case has its own scenario file which specifies several other input files needed for the test case, including the launch vehicle file and the simulation control file. The launch vehicle file describes the dimensions and mass properties of each of two stages, as well as the location and capabilities of separation motors and thrusters. The simulation control file specifies how long to run, what time step to use, whether to stop if stage re-contact occurs, whether to model pushers or motors, whether motor/pusher force is uniform, a linear gradient across the vehicle, or random, and more. All the output files from a particular test case have file names based on the file name of that test case's scenario file, but with a different extension. This helps keep the files for a particular test case logically grouped. To simplify operation even further, all test cases are grouped together and executed from a common routine, so that if there is a change in any input file or update to any algorithm, the output of all scenarios can be re-created with one command.

MATLAB is sufficient for graphing simulation data, but MATLAB is difficult to create geometry with, and so it is hard to use to depict moving objects. To help debug the MATLAB simulation, a short C++ program, named "twoStages", was written that displays the location of the stages and their reference frames throughout the simulation time span. The C++ program uses the standard OpenGL 3D graphics library to draw the geometry. The geometry is simple; there is no "eye candy". The stage tankage and skirts and the engines are drawn as simple cylinders with tops and bottoms. The program itself does not perform any dynamics computation; that is the job of the MATLAB simulation. The program reads in the state record file and simply animates the contents.

6.2 Results of Simulation

Several of the analytical results of Chapter IV were coded in MATLAB and compared against the 3D simulation described earlier. The specific cases studied were (1) the thrust transient of the spent-stage

main engine as an impulse, (2) separation motors on the spent stage with uniform thrust, (3) separation motors on the spent stage with a lateral thrust gradient, (4) pneumatic pushers with uniform force, (5) pneumatic pushers with a lateral force gradient, and (6) mass offset of a spent-stage main engine due to gimbaling.

6.2.1 Main Engine Thrust Transient

From a given exponentially-declining profile of the main-engine thrust cutoff, an equivalent impulse was calculated using the results of Chapter IV. Then a short-duration constant force with equivalent total impulse was determined. A one-dimensional MATLAB simulation was conducted using this constant force. For purposes of comparison, a full 3D simulation with the actual thrust cutoff profile was performed.

Figure 6.1 depicts the spent stage velocity due to the thrust transient from both the 1D model and from simulation. The velocity from 3D simulation monotonically approaches 0.3 m/s from below, while the 1D model predicts a final velocity about 10% lower. A possible source of error is numerical error resulting from modeling an impulse over a very few time steps. The constant force of the impulse model is spread out, for simulation purposes over 0.004 s, only 4 time steps. The steep rise and fall may cause the ODE45 integrator routine in MATLAB to significantly shorten its internal step size to meet error tolerance requirements. Note the brief overshoot in the impulse model before leveling off, which is expected for the numerical solution of the response to an impulse loading.

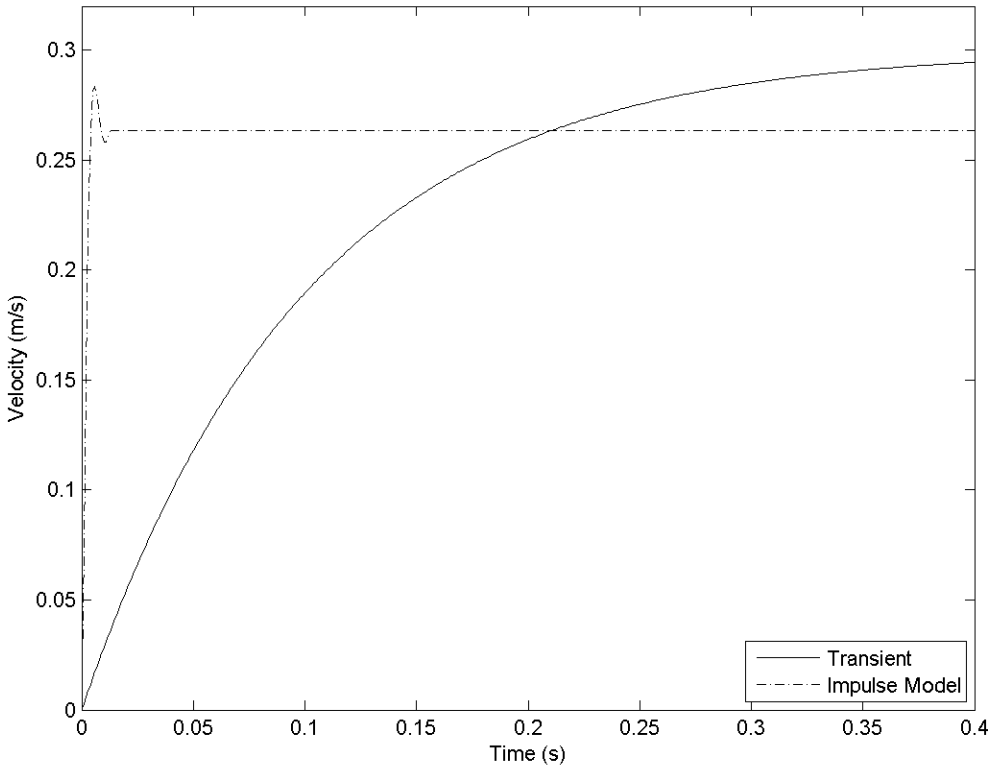

Figure 6.1: Thrust Transient Impulse Model Performance

6.2.2 Separation Motors with Uniform Thrust

A two-dimensional simulation (state x, y, and θ about the Z axis) based on the force and moment equations for uniform thrust separation motors presented in Chapter IV was developed. Four equal retro-firing motors were present on the spent stage. Only the spent stage was simulated, since the ongoing stage is not affected by the spent stage motors. The same scenario was simulated with 3D simulation.

The agreement between the simulation of the analytic model and the full 3D simulation was excellent in this simple case. Figure 6.2 shows the spent stage longitudinal (x axis) velocities, which are very close during thrust ($t \leq 0.4\ s$) and within 5% thereafter.

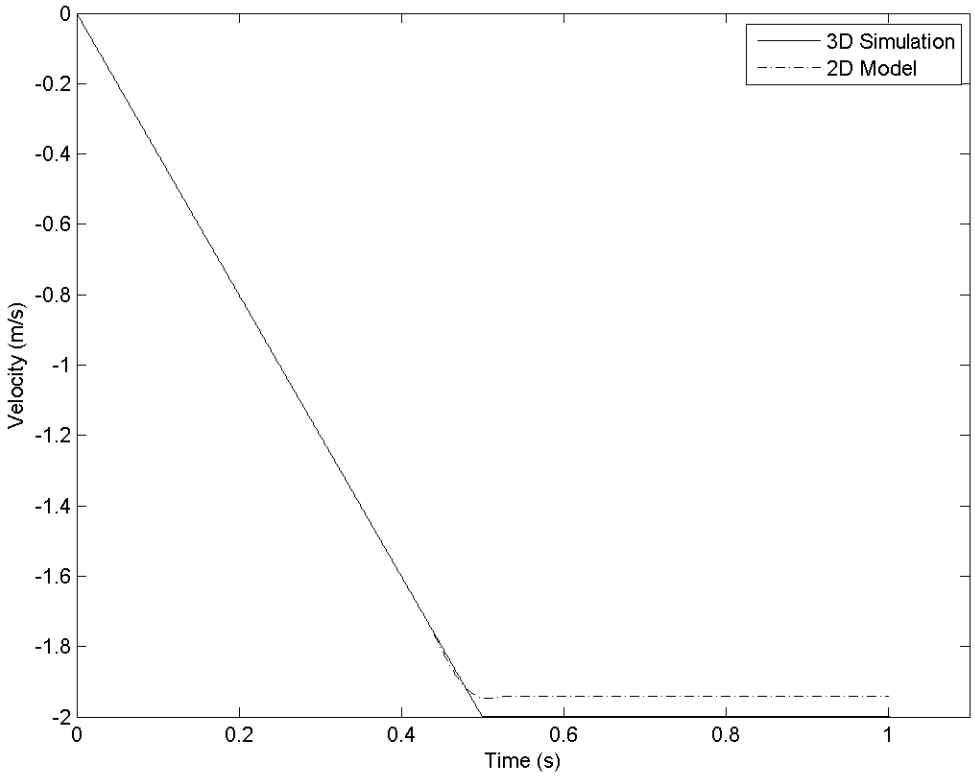

Figure 6.2: Uniform Separation Motors Model Performance

6.2.3 Separation Motors with Lateral Thrust Gradient

The previous uniform thrust separation motor case was modified to model a gradient in the motor performance across the y axis of the spent stage. Figure 6.3, depicting spent-stage positions, and Figure 6.4, showing the angular positions of the same stage, indicate that the results from 2D and 3D calculations are again close, especially during thrust. A slight velocity discrepancy is present after thrust cut-off, evident in the different slopes for 3D simulation and the 2D model in Figure 6.3.

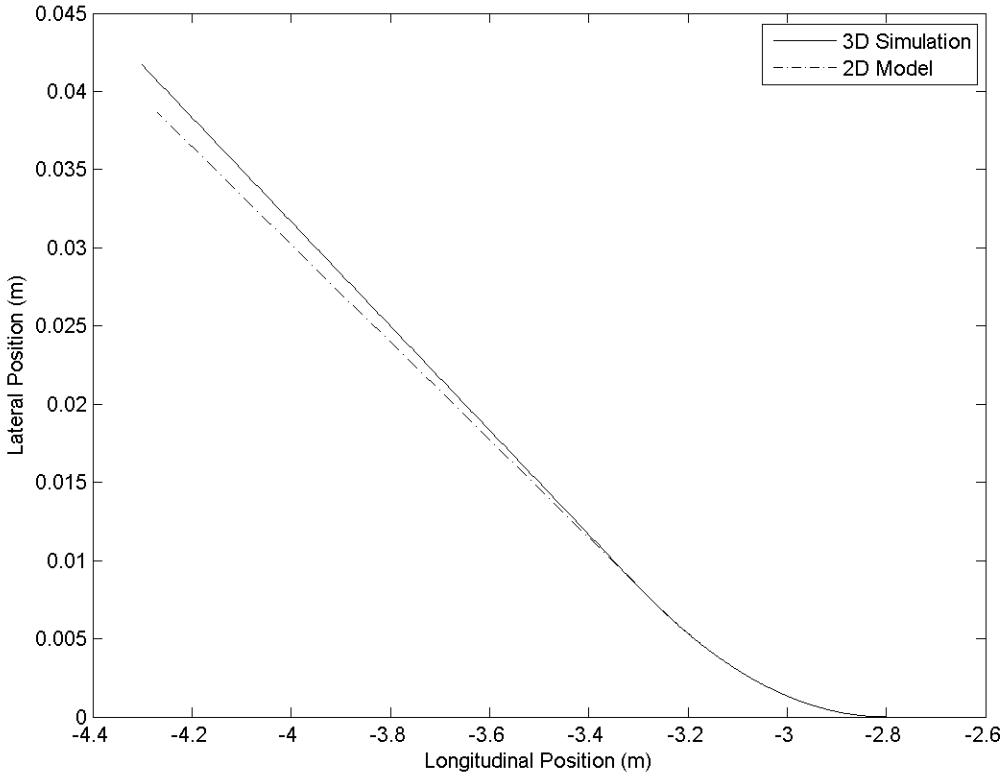

Figure 6.3: Separation Motors with Gradient Spent Stage Motion

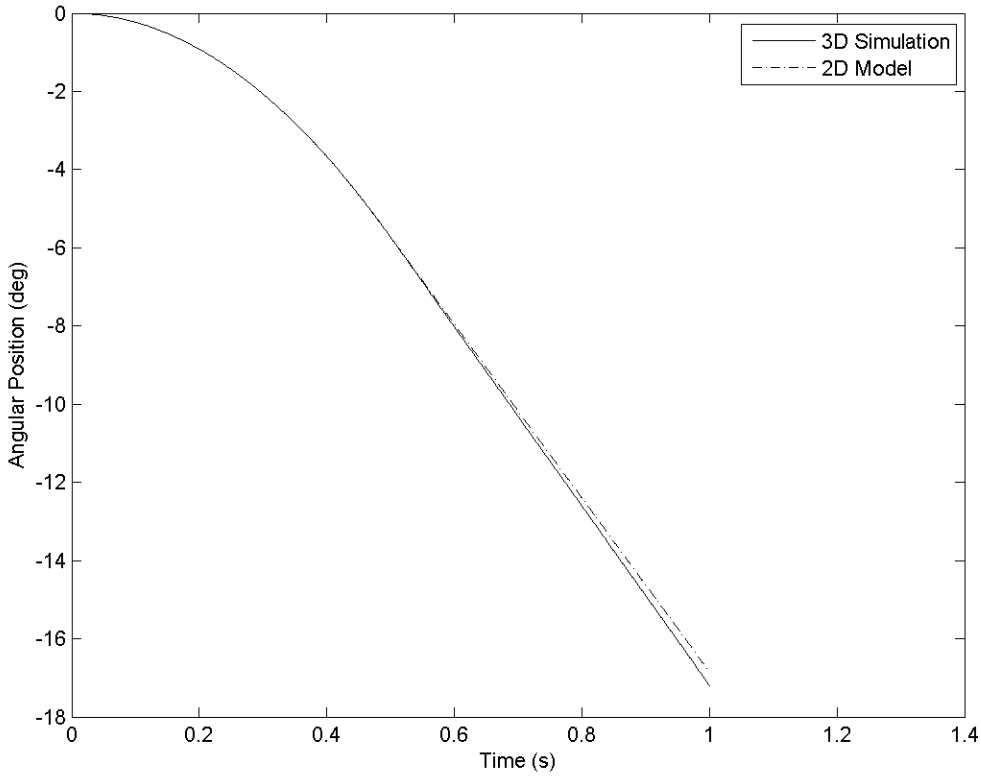

Figure 6.4: Separation Motors with Gradient Spent Stage Angular Motion

6.2.4 Pneumatic Pushers with Uniform Force

A two-dimensional analysis based on the force and moment equations for uniform force pneumatic pushers presented in Chapter IV was developed. Eight equal pushers were modeled between the two stages. Both the spent stage and ongoing stage were modeled, because, unlike separation motors, both stages are affected by the pushers. The MATLAB-based three-dimensional code was used to simulate this case as well.

Agreement between the results of the analytic model and of the full 3D simulation was good during contact (when the pushers can exert force), but resulted in different separation velocities (about 10%), as shown in Figures 6.5 and 6.6 for the spent stage and ongoing stage, respectively. The simulation using the analytical model exhibited some overshoot as well. The sharp cutoff in pusher force when contact is lost (at $t \approx 1.3\ s$) is believed to contribute to the overshoot and velocity error. As the ODE

solver marches back and forth in time to minimize computational error, it finds a point in time before which the pusher is in contact and the force is high, and after which the pusher is not in contact and the force is low. No matter how short the time step is made, the ODE solver will not find an intermediate value.

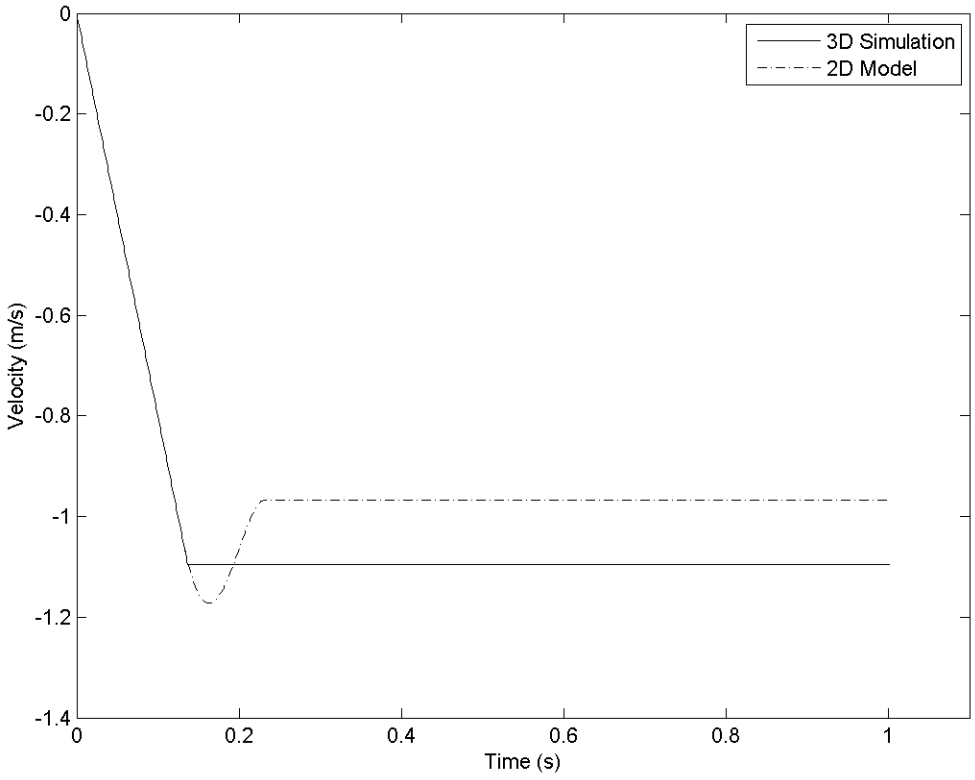

Figure 6.5: Spent Stage Velocity due to Uniform Pushers

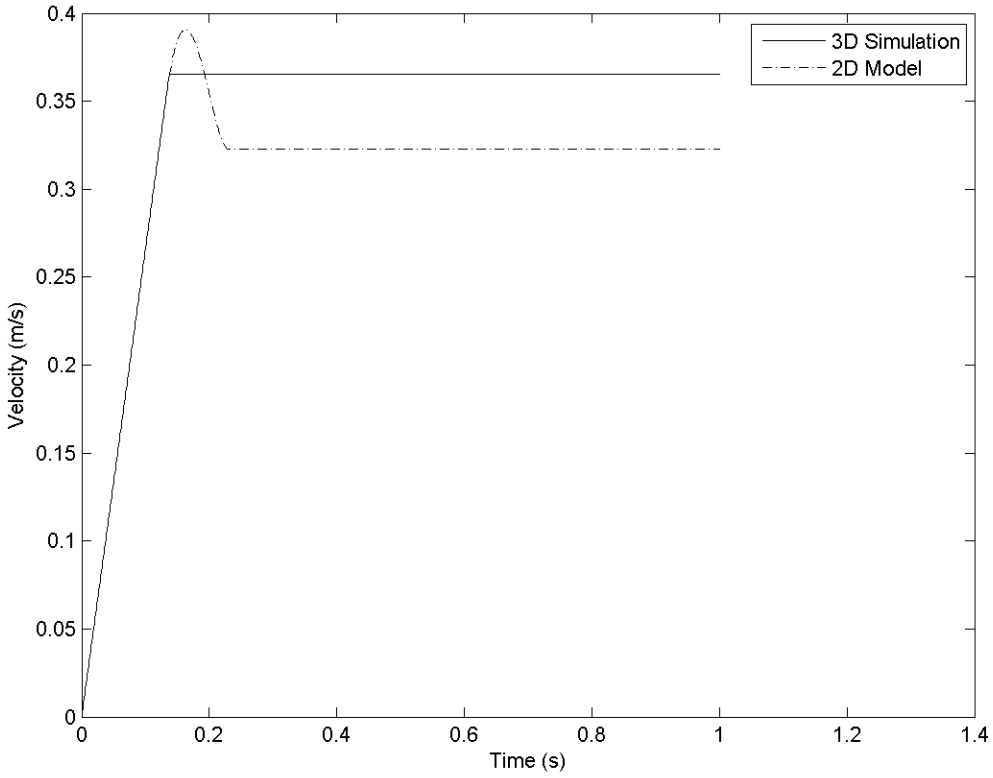

Figure 6.6: Ongoing Stage Velocity due to Uniform Pushers

6.2.5 Pneumatic Pushers with Lateral Force Gradient

In order to model a gradient in the pneumatic pusher force across the Y axis of the spent stage, the uniform force pusher case was modified. Comparisons of the 2D and 3D results are given in Figures 6.7 through 6.10. The motion of the spent stage is shown in Figures 6.7 and 6.8, whereas the motion of the ongoing stage is shown in Figures 6.9 and 6.10. Figures 6.8 and 6.10 depict the growth in stage angles θ_{s_1} and θ_{s_2} for both stages resulting from the unequal pusher forces. Figures 6.7 and 6.9 show that, in both simulations, even though the stages are rotating about their z axes, the rectilinear motion is largely confined to longitudinal separation, with very little lateral motion. There is a residual velocity discrepancy in both stages.

Numerical accuracy aside, there is an important difference between the 3D simulation and the 2D model based on the analytical result, and that is the nature of modeling pusher contact. For 3D simulation, each pusher and its location is modeled individually and in detail. The pushers lose contact one at a time as an uneven separation takes place. The 2D model simply declares that all pushers to be in contact when the stages are closer than the pusher length, or all pushers to be out of contact (no force) when they are separated further. Early during separation in the uneven case, and always in the uniform case, all pushers are in contact and one would expect the results of 3D simulation and the 2D model to compare well. In the time region where contact is gradually being lost, one would expect to see the greatest difference in behavior in final imparted velocities.

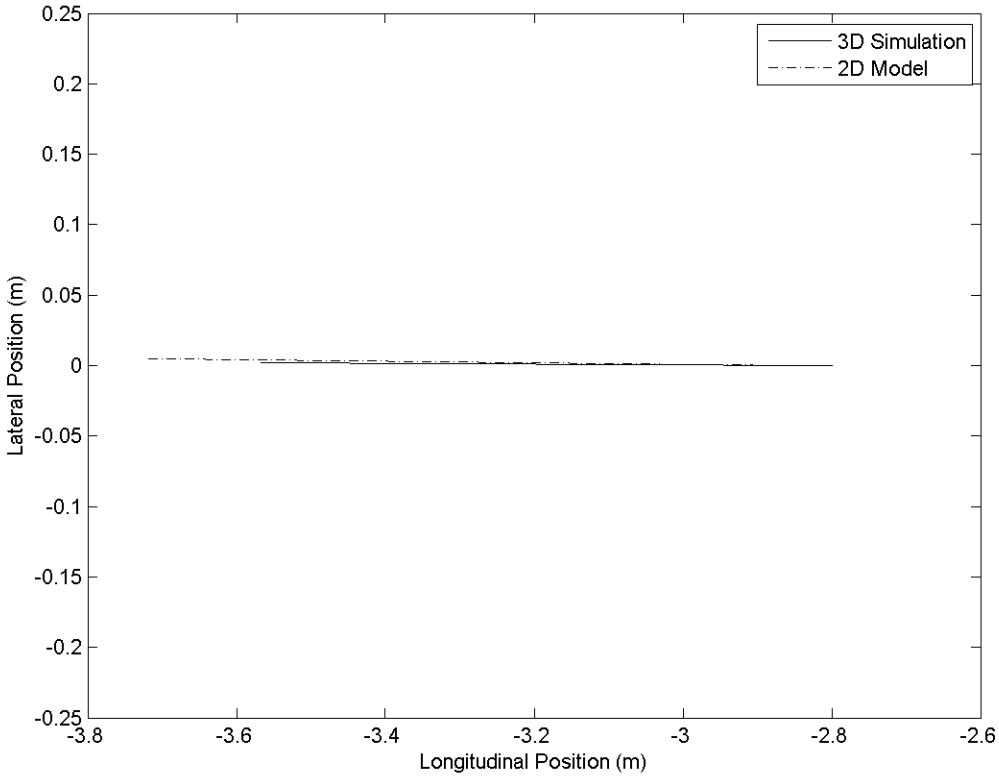

Figure 6.7: Spent Stage Motion due to Pushers with Gradient

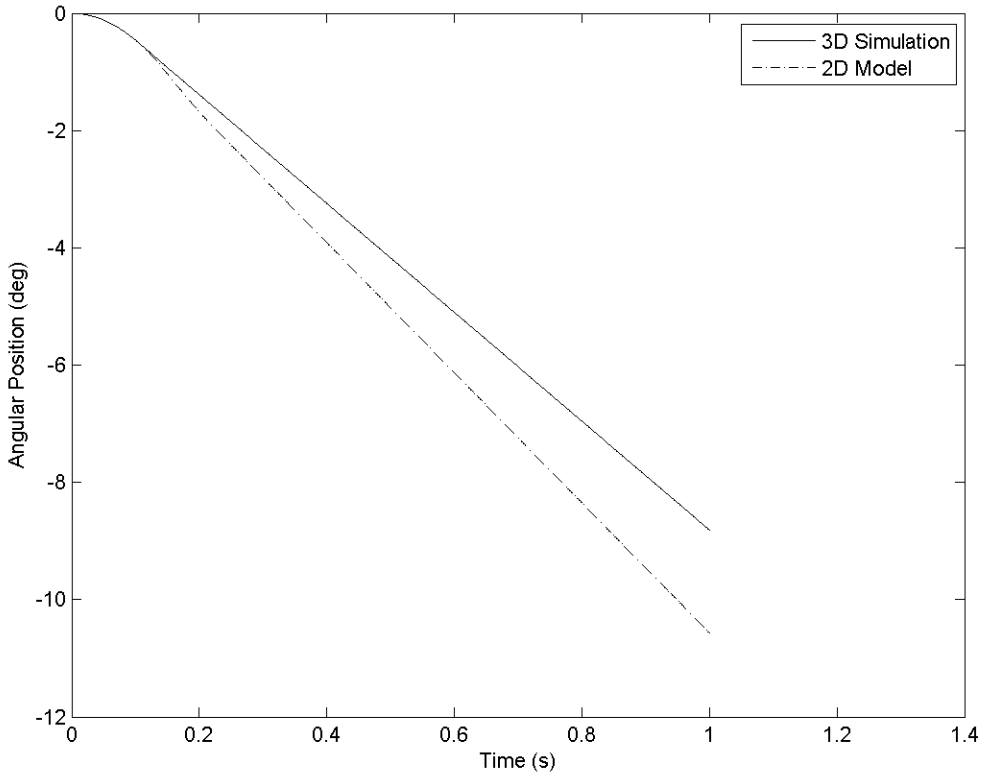

Figure 6.8: Spent Stage Angular Motion due to Pushers with Gradient

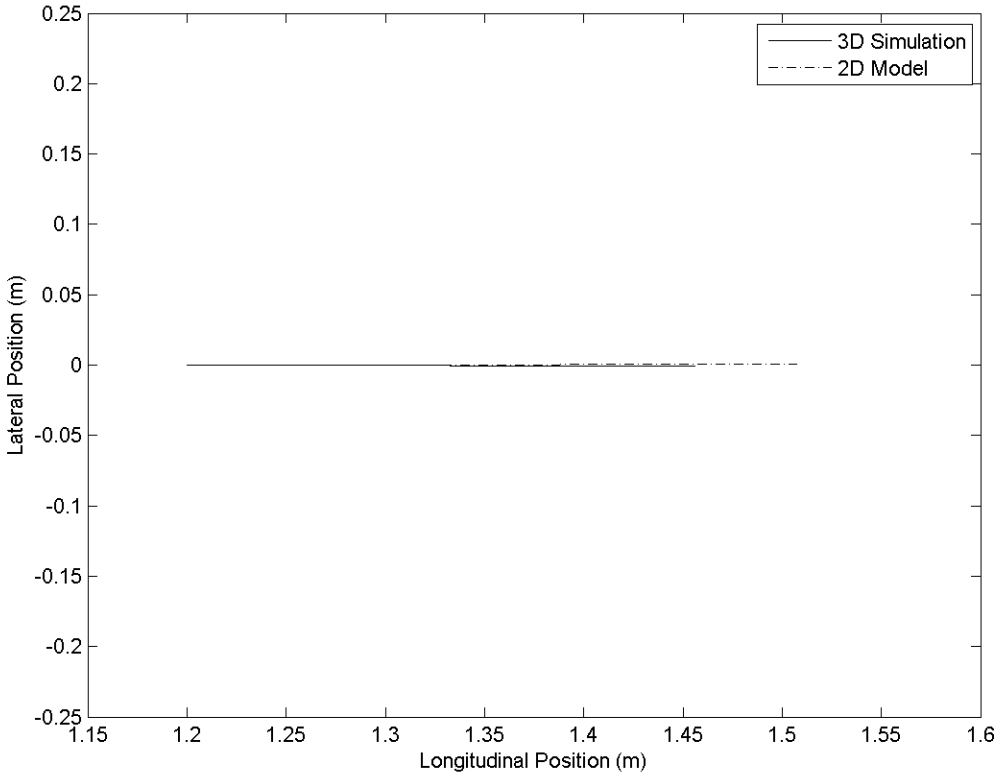

Figure 6.9: Ongoing Stage Motion due to Pushers with Gradient

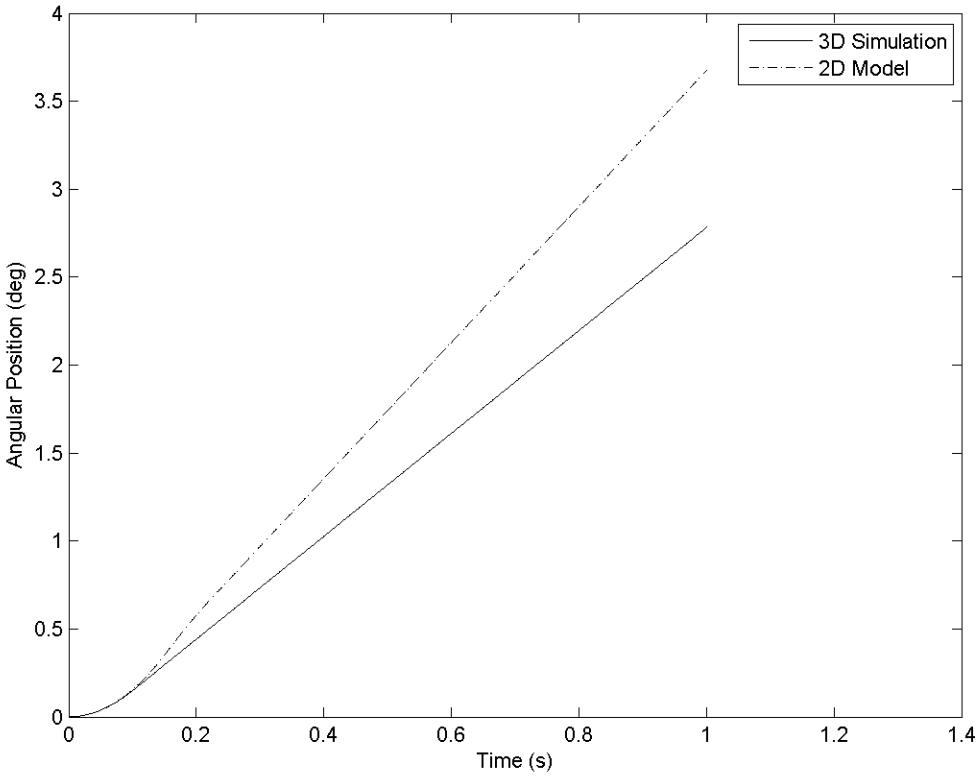

Figure 6.10: Ongoing Stage Angular Motion due to Pushers with Gradient

6.2.6 Main Engine Mass Offset

The case of main-engine mass offset is of interest, because a lateral displacement of the spent stage CM would result in stage rotation even with nominal separation devices. If that CM displacement is large enough, re-contact may occur. To shed some light on this behavior, the 2D simulation for the uniform separation motors case was modified to use the analytic result for main engine mass offset presented in Chapter IV, and the numbers were contrived to lead to a stage CM offset of 0.1 m. To accompany this model, a scenario for 3D simulation was developed with the CM offset by 0.1 m as well. Agreement between the two-dimensional results and the three-dimensional results was good for both rectilinear motion (shown in Figure 6.11) and angular motion (shown in Figure 6.12).

In order to achieve a CM offset of 0.1 m on the spent stage (2 m diameter, 1000 kg dry mass, about 4m tankage length) using engine offset only required an engine of 400 kg (dry mass fraction 0.40),

length l of engine CM from gimbal of 1m, and gimbal angle δ of 0.25 rad (14.3 degrees), all very large numbers, and ones not likely to be encountered in a real booster stage. The numbers have to be contrived to make engine mass offset dominate the dynamics.

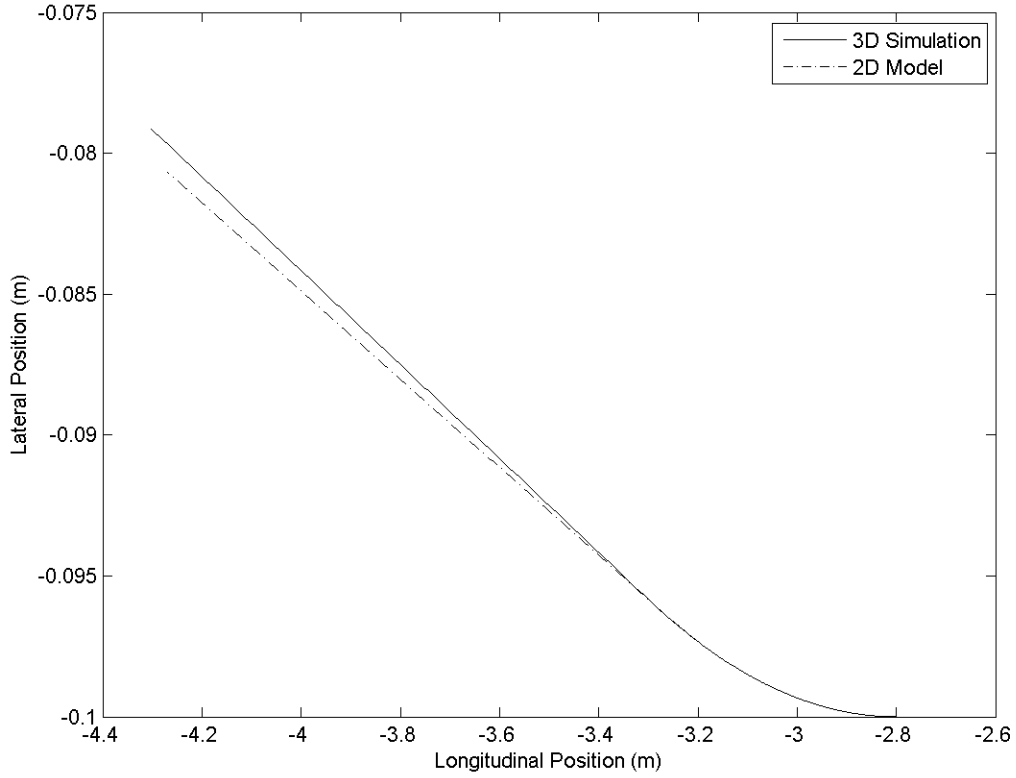

Figure 6.11: Spent Stage Motion due to Engine Mass Offset

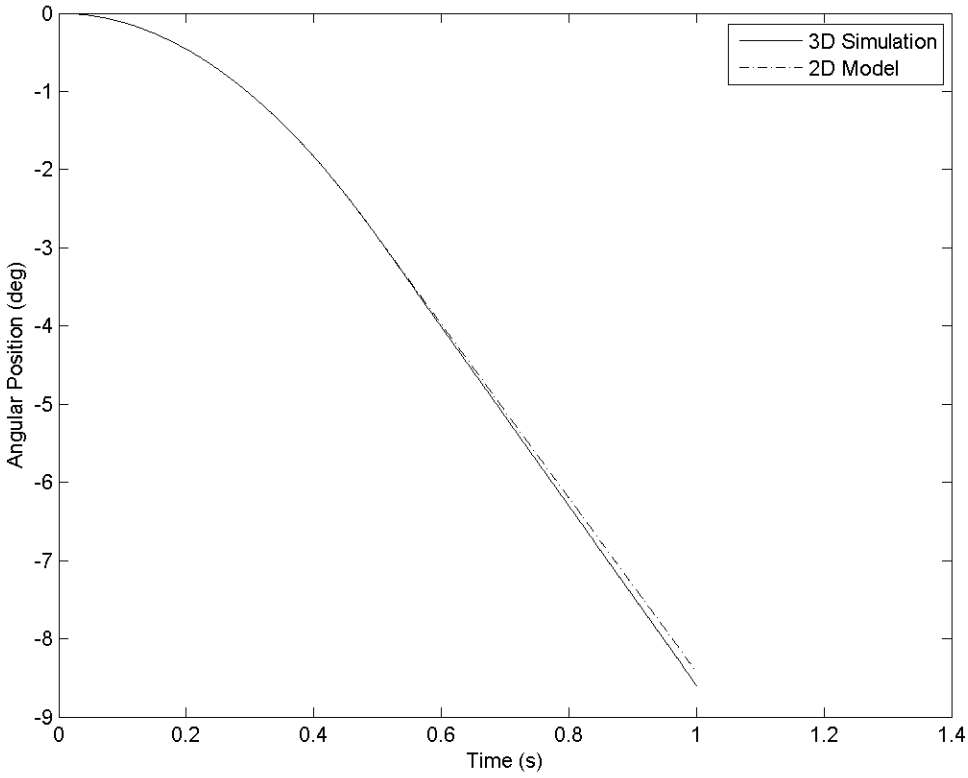

Figure 6.12: Spent Stage Angular Motion due to Engine Mass Offset

CHAPTER VII

CONCLUSIONS

Full three-dimensional equations of motion for separation analysis of launch-vehicle stages were developed. Simplified analytical models for separation with main engine thrust transient, uniform and non-uniform separation motors, uniform and non-uniform pneumatic pushers, and main engine mass offset were derived and presented. These analytical models were implemented as simple simulations and compared with results from a fully three-dimensional simulation implementing the full equations of motion.

In all cases, the comparisons between the analytical model and the 3D simulation were fairly good. When an engine thrust transient is modeled as an impulse and then simulated, numerical issues can enter into the results, resulting in an impulse model that underestimates the final velocity. Agreement was excellent for both the separation-motors model and the mass offset model. Also, modeling pushers simply with a 2D force/moment model can lead to inaccuracy in the region where individual pushers are losing contact one at a time, because such a model does not consider contact at the individual pusher level, but globally.

The full three-dimensional model for pusher contact, and the analytic expressions for pusher force and moment in the case where the pusher has a gradient in the lateral direction, are believed to constitute a new and unique contribution to separation and re-contact analysis.

CHAPTER VIII

FUTURE RESEARCH

Possible directions for future research along the lines of this thesis include the study of behavior immediately after re-contact, the examination of first stage and parallel booster separation at much lower altitudes, and a look at separation of nose fairings. This thesis did not explore what happens after two stages contact. During a re-contact, momentum is exchanged, some losses probably occur due to friction, slosh may be induced in the propellants of the ongoing stage, and the control system of the ongoing stage will have to recover. For separations in the lower atmosphere, aerodynamics, which was ignored here, would play an important role. It would be necessary to model the aerodynamic forces and moments on each stage while in close proximity and at odd orientations to the other. The separation of nose fairings for payload involves a different set of re-contact conditions not explored in this thesis. While the same equations of motion apply, the separation devices and directions of force are different, since most payload shrouds split longitudinally and fall away to the sides, and the "spent" device is ahead of the ongoing stage. Separation of parallel-burning boosters from a central core stage also represents a different set of re-contact conditions than those examined in this thesis.

APPENDICES

APPENDIX A

REPRESENTATION OF ATTITUDE

Describing the orientation of a body in 3-space, and, more generally, describing the relationship between two coordinate systems, is necessary for attitude dynamics. There are many ways to mathematically describe attitude [1, 10, 11, 12], but only 3 are common for practical implementations: Euler angles, Direction Cosine Matrices (DCMs), and quaternions.

A.1 Euler Angles

Euler angles are an ordered set of 3 angles defining the angular relationship between two arbitrary coordinate frames. The relationship is described by 3 rotations, each rotation in turn by a specified angle about a coordinate axis.

Each angle describes a rotation about one coordinate axis. Consecutive rotations must be about different axes. Since any one of $\{X, Y, Z\}$ can be selected for the first axis of rotation, only the other two axes are available for the second axis of rotation. For the third axis, all but the second axis are available, for a total of $3 \times 2 \times 2 = 12$ possible Euler angle schemes. Appendix C of Regan [1] enumerates all of these and gives the full, expanded set of rotation matrices for each.

For example, the rotation matrices for a 3-2-3 transformation (that is, first rotation about Z, second about Y, and last about the new Z) are

$$C_3(\theta_1)C_2(\theta_2)C_3(\theta_3) = \begin{bmatrix} \cos\theta_1 & \sin\theta_1 & 0 \\ -\sin\theta_1 & \cos\theta_1 & 0 \\ 0 & 0 & 1 \end{bmatrix} \begin{bmatrix} \cos\theta_2 & 0 & -\sin\theta_2 \\ 0 & 1 & 0 \\ \sin\theta_2 & 0 & \cos\theta_2 \end{bmatrix} \begin{bmatrix} \cos\theta_3 & \sin\theta_3 & 0 \\ -\sin\theta_3 & \cos\theta_3 & 0 \\ 0 & 0 & 1 \end{bmatrix}. \quad \text{(A.1)}$$

This is the transformation matrix between the $\{X, Y, Z\}$ frame and the frame resulting from the three rotations. Euler angles are intuitive and easy to visualize. They do not require any normalization, although they do often require bounding to the ranges $[0,2\pi)$ or $[-\pi, \pi)$, which requires modulo operations.

But integrating Euler angles results in transcendental equations. The kinematic equations also contain trigonometric terms:

$$\begin{bmatrix} \dot{\theta}_1 \\ \dot{\theta}_2 \\ \dot{\theta}_3 \end{bmatrix} = \begin{bmatrix} \frac{\cos\theta_1 \cos\theta_2}{\sin\theta_2} & \frac{-\sin\theta_1 \cos\theta_2}{\sin\theta_2} & 1 \\ \sin\theta_1 & \cos\theta_1 & 0 \\ \frac{-\cos\theta_1}{\sin\theta_2} & \frac{\sin\theta_1}{\sin\theta_2} & 0 \end{bmatrix} \begin{bmatrix} \omega_1 \\ \omega_2 \\ \omega_3 \end{bmatrix}, \tag{A.2}$$

where $(\omega_1, \omega_2, \omega_3)$ are the angular velocities about the rotating body axes. These are computationally expensive to integrate. Figure A.1 shows an example of a set of Euler angles, in this case, the sequence 1-2-3 (that is, first rotation about the original X axis, second rotation about the Y axis, and the last rotation about the Z axis).

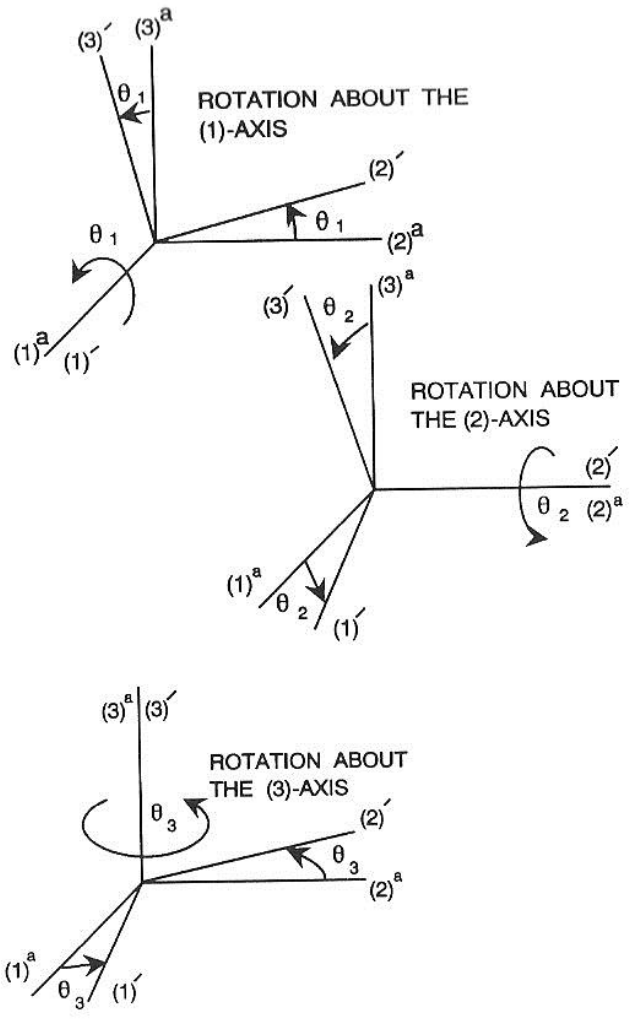

Figure A.1: Euler Angles (used by permission)

A.2 Direction Cosine Matrices

A DCM is a 3×3 matrix describing a complete rotation from one coordinate system to another. Each element of the matrix is a direction cosine, as seen in Figure A.2. The first (second, third) column is the "FROM" X (Y, Z) axis expressed in the "TO" coordinate system. The first (second, third) row is the "TO" X (Y, Z) axis expressed in the "FROM" coordinate system. Premultiplying a vector expressed in one frame by a DCM transforms that vector to another coordinate system.

DCMs have several mathematical properties that make them a quite advantageous representation of attitude. First, DCMs are orthogonal. Each row is a vector perpendicular to the other two rows. If row one is considered the $\vec{x}$ vector, the second row $\vec{y}$, and the last $\vec{z}$, then the familiar relations between coordinate axes hold: $\vec{x} \times \vec{y} = \vec{z}; \vec{y} \times \vec{z} = \vec{x}; \vec{z} \times \vec{x} = \vec{y}$. DCMs are also normal: each row is a vector of unit length. Since DCMs are both orthogonal and normal, they are also orthonormal. An important property of orthonormal matrices is that the inverse is equal to the transpose, making inversion trivial. That also means the columns share the same vector properties as the rows: that is, they are unit vectors orthogonal to each other.

The concatenation of 3 rotation matrices based on Euler angle sequences will produce a DCM.

DCMs are also intuitive and easy to visualize. Each row is the unit vector specifying a coordinate axis of the "from" system in the "to" system's coordinates. Because DCMs are orthonormal, and their inverse is simply their transpose, each column is the unit vector specifying a coordinate axis of the "to" system in the "from" system's coordinates.

A DCM is easy to construct from just two non-parallel vectors. This pair of vectors, when crossed, produces a third vector. Crossing one of the original two with this out-of-plane vector produces a third vector perpendicular to both, forming a complete orthogonal right-handed system.

For any arbitrary rotation, there is a unique DCM corresponding to it.

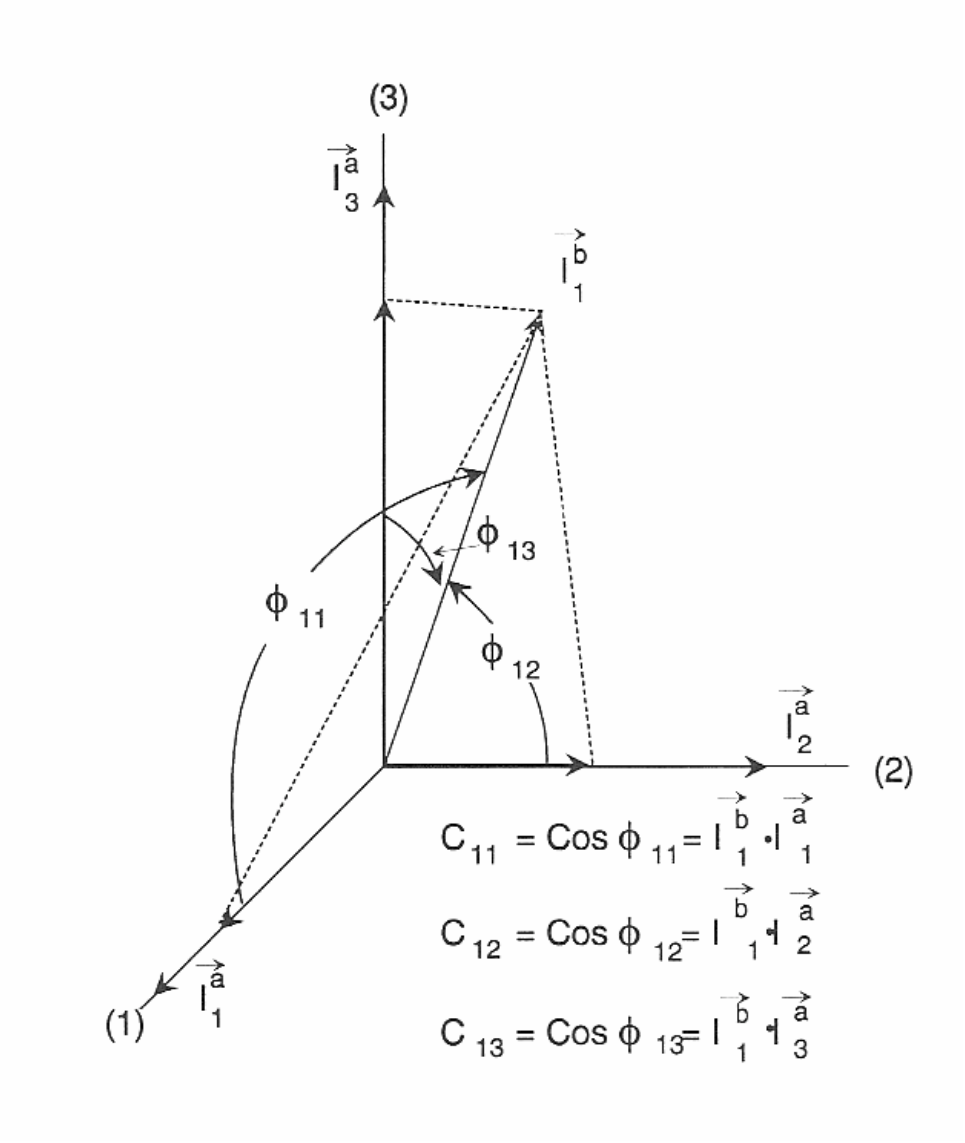

Figure A.2: Direction Cosines (used by permission)

DCMs do have some disadvantages, however. They are hard to keep orthonormal as state is advanced, that is, as the angular kinematic equations, relating angular velocity to angular position, are integrated, the rows and columns gradually become non-perpendicular: $\vec{x} \cdot \vec{y} \neq 0$, for example. As integration progresses, if no special measures are taken, the rows and columns also become non-normalized, that is, they become non-unit in length: for instance, $\|\vec{x}\| \neq 1$. To prevent this, regular normalization and orthogonalization of the DCM is required. Every few dozen integration steps (the actual number required varies with floating point precision used, step size, and other factors), time has to be taken to refresh the matrix, to restore the DCM to completely orthonormal. This step requires 3 matrix multiplies and a matrix subtraction, plus scaling.

Unlike the Euler equation, the DCM kinematic equations are linear but numerous. The computer must integrate 9 ODEs to advance state, but only 6 are independent. That is, one could integrate just 6 of the equations and find the other 3 quantities from simple algebraic relations among the 9.

$$\begin{array}{lll} \dot{C}_{11} = C_{12}\omega_3 - C_{13}\omega_2 & \dot{C}_{12} = C_{13}\omega_1 - C_{11}\omega_3 & \dot{C}_{13} = C_{11}\omega_2 - C_{12}\omega_1 \\ \dot{C}_{21} = C_{22}\omega_3 - C_{23}\omega_2 & \dot{C}_{22} = C_{23}\omega_1 - C_{21}\omega_3 & \dot{C}_{23} = C_{21}\omega_2 - C_{22}\omega_1 \\ \dot{C}_{31} = C_{32}\omega_3 - C_{33}\omega_2 & \dot{C}_{32} = C_{33}\omega_1 - C_{31}\omega_3 & \dot{C}_{33} = C_{31}\omega_2 - C_{32}\omega_1 \,, \end{array} \tag{A.3}$$

where $(\omega_1, \omega_2, \omega_3)$ are the angular velocities about the rotating body axes. This is a large number of members. All operations with this set are expensive. The above kinematic equations, if advantage is not taken of the redundancy inherent among them, require 18 floating point multiplies and 9 adds, and 9 ODEs have to be integrated. Even taking account of the dependencies among the equations, a minimum of 6 ODEs must be integrated.

A.3 Quaternions

Quaternions were developed by Hamilton around 1845, and so actually precede the development of vector algebra. They are an ordered set of 4 numbers (q_1, q_2, q_3, q_4) describing a rotation. The triplet (q_1, q_2, q_3) is a vector portion, and q_4 is a scalar. In many computer implementations, especially in the C programming language, the quaternion is represented as (q_0, q_1, q_2, q_3), where q_0 is the scalar portion.

If (x, y, z) is a vector along the axis of rotation, and φ is the twist (angle of rotation) about that axis, then

$$\begin{aligned} q_1 &= x \sin\frac{\varphi}{2} \\ q_2 &= y \sin\frac{\varphi}{2} \\ q_3 &= z \sin\frac{\varphi}{2} \\ q_4 &= \cos\frac{\varphi}{2}\,. \end{aligned} \tag{A.4}$$

Quaternions in practice are usually normalized to a unit length. Also, it is often required for mathematical convenience to keep the real portion (q_4 in this case) positive.

They are not intuitive. It is difficult to just look at a quaternion and tell what rotation it is describing. A novice's frequent first attempt at understanding is useful but wrong: a 3D vector plus a "twist" angle about that vector. Although (x, y, z, φ) certainly uniquely describes a rotation, it does not share the mathematical properties that make quaternions useful.

They cannot be visualized readily. Even attitude dynamics experts, who work with quaternions every day and prefer them mathematically, result to transformation to DCMs and Euler angles to understand where the quaternion is pointing.

Quaternions can be hard to interpolate. Keeping the real part q_4 positive results in "reflections" during rotations at what would have been real-part zero crossings. Instead of a zero crossing, there is an undifferentiable point where q_4 hits zero and immediately returns positive, with the negative of the slope (v. time) it had prior to zero crossing. These points require special handling in software.

Kinematic equations are just 4 linear ODEs.

$$\begin{aligned} \dot{q}_1 &= \frac{1}{2}\left(\omega_1 q_4 - \omega_2 q_3 + \omega_3 q_2\right) \\ \dot{q}_2 &= \frac{1}{2}\left(\omega_1 q_3 + \omega_2 q_4 - \omega_3 q_1\right) \\ \dot{q}_3 &= \frac{1}{2}\left(-\omega_1 q_2 + \omega_2 q_1 + \omega_3 q_4\right) \\ \dot{q}_4 &= \frac{1}{2}\left(-\omega_1 q_1 - \omega_2 q_2 - \omega_3 q_3\right). \end{aligned} \tag{A.5}$$

The above equations require 16 multiplies, 8 adds, and the integration of 4 ODEs.

Normalization of quaternions is easy:

$$\boldsymbol{q}_{Norm} = \frac{\boldsymbol{q}}{\|\boldsymbol{q}\|}. \tag{A.7}$$

This requires 8 multiplies, 3 adds, a square root, and a reciprocal. In practice, quaternions also require normalization less often than DCMs. Quaternions are, by definition, orthogonal, and therefore orthogonalization is not needed, just normalization.

A.4 Selecting an Appropriate Representation for Simulation

The main attitude representation for the simulation is the quaternion form. Quaternions have fewer elements than DCMs, requiring only 4 linear ODEs to be integrated. Orthogonalization is unnecessary, and normalization is easier and less frequent.

Euler angles will still be necessary as an input and output format so that the simulation can present data in a form that can be readily interpreted. DCMs are helpful for transforming between quaternions and Euler angles. DCMs are also convenient for depicting the vector triads of coordinate axes, since each column is a unit vector in the direction of a coordinate axis. Though they may not form part of the core integrations in this thesis, both Euler angles and DCMs will be necessary and prevalent throughout the simulation.

APPENDIX B

ASSESSMENT OF NEGLIGIBLE FORCES

Chapter III describes why thrust and the force applied by separation mechanisms cannot be neglected in the separation problem. This appendix shows with several examples why the aerodynamic and gravity forces can be ignored for the separation problems of interest to this thesis, namely, those of relative motion at very high altitude.

B.1 Aerodynamic Forces

At the altitude being considered for this analysis, aerodynamic forces are not significant enough to have a large effect during the maximum 10-second span, though for a longer time frame there certainly would be an effect, but the trends in separation by then are well established. For example, for a booster of 3 m diameter at the upper edge of the tenable atmosphere, about 100 km altitude, using an exponential atmosphere model, the density of air is

$$\rho = \rho_0 e^{-\frac{h}{H}}, \tag{B.1}$$

where $\rho_0 \equiv sea\ level\ atmosphere\ density = 1.752 \frac{kg}{m^3}$, $H \equiv atmosphere\ scale\ height = 6.7km$,

$$\rho = 1.752 \frac{kg}{m^3} e^{-\frac{100km}{6.7km}} = 5.775 \times 10^{-7} \left(\frac{kg}{m^3}\right).$$

The drag (force) at orbital velocity, $v = 7{,}905\ m/s$ is estimated to be

$$D = \frac{1}{2} \rho C_D S v^2 \tag{B.2}$$

$$= \frac{1}{2} \times 5.775 \times 10^{-7} \left(\frac{kg}{m^3}\right) \times \pi \times 1.5^2 m^2 \times \left(7905 \frac{m}{s}\right)^2$$

$$= 128\ N\ .$$

This force is too small to have a significant effect on a 3 m stage in the 10-ton mass range over just 10 s.

An aerodynamic torque would be similarly negligible over brief periods. An analysis at lower altitude would have to consider aerodynamic forces to be complete. Most separations are at velocities well into the hypersonic region, and viscosity cannot be neglected if atmospheric density is sufficient to be in continuum. Staging is a particularly difficult problem, because it involves two bodies in close proximity so the flow around each stage depends on the flow around the other. Motion at hypersonic velocities within the tenable atmosphere is not considered in this thesis.

B.2 Gravity

Gravity is certainly significant at 100 km, often considered the edge of the "tenable atmosphere," being almost 97% of its value at Earth's surface. Since the force of gravity F_{grav} at a distance r from the center of the earth is given in [8] as

$$F_{grav} = \frac{\mu}{r^2}, \tag{B.3}$$

then

$$\frac{F_{alt}}{F_{surf}} = \frac{\frac{\mu}{r_{alt}^2}}{\frac{\mu}{r_{surf}^2}} \tag{B.4}$$

$$= \frac{r_{surf}^2}{r_{alt}^2}$$

$$= \left(\frac{6378\ km}{6378\ km + 100\ km}\right)^2$$

$$\approx 0.97\ .$$

But gravity affects the vehicle as a whole and the two stages mostly equally. Since this is a separation problem, only relative motion is of interest. Gravity is not a major contributor to the relative motion on this short time scale (less than 10 s).

Even should the mass centers of the stages be as much as 100 m apart and the dimensions of the stages be very large (so that re-contact is still a concern at that distance), the difference in gravity acting on the two stages is exceedingly small.

$$dh = r_2 - r_1 \tag{B.5}$$

$$\left(\frac{\mu}{r_1^2} - \frac{\mu}{r_2^2}\right) = \frac{\mu(r_2^2 - r_1^2)}{(r_1 r_2)^2} = \frac{\mu\left(((r_1 + dh)^2 - r_1^2)\right)}{\left(r_1 (r_1 + dh)\right)^2}. \tag{B.6}$$

Assume $dh << r_1$ so that

$$\approx \mu \frac{2 r_1 dh + dh^2}{r_1^4}$$

$$= \mu 2 \frac{r_1 dh}{r_1^4}$$

$$= \mu \frac{2dh}{r_1^3}$$

$$= 3.986 \times 10^5 \left(\frac{\text{km}^3}{\text{s}^2}\right) \times 2 \times \frac{0.1 \text{ km}}{(6378 \text{ km} + 100 \text{ km})^3}$$

$$= 0.00029 \frac{\text{m}}{\text{s}^2}.$$

This is less than 0.01% of gravitational force and cannot lead to any significant relative displacement over 10 s.

Gravity torques could be measureable on time scales of 100 s and significant on scales of orbital period (an hour and beyond) but is insignificant over 10 s. Even with a very prolate (rod-like) body such as a booster stage, where the moment of inertia about the longitudinal (roll) axis can be more than an order of magnitude smaller than those of the yaw and pitch moments of inertia, the time scale of significant motion is well beyond the period of interest. Following [1], the moment about the pitch axis (Z-axis) is

$$M_z = 3\frac{\mu(a_{13}a_{23})}{R_0^3}\left(I_{yy} - I_{xx}\right). \tag{B.7}$$

The above is Equation F.8 of [1]. Assume that the nose is up by a 45° angle; that is, assume the flight path angle $\gamma = -45°$. That means $a_{13} = a_{23} = 0.707$. Assume an average density half that of water for a prolate stage 12m long and 3m diameter

$$m = \pi r^2 l \rho \tag{B.8}$$

$$= \pi\,(1.5\text{ m})^2 12\text{ m}\left(500\frac{\text{kg}}{\text{m}^3}\right)$$

$$= 42412\text{ kg.}$$

$$I_{xx} = \frac{1}{2} \times m \times r^2 \tag{B.9}$$

$$= \frac{1}{2} * 42412\text{ kg} * (1.5\text{ m})^2$$

$$= 47714\text{ kg m}^2$$

$$I_{yy} = \frac{1}{12} m \times (3r^2 + ell^2) \tag{B.10}$$

$$= \frac{1}{12}(42412\text{ kg})(3 \times (1.5\text{ m})^2 + 12\text{ m}^2)$$

$$= 532800\text{ kg m}^2\text{ .}$$

Note that $I_{yy} \gg I_{xx}$.

$$M_z = \left(\frac{3 \times 3.986\text{E14 (kg}^3)(\text{s}^{-2}) \times 0.717 \times 0.717}{(6478145\text{m})^3}\right)(532800\text{ kg m}^2 - 47714\text{ kg m}^2)$$

$$= 1.067\text{ Nm .}$$

Hence the torque is trivial for such a heavy stage, too slight to generate much velocity within 10 s.

In summary, it is shown above that gravity's contribution to relative motion, whether to induce translation or rotation, is very small over these dimensions and small time scope and can be safely neglected for the separation problem.

APPENDIX C

AN ALTERNATIVE METHOD FOR PUSHER CONTACT POINT

College calculus books, such as Purcell [19], show how to find the intersection of a line and a plane in three dimensions if the plane is a coordinate plane. The methods used therein form the basis of the approach described below for finding the location on the ongoing stage that the pneumatic pushers are pushing against.

It is necessary to transform the position of the pusher end on the spent stage, the "u" end, and the direction of the pusher to a frame parallel to the ongoing stage station coordinates with the origin in the base plane. That way one can just find the piercing points in the YZ plane (that is, the ongoing stage base plane where the pusher patches reside).

First the origin of the spent stage station coordinates must be described relative to a known reference:

$$\vec{r}_{s_1}^{\,b_1} = -\vec{r}_{cm_1}^{\,s_1} \tag{C.1}$$

$$\vec{r}_{s_1}^{\,f} = \vec{r}_{cm_1}^{\,f} + \boldsymbol{C}_{b_1}^{f}\vec{r}_{s_1}^{\,b_1} = \vec{r}_{cm_1}^{\,f} - \boldsymbol{C}_{b_1}^{f}\vec{r}_{cm_1}^{\,s_1} \tag{C.2}$$

$$\vec{r}_{s_1}^{\,f} = \vec{r}_{cm_1}^{\,f} - \boldsymbol{C}_{p_1}^{f}\boldsymbol{C}_{b_1}^{p_1}\vec{r}_{cm_1}^{\,s_1}\,. \tag{C.3}$$

And likewise for the ongoing stage:

$$\vec{r}_{s_2}^{\,f} = \vec{r}_{cm_2}^{\,f} - \boldsymbol{C}_{p_2}^{f}\boldsymbol{C}_{b_2}^{p_2}\vec{r}_{cm_2}^{\,s_2}\,. \tag{C.4}$$

Transform position of the pusher u end to ongoing stage station coordinates:

$$\vec{r}_{u_j}^{\,f} = \vec{r}_{s_1}^{\,f} + \boldsymbol{C}_{b_1}^{f}\vec{r}_{u_j}^{\,s_1} \tag{C.5}$$

$$= \vec{r}_{cm_1}^{\,f} - \boldsymbol{C}_{p_1}^{f}\boldsymbol{C}_{b_1}^{p_1}\vec{r}_{cm_1}^{\,s_1} + \boldsymbol{C}_{p_1}^{f}\boldsymbol{C}_{b_1}^{p_1}\vec{r}_{u_j}^{\,s_1}$$

$$= \vec{r}_{cm_1}^{\,f} + \boldsymbol{C}_{p_1}^{f}\boldsymbol{C}_{b_1}^{p_1}(\vec{r}_{u_j}^{\,s_1} - \vec{r}_{cm_1}^{\,s_1})$$

$$\vec{\mathrm{r}}_{u_j}^{s_2} = \boldsymbol{C}_f^{b_2}\left(\vec{\mathrm{r}}_{u_j}^{f} - \vec{\mathrm{r}}_{s_1}^{f}\right) = \boldsymbol{C}_{p_2}^{b_2}\boldsymbol{C}_f^{p_2}\left(\vec{\mathrm{r}}_{u_j}^{f} - \vec{\mathrm{r}}_{s_1}^{f}\right) \tag{C.6}$$

$$= \boldsymbol{C}_{p_2}^{b_2}\boldsymbol{C}_f^{p_2}\left(\left(\vec{\mathrm{r}}_{cm_1}^{f} + \boldsymbol{C}_{p_1}^{f}\boldsymbol{C}_{b_1}^{p_1}\left(\vec{\mathrm{r}}_{u_j}^{s_1} - \vec{\mathrm{r}}_{cm_1}^{s_1}\right)\right) - \left(\vec{\mathrm{r}}_{cm_1}^{f} - \boldsymbol{C}_{p_1}^{f}\boldsymbol{C}_{b_1}^{p_1}\vec{\mathrm{r}}_{cm_1}^{s_1}\right)\right)$$

$$= \boldsymbol{C}_{p_2}^{b_2}\boldsymbol{C}_f^{p_2}\left(\boldsymbol{C}_{p_1}^{f}\boldsymbol{C}_{b_1}^{p_1}\left(\vec{\mathrm{r}}_{u_j}^{s_1} - \vec{\mathrm{r}}_{cm_1}^{s_1}\right) + \boldsymbol{C}_{p_1}^{f}\boldsymbol{C}_{b_1}^{p_1}\vec{\mathrm{r}}_{cm_1}^{s_1}\right)$$

$$\vec{\mathrm{r}}_{u_j}^{s_2} = \boldsymbol{C}_{p_2}^{b_2}\boldsymbol{C}_f^{p_2}\boldsymbol{C}_{p_1}^{f}\boldsymbol{C}_{b_1}^{p_1}\vec{\mathrm{r}}_{u_j}^{s_1}. \tag{C.7}$$

Now get that position in the base plane relative to the center of this pusher's patch.

$$\vec{\mathrm{r}}_{w_j}^{s_2} \equiv position\ of\ j^{th} pusher\ patch\ center\ of\ ongoing\ stage\ in\ station\ coordinates$$

The w_j coordinate system is parallel to the ongoing stage station coordinates with origin at the j^{th} pusher's patch.

$$\vec{\mathrm{r}}_{u_j}^{w_j} = \vec{\mathrm{r}}_{u_j}^{s_2} - \vec{\mathrm{r}}_{w_j}^{s_2}. \tag{C.8}$$

Transform the direction of the pusher's pointing vector to ongoing stage station coordinates:

$$\vec{\mathrm{d}}_j^{s_1} = \vec{\mathrm{i}}_1^{s_1} = \begin{bmatrix}1\\0\\0\end{bmatrix} \tag{C.9}$$

$$\vec{\mathrm{d}}_j^{f} = \boldsymbol{C}_{s_1}^{f}\begin{bmatrix}1\\0\\0\end{bmatrix} = \boldsymbol{C}_{b_1}^{f}\begin{bmatrix}1\\0\\0\end{bmatrix} \tag{C.10}$$

$$\vec{\mathrm{d}}_j^{s_2} = \boldsymbol{C}_f^{s_2}\vec{\mathrm{d}}_j^{f} = \boldsymbol{C}_f^{b_2}\vec{\mathrm{d}}_j^{f} = \boldsymbol{C}_f^{b_2}\boldsymbol{C}_{b_1}^{f}\begin{bmatrix}1\\0\\0\end{bmatrix}. \tag{C.11}$$

In terms of D.C.M.s that are readily available,

$$\vec{\mathrm{d}}_j^{s_2} = \boldsymbol{C}_{p_2}^{b_2}\boldsymbol{C}_f^{p_2}\boldsymbol{C}_{p_1}^{f}\boldsymbol{C}_{b_1}^{p_1}\begin{bmatrix}1\\0\\0\end{bmatrix}. \tag{C.12}$$

Now we test for the intersection of a line and a plane. The line is simply that corresponding to the base and pointing vector of the pusher. The plane is that of the $(Y^{w_j}Z^{w_j})$ base plane, in this case centered at the pusher patch, the origin of the w_j system. The test is simpler since the plane is a coordinate plane.

The point-plus-vector of the pusher must be expressed as an equation of the line. In Purcell, the symmetric equations of the line passing through point (x_1, y_1, z_1) parallel to the vector $\boldsymbol{a} = [a_1, a_2, a_3]$ is

$$\frac{x - x_1}{a_1} = \frac{y - y_1}{a_2} = \frac{z - z_1}{a_3}, \tag{C.13}$$

so that

$$y = \frac{a_2}{a_1}(x - x_1) + y_1$$
$$z = \frac{a_3}{a_1}(x - x_1) + z_1 \,. \tag{C.14}$$

Since in the $(Y^{w_j}Z^{w_j})$ base plane $x = 0$,

$$y = -\frac{a_2}{a_1}x_1 + y_1$$
$$z = -\frac{a_3}{a_1}x_1 + z_1 \,. \tag{C.15}$$

This approach has problems with the general case, where vector $\boldsymbol{a}$ could be nearly parallel to a coordinate plane. In such an event, the denominators of the symmetric equations can become very small. It is important to use the above equations only when one is sure that a substantial X component exists, so that a_1 going to zero does not cause problems. Since in our particular case, the stages are nearly aligned at the beginning of separation and hopefully don't grow to more than a few degrees of misalignment during separation, the assumption of a sufficient X component is realistic.

The result of the above computation is the point of contact of the pusher in the ongoing stage's base plane.

$$\vec{\mathrm{r}}_{v_j}^{\,w_j} = \begin{bmatrix} 0 \\ y \\ z \end{bmatrix}. \tag{C.16}$$

The vector from the pusher base (the u end) to this point is

$$\vec{\mathrm{r}}_{uv_j}^{\,w_j} = \vec{\mathrm{r}}_{v_j}^{\,w_j} - \vec{\mathrm{r}}_{u_j}^{\,w_j} \,. \tag{C.17}$$

If the magnitude of the vector exceeds the pusher maximum extent L_{pusher}, the pusher does not reach the ongoing stage.

$$m_j = \begin{cases} 0, & \left\| \vec{\mathrm{r}}_{uv_j}^{\,w_j} \right\| > L_{pusher} \\ 1, & \left\| \vec{\mathrm{r}}_{uv_j}^{\,w_j} \right\| \le L_{pusher} \,. \end{cases} \tag{C.18}$$

The position vector from the center of the contact patch on the ongoing stage to the v intercept point in the base plane is

$$\vec{\mathrm{r}}_{wv_j}^{\,w_j} = \vec{\mathrm{r}}_{v_j}^{\,w_j} - \vec{\mathrm{r}}_{w_j}^{\,w_j} = \begin{bmatrix} 0 \\ y \\ z \end{bmatrix} - \begin{bmatrix} 0 \\ 0 \\ 0 \end{bmatrix} = \begin{bmatrix} 0 \\ y \\ z \end{bmatrix}. \tag{C.19}$$

If the magnitude of the vector exceeds the radius of the contact patch r_{patch}, the pusher does not exert any force on the ongoing stage.

$$\left\|\vec{\mathrm{r}}_{wv_j}^{w_j}\right\| = \sqrt{y^2 + z^2} \leq r_{patch} \tag{C.20}$$

$$n_j = \begin{cases} 0, & \left\|\vec{\mathrm{r}}_{wv_j}^{w_j}\right\| > r_{patch} \\ 1, & \left\|\vec{\mathrm{r}}_{wv_j}^{w_j}\right\| \leq r_{patch} \end{cases}. \tag{C.21}$$

APPENDIX D

SUMS OF SINES AND COSINES

This section is an application of the techniques described in Section 9.2, pp. 388-391 of [15].

Recall the Euler's relation for complex numbers

$$cos\theta + j\, sin\,\theta = e^{j\theta}\,, \tag{D.1}$$

where j is the imaginary unit (square root of -1). From the above relation may be derived the complex definitions of sine and cosine:

$$\sin\theta = \frac{e^{j\theta} - e^{-j\theta}}{2j} \tag{D.2}$$

$$\cos\theta = \frac{e^{j\theta} + e^{-j\theta}}{2}. \tag{D.3}$$

A problem of interest is the total of the X and Y components of a quantity that is uniformly distributed about the circumference of a unit circle at discrete intervals:

$$S_X = \sum_{i=0}^{n-1} \cos\frac{2\pi i}{n} \tag{D.4}$$

$$S_Y = \sum_{i=0}^{n-1} \sin\frac{2\pi i}{n}. \tag{D.5}$$

Starting with the S_Y sum,

$$\sum_{i=0}^{n-1} \sin\frac{2\pi i}{n} = \sum_{i=0}^{n-1} \frac{e^{\frac{j2\pi i}{n}} - e^{-\frac{j2\pi i}{n}}}{2j} = \frac{1}{2j}\left\{\sum_{i=0}^{n-1} e^{\frac{j2\pi i}{n}} - \sum_{i=0}^{n-1} e^{-\frac{j2\pi i}{n}}\right\}. \tag{D.6}$$

The sum of a finite arithmetic series is

$$S_n = \sum_{i=0}^{n-1} a^i = \frac{1-a^n}{1-a}. \tag{D.7}$$

Equating a with $e^{\frac{j2\pi}{n}}$ in the first sum and with $e^{-\frac{j2\pi}{n}}$ in the second sum

$$\sum_{i=0}^{n-1} \sin\frac{2\pi i}{n} = \frac{1}{2j}\left\{\frac{1-e^{j2\pi}}{1-e^{\frac{j2\pi}{n}}} - \frac{1-e^{-j2\pi}}{1-e^{-\frac{j2\pi}{n}}}\right\}. \tag{D.8}$$

Observe that since $e^{j2\pi i} = 0$ in every integer i, the two numerators are always zero. However, a singularity exists in the above relation when either $1 - e^{\frac{j2\pi}{n}} = 0$ or $1 - e^{-\frac{j2\pi}{n}} = 0$. In either case, this is satisfied only when $n = 1$. In such cases, the finite sum equation will not work, and the sum has to be evaluated by hand. This is not as bad as it sounds, because the one case where the sum fails is the trivial case of one discrete quantity. That trivial case also evaluates to zero, so that

$$\sum_{i=0}^{n-1} \sin\frac{2\pi i}{n} = 0 \; for \; all \; n > 0\,. \tag{D.9}$$

Working similarly for the cosine summation,

$$\begin{aligned}\sum_{i=0}^{n-1} \cos\frac{2\pi i}{n} = \sum_{i=0}^{n-1} \frac{e^{\frac{j2\pi i}{n}} + e^{-\frac{j2\pi i}{n}}}{2} &= \frac{1}{2}\left\{\sum_{i=0}^{n-1} e^{\frac{j2\pi i}{n}} - \sum_{i=0}^{n-1} e^{-\frac{j2\pi i}{n}}\right\} \\ &= \frac{1}{2}\left\{\frac{1-e^{j2\pi}}{1-e^{\frac{j2\pi}{n}}} + \frac{1-e^{-j2\pi}}{1-e^{-\frac{j2\pi}{n}}}\right\}.\end{aligned} \tag{D.10}$$

Like the sine case, the numerators are both zero, and a singularity exists for the case of $n = 1$, so that for every $n > 1$, the sum is zero, and the $n = 1$ case has to be evaluated by hand, not using the series sum. This gives

$$\sum_{i=0}^{n-1} \cos\frac{2\pi i}{n} = \begin{cases}1, & n = 1 \\ 0, & n > 1\,.\end{cases} \tag{D.11}$$

Next, the case of twice the previous angle (i.e., $\frac{2\pi i}{n}$) is examined.

$$S_X = \sum_{i=0}^{n-1} \cos\frac{4\pi i}{n} \tag{D.12}$$

$$S_Y = \sum_{i=0}^{n-1} \sin\frac{4\pi i}{n} \tag{D.13}$$

Proceeding along similar principles, with this time $a = \frac{j4\pi}{n}$,

$$\sum_{i=0}^{n-1} \sin\frac{4\pi i}{n} = \sum_{i=0}^{n-1} \frac{e^{\frac{j4\pi i}{n}} - e^{-\frac{j4\pi i}{n}}}{2j} = \frac{1}{2j}\left\{\sum_{i=0}^{n-1} e^{\frac{j4\pi i}{n}} - \sum_{i=0}^{n-1} e^{-\frac{j4\pi i}{n}}\right\}$$
$$= \frac{1}{2j}\left\{\frac{1-e^{j4\pi}}{1-e^{\frac{j4\pi}{n}}} - \frac{1-e^{-j4\pi}}{1-e^{-\frac{j4\pi}{n}}}\right\}. \tag{D.14}$$

Since $e^{j4\pi} = e^{-j4\pi} = 0$, the numerators in the above sums are always zero. But singularities arise in the denominators again. There exist n where the denominators are zero.

$$1 - e^{\frac{j4\pi}{n}} = 0;\ \ e^{\frac{j4\pi}{n}} = 1$$

$$1 - e^{-\frac{j4\pi}{n}} = 0;\ \ e^{-\frac{j4\pi}{n}} = 1.$$

This is only satisfied in either case when $n = 1$ or $n = 2$. Evaluating those two cases by hand yields the following for all cases.

$$\sum_{i=0}^{n-1} \sin\frac{4\pi i}{n} = 0\,. \tag{D.15}$$

Similarly, for cosines,

$$\sum_{i=0}^{n-1} \cos\frac{4\pi i}{n} = \sum_{i=0}^{n-1} \frac{e^{\frac{j4\pi i}{n}} + e^{-\frac{j4\pi i}{n}}}{2} = \frac{1}{2}\left\{\sum_{i=0}^{n-1} e^{\frac{j4\pi i}{n}} + \sum_{i=0}^{n-1} e^{-\frac{j4\pi i}{n}}\right\}$$
$$= \frac{1}{2}\left\{\frac{1-e^{j4\pi}}{1-e^{\frac{j4\pi}{n}}} + \frac{1-e^{-j4\pi}}{1-e^{-\frac{j4\pi}{n}}}\right\} \tag{D.16}$$

which has the same singularities, so that

$$\sum_{i=0}^{n-1} \cos\frac{4\pi i}{n} = \begin{cases} 1, & n = 1 \\ 2, & n = 2 \\ 0, & n \geq 3\,. \end{cases} \tag{D.17}$$

APPENDIX E

DERIVATIONS

Analytical expressions based on the simplified two-dimensional geometry of separation and re-contact need to be developed to permit insight into the re-contact problem.

E.1 Geometry of Separation and Re-contact

The state of the second (ongoing) stage relative to the first (spent) stage, which is considered fixed, may be represented in two dimensions as

$$s(t) = \{ x, \dot{x}, \ddot{x}, y, \dot{y}, \ddot{y}, \theta, \dot{\theta}, \ddot{\theta} \}. \tag{E.1}$$

Assume (at worst) constant acceleration. What is the state of any location on the ongoing stage at time t? Let

$$r_x, r_y \equiv the\ location\ of\ a\ point\ relative\ to\ stage\ C.M.$$

From Regan [1],

$$\frac{d\vec{R}}{dt}|_f = \frac{d\vec{R}_o}{dt}|_f + \frac{d\vec{r}}{dt}|_m + \vec{\omega}_{m\backslash f} \times \vec{r} \tag{E.4}$$

and

$$\frac{d^2\vec{R}}{dt^2}|_f = \frac{d^2\vec{R}_o}{dt^2}|_f + \frac{d^2\vec{r}}{dt^2}|_m + \frac{d\vec{\omega}_{m\backslash f}}{dt} \times \vec{r} + 2\vec{\omega}_{m\backslash f} \times \frac{d\vec{r}}{dt}|_m + \vec{\omega}_{m\backslash f} \times \left(\vec{\omega}_{m\backslash f} \times \vec{r}\right). \tag{E.5}$$

For rigid bodies, $\frac{d\vec{r}}{dt}|_m = \frac{d^2\vec{r}}{dt^2}|_m = 0$, so that

$$\frac{d\vec{R}}{dt}|_f = \frac{d\vec{R}_o}{dt}|_f + \vec{\omega}_{m\backslash f} \times \vec{r} \tag{E.6}$$

$$\frac{d^2\vec{R}}{dt^2}|_f = \frac{d^2\vec{R}_o}{dt^2}|_f + \frac{d\vec{\omega}_{m\backslash f}}{dt} \times \vec{r} + \vec{\omega}_{m\backslash f} \times \left(\vec{\omega}_{m\backslash f} \times \vec{r}\right). \tag{E.7}$$

Reducing to two dimensions in the XZ plane (all rotations are about the Y axis, so that $\vec{\omega}_{m\backslash f} = \omega\vec{\imath}_2$),

$$\frac{d\vec{R}}{dt}|_f = \frac{d\vec{R}_o}{dt}|_f + \omega\vec{\imath}_2 \times \left(r_{x_m}\vec{\imath}_1 + r_{z_m}\vec{\imath}_3\right) = \frac{d\vec{R}_o}{dt} - \omega r_{x_m}\vec{\imath}_3 + \omega r_{z_m}\vec{\imath}_1 \tag{E.8}$$

$$\frac{d^2\vec{R}}{dt^2}|_f = \frac{d^2\vec{R}_o}{dt^2}|_f + \alpha\vec{\imath}_2 \times \left(r_{x_m}\vec{\imath}_1 + r_{z_m}\vec{\imath}_3\right) + \omega\vec{\imath}_2 \times \left[\omega\vec{\imath}_2 \times \left(r_{x_m}\vec{\imath}_1 + r_{z_m}\vec{\imath}_3\right)\right] \tag{E.9}$$

$$= \frac{d^2\vec{R}_o}{dt^2}|_f - \alpha r_{x_m}\vec{\imath}_3 + \alpha r_{z_m}\vec{\imath}_1 + \omega\vec{\imath}_2 \times \left[-\omega r_{x_m}\vec{\imath}_3 + \omega r_{z_m}\vec{\imath}_1\right] \tag{E.10}$$

$$= \frac{d^2\vec{R}_o}{dt^2}|_f - \alpha r_{x_m}\vec{\imath}_3 + \alpha r_{z_m}\vec{\imath}_1 - \omega^2 r_{x_m}\vec{\imath}_1 - \omega^2 r_{z_m}\vec{\imath}_3. \tag{E.11}$$

For now, in the first case, assume constant velocity and angular velocity. Let v_{r_x} and v_{r_y} be velocities of point R on the ongoing stage, v_{o_x} and v_{o_y} be velocities of the ongoing stage CM, and ω be the angular velocity of the ongoing stage.

$$v_{r_x} = v_{o_x} + \omega r_{z_m} \tag{E.12}$$

$$v_{r_z} = v_{o_z} - \omega r_{x_m} \tag{E.13}$$

$$x = x_o + v_{r_x}t = x_o + \left(v_{o_x} + \omega r_{z_m}\right)t \tag{E.14}$$

$$z = z_o + v_{r_z}t = z_o + \left(v_{o_z} - \omega r_{x_m}\right)t \tag{E.15}$$

$$\begin{bmatrix} x_a^s \\ y_a^s \end{bmatrix} = \begin{bmatrix} \cos\theta & -\sin\theta \\ \sin\theta & \cos\theta \end{bmatrix}\begin{bmatrix} x_a^o \\ y_a^o \end{bmatrix} + \begin{bmatrix} x_{CM_o}^s \\ y_{CM_o}^s \end{bmatrix}. \tag{E.16}$$

From Regan's Equation 5.13, p. 116,

$$\begin{bmatrix} v_{x_a}^s \\ v_{y_a}^s \end{bmatrix} = \begin{bmatrix} v_{x_{CM_o}}^s \\ v_{y_{CM_o}}^s \end{bmatrix} + \begin{bmatrix} \cos\theta & -\sin\theta \\ \sin\theta & \cos\theta \end{bmatrix}\left[\begin{bmatrix} v_{x_a}^o \\ v_{y_a}^o \end{bmatrix} + \begin{bmatrix} 0 & -\omega \\ \omega & 0 \end{bmatrix}\begin{bmatrix} x_a^o \\ y_a^o \end{bmatrix}\right] \tag{E.17}$$

$$= \begin{bmatrix} v_{x_{CM_o}}^s \\ v_{y_{CM_o}}^s \end{bmatrix} + \begin{bmatrix} -\omega\sin\theta & -\omega\cos\theta \\ \omega\cos\theta & -\omega\sin\theta \end{bmatrix}\begin{bmatrix} x_a^o \\ y_a^o \end{bmatrix} \tag{E.18}$$

For constant ω, $\theta = \theta_0 + \omega t$; $x^s_{CM_o} = x^s_{CM_o}(0) + v^s_{x_{CM_o}} t$; $y^s_{CM_o} = y^s_{CM_o}(0) + v^s_{y_{CM_o}} t$.

$$\begin{bmatrix} x^s_a \\ y^s_a \end{bmatrix} = \begin{bmatrix} \cos(\theta_o + \omega t) & -\sin(\theta_0 + \omega t) \\ \sin(\theta_0 + \omega t) & \cos(\theta_0 + \omega t) \end{bmatrix} \begin{bmatrix} x^o_a \\ y^o_a \end{bmatrix} + \begin{bmatrix} x^s_{CM_o}(0) + v^s_{x_{CM_o}} t \\ y^s_{CM_o}(0) + v^s_{y_{CM_o}} t \end{bmatrix}. \tag{E.19}$$

Assume that $\theta = \theta_0 + \omega t$ is a small angle and never grows beyond a small angle.

$$\begin{bmatrix} x^s_a \\ y^s_a \end{bmatrix} = \begin{bmatrix} 1 & -\theta_0 - \omega t \\ \theta_0 + \omega t & 1 \end{bmatrix} \begin{bmatrix} x^o_a \\ y^o_a \end{bmatrix} + \begin{bmatrix} x^s_{CM_o}(0) + v^s_{x_{CM_o}} t \\ y^s_{CM_o}(0) + v^s_{y_{CM_o}} t \end{bmatrix} \tag{E.20}$$

In non-matrix format,

$$x^s_a = x^o_a + x^s_{CM}(0) - \theta_0 y^o_a + \left(v^s_{x_{CM_o}} - \omega y^o_a \right) t \tag{E.21}$$

$$y^s_a = y^o_a + y^s_{CM}(0) + \theta_0 x^o_a + \left(v^s_{y_{CM_o}} + \omega x^o_a \right) t\,. \tag{E.22}$$

This is a linear trajectory for any point on the ongoing stage,

$$x = x_o + m_1 t \tag{E.23}$$

$$y = y_o + m_2 t\,. \tag{E.24}$$

The re-contact problem is basically the question, "Does point A reach the forward skirt tip point B's y before A reaches B's x? If so, then point A contacts the spent stage somewhere to the stern of point B.

E.1.1 Approach One

Combining the above linear parametric equations into one in the variables x and y,

$$t = \frac{x - x_o}{m_1} \tag{E.25}$$

$$y = y_o + \frac{m_2}{m_1}(x - x_o) \tag{E.26}$$

Or

$$\begin{aligned} y^s_a = {} & y^o_a + y^s_{CM_o}(0) + \theta_0 x^o_a \\ & + \frac{v^s_{y_{CM_o}} + \omega x^o_a}{v^s_{x_{CM_o}} - \omega y^o_a} [x^s_a - (x^o_a + x^s_{CM}(0) - \theta_0 y^o_a)] \end{aligned} \tag{E.27}$$

This is the trajectory of the point A of the ongoing stage in the coordinates of the spent stage and is given as (x_a^s, y_a^s). When $y_a^s = r_b \equiv inner\ radius\ of\ the\ forward\ skirt$, then re-contact may have occurred. The only unknown is x_a^s. If $x_a^s > h_B$, re-contact does not happen. If $x_a^s \leq h_B$, re-contact occurs.

Simplified, what is $x = x_2$, if $y = y_2$?

$$y_2 = y_o + \frac{m_2}{m_1}(x - x_o) \tag{E.28}$$

$$\frac{m_1}{m_2}(y_2 - y_o) + x_o = x = x_2\,. \tag{E.29}$$

Or, specifically,

$$\frac{v_{x_{CM_o}}^s - \omega y_a^o}{v_{y_{CM_o}}^s + \omega x_a^o}\left(r_B - y_a^o - y_{CM_o}^s(0) - \theta_0 x_a^o\right) - x_a^o - x_{CM}^s(0) + \theta_0 y_a^o = x = h_B\,. \tag{E.30}$$

Now, this happens at time $t = t_2$.

$$t_2 = \frac{x_2 - x_o}{m_1} = \frac{y_2 - y_o}{m_2} \tag{E.31}$$

Or

$$t_2 = \frac{h_B - x_a^o - x_{CM}^s(0) + \theta_0 y_a^o}{v_{x_{CM_o}}^s - \omega y_a^o} = \frac{r_B - y_a^o - y_{CM_o}^s(0) - \theta_0 x_a^o}{v_{y_{CM_o}}^s + \omega x_a^o}. \tag{E.32}$$

E.1.2 Approach Two

Instead of eliminating t as in Approach One, one may solve for t at $y_a^s = r_B$, then solve for x_a^s at that time, which is h_B.

$$\frac{y_2 - y_o}{m_2} = t_2 \tag{E.33}$$

$$x_2 = x_o + m_1 t_2 \tag{E.34}$$

So

$$t_2 = \frac{r_B - y_a^o - y_{CM_o}^s(0) - \theta_0 x_a^o}{v_{y_{CM_o}}^s + \omega x_a^o} \tag{E.35}$$

Then t_2 is plugged immediately into the x relation.

$$h_B = x_a^o + x_{CM}^s(0) - \theta_0 y_a^o + \left(v_{x_{CM_o}}^s - \omega y_a^o\right) t_2 \,. \tag{E.36}$$

This is conceptually the same; the process, though, is much simpler.

E.1.3 Acceleration

What if acceleration cannot be ignored? That is, velocities are not constant, and the rates before cutoff are sufficiently slow to not be amenable to modeling as impulses? Then

$$\theta_s = \theta_o + \ (\omega - \omega_o)t + \frac{1}{2}\alpha t^2 \tag{E.37}$$

$$x_{CM_o}^s = x_{CM_o}^s(0) + \left(v_{x_{CM_o}}^s - v_{x_{CM_o}}^s(0)\right) t + \frac{1}{2} a_x^s t^2 \tag{E.38}$$

$$y_{CM_o}^s = y_{CM_o}^s(0) + \left(v_{y_{CM_o}}^s - v_{y_{CM_o}}^s(0)\right) t + \frac{1}{2} a_y^s t^2 \,. \tag{E.39}$$

In the case of pneumatic pushers, at least, there are various "epochs" as each pusher loses contact in turn, so the time t_o, the starting positions $(\theta_o, x_{CM_o}^s(0), y_{CM_o}^s(0))$ and initial velocities of each epoch $(\omega, v_{x_{CM_o}}^s(0), v_{y_{CM_o}}^s(0)$) are important.

Expanding in matrix form,

$$\begin{bmatrix} x_a^s \\ y_a^s \end{bmatrix}$$

$$= \begin{bmatrix} \cos(\theta_o + \ (\omega - \omega_o)t + \frac{1}{2}\alpha t^2) & -\sin(\theta_o + \ (\omega - \omega_o)t + \frac{1}{2}\alpha t^2) \\ \sin(\theta_o + \ (\omega - \omega_o)t + \frac{1}{2}\alpha t^2) & \cos(\theta_o + \ (\omega - \omega_o)t + \frac{1}{2}\alpha t^2) \end{bmatrix} \begin{bmatrix} x_a^o \\ y_a^o \end{bmatrix} \tag{E.40}$$

$$+ \begin{bmatrix} x_{CM_o}^s(0) + \left(v_{x_{CM_o}}^s - v_{x_{CM_o}}^s(0)\right) t + \frac{1}{2} a_x^s t^2 \\ y_{CM_o}^s(0) + \left(v_{y_{CM_o}}^s - v_{y_{CM_o}}^s(0)\right) t + \frac{1}{2} a_y^s t^2 \end{bmatrix}.$$

With the small angle assumption still on θ,

$$= \begin{bmatrix} 1 & -(\theta_o + (\omega - \omega_o)t + \frac{1}{2}\alpha t^2) \\ (\theta_o + (\omega - \omega_o)t + \frac{1}{2}\alpha t^2) & 1 \end{bmatrix} \begin{bmatrix} x_a^o \\ y_a^o \end{bmatrix} + \begin{bmatrix} x_{CM_o}^s(0) + \left(v_{x_{CM_o}}^s - v_{x_{CM_o}}^s(0)\right)t + \frac{1}{2}a_x^s t^2 \\ y_{CM_o}^s(0) + \left(v_{y_{CM_o}}^s - v_{y_{CM_o}}^s(0)\right)t + \frac{1}{2}a_y^s t^2 \end{bmatrix} \tag{E.41}$$

$$x_a^s = x_a^o + x_{CM}^s(0) - \theta_0 y_a^o + \left(v_{x_{CM_o}}^s - v_{x_{CM_o}}^s(0) - (\omega - \omega_o)y_a^o\right)t + \frac{1}{2}(a_x^s - \alpha y_a^o)t^2 \tag{E.42}$$

$$y_a^s = y_a^o + y_{CM}^s(0) + \theta_0 x_a^o + \left(v_{y_{CM_o}}^s - v_{y_{CM_o}}^s(0) + (\omega - \omega_o)x_a^o\right)t + \frac{1}{2}\left(a_y^s - \alpha x_a^o\right)t^2 . \tag{E.43}$$

These two equations represent two parabolas, $x_a^s(t)$ and $y_a^s(t)$, of the form

$$x(t) = x_0 + m_1 t + c_1 t^2 \tag{E.44}$$

$$y(t) = y_0 + m_2 t + c_2 t^2 . \tag{E.45}$$

Using the binomial theorem to solve the $x(t)$ equation for t is simple enough, but elimination of the time parameter t to achieve lateral position $y(x)$, that is, as a function of longitudinal position x, is arduous and unenlightening, since the expression does not readily simplify. However, numerical evaluation is straightforward.

E.2 Separation Thrusters

Assume C.M. on stage centerline which is coincident with the body X axis.

$$\vec{F_i} \equiv force\ of\ i^{th}\ motor\ in\ station\ coordinates$$

$$\vec{r_i} \equiv position\ of\ i^{th} motor\ in\ station\ coordinates$$

$$n \equiv number\ of separation\ motors$$

$$\vec{F}_{sep} = \sum_{i=0}^{n-1} \vec{F}_i \; ; \; \vec{M}_{sep} = \sum_{i=0}^{n-1} \vec{r}_i \times \vec{F}_i \tag{E.46}$$

Assume that all the motors produce the same force vector, that is, the same magnitude and direction, but exerted at different locations. For $\vec{F}_i = \vec{F} = F_c\vec{p}$, where$F_c$is the scalar value of the common per-motor force, and $\vec{p}$ is the direction of that force.

$$\vec{F}_{sep} = \sum_{i=0}^{n-1} \vec{F} = \sum_{i=0}^{n-1} F_c\vec{p} = nF_c\vec{p} \tag{E.47}$$

$$\vec{M}_{sep} = \sum_{i=0}^{n-1} \vec{r}_i \times \vec{F}_i = F_c \sum_{i=0}^{n-1} \vec{r}_i \times \vec{p}\,. \tag{E.48}$$

If the motor force is parallel to the longitudinal axis (the centerline), the X station coordinate axis, then

$$\vec{p} = \vec{\imath} \tag{E.49}$$

$$\vec{F}_{sep} = nF_c\vec{\imath} \tag{E.50}$$

$$\vec{M}_{sep} = F_c \sum_{i=0}^{n-1} \vec{r}_i \times \vec{\imath}\,. \tag{E.51}$$

If the motors are mounted circumferentially on the skirt at the same radius h and at the same distance along the X axis from the C.M. l, then

$$\vec{r}_i = l\vec{\imath} + h\left(\vec{\jmath}cos\theta_i + \vec{k}sin\theta_i\right), \tag{E.52}$$

where

$$l \equiv distance\ from\ C.M.\ to\ plane\ of\ motor\ ring$$

$$h \equiv radius\ of\ motor\ ring$$

$$\theta_i \equiv angle\ of\ i^{th} motor\ on\ ring, measured\ from\ Y\ axis\ toward\ Z$$

$$\theta_i = \frac{360i}{n}\deg = \frac{2\pi i}{n} rad$$

$$\vec{M}_{sep} = F_c \sum_{i=0}^{n-1} [l\vec{\imath} + h(\vec{\jmath}cos\frac{2\pi i}{n} + \vec{k}sin\frac{2\pi i}{n})] \times \vec{\imath}\,. \tag{E.53}$$

Since $\vec{\imath} \times \vec{\imath} = 0$, all of the terms related to longitudinal distance from the C.M., i.e., those involving $l\vec{\imath}$, drop out.

$$\vec{M}_{sep} = F_c h \sum_{i=0}^{n-1} (\vec{\jmath}sin\frac{2\pi i}{n} - \vec{k}cos\frac{2\pi i}{n}) \tag{E.54}$$

$$= F_c h \left\{ \vec{j} \sum_{i=0}^{n-1} \sin\frac{2\pi i}{n} - \vec{k} \sum_{i=0}^{n-1} \cos\frac{2\pi i}{n} \right\}. \tag{E.55}$$

Using the sums of finite sine and cosines from Appendix C,

$$\vec{M}_{sep} = \begin{cases} \vec{0}, & n > 1 \\ -hF_c\vec{k}, & n = 1 \end{cases}. \tag{E.56}$$

This is the intuitively expected result. When there is only one separation thruster, the moment it causes is unbalanced; when there are more thrusters, they balance out, netting no moment.

The next case to be considered is when the circumferentially-mounted thrusters still point in the same direction but that vary in thrust magnitude. The stage C.M. remains on the centerline (the body X axis). All thrust is still exerted parallel to the centerline. All motors are still mounted in a ring at the same radius and distance from the C.M. The difference is that now the magnitude of a thruster's force will vary linearly with its position along the Y coordinate axis, across the stage.

The force is modified so that it may vary between motors.

$$\vec{F}_i = F_i\vec{p}, where\ F_i is\ the\ scalar\ force\ of\ each\ motor$$

$$= F_i\vec{\imath}\,, since\ \vec{p} = \vec{\imath}$$

The positions remain the same:

$$\vec{r}_i = l\vec{\imath} + h\left(\vec{j}cos\theta_i + \vec{k}sin\theta_i\right). \tag{E.57}$$

The linearly-varying (with Y) scalar force is given by

$$F_i = F_{base} + dF\ y_i\,, \tag{E.58}$$

where

$$F_{base} \equiv constant\ component\ of\ force\ across\ all\ motors$$

$$dF \equiv component\ of\ force\ varying\ with\ Y\ distance$$

$$y_i \equiv the\ Y\ component\ of\ the\ i^{th}\ motor$$

$$y_i = h\cos\theta_i\,. \tag{E.59}$$

Starting with the total forces of separation,

$$\vec{F}_{sep} = \sum_{i=0}^{n-1} \vec{F}_i = \sum_{i=0}^{n-1} F_i\vec{\imath} = \vec{\imath} \sum_{i=0}^{n-1} (F_{base} + dF\ y_i) \tag{E.60}$$

$$= \vec{\imath} \sum_{i=0}^{n-1} (F_{base} + \ dF \ h \cos\theta_i) \tag{E.61}$$

$$= \vec{\imath} \left\{ n \ F_{base} + \ dFh \sum_{i=0}^{n-1} \cos\theta_i \right\} \tag{E.62}$$

$$= \vec{\imath} \left\{ n \ F_{base} + \ dFh \sum_{i=0}^{n-1} \cos\frac{2\pi i}{n} \right\}. \tag{E.63}$$

As shown in Appendix C, the cosine sum is zero for every $n \geq 1$.

$$\vec{F}_{sep} = \begin{cases} \vec{\imath} \, n \, F_{base}, n \geq 2 \\ \vec{\imath} \, \{n \, F_{base} + \ dFh\}, n = 1 \, . \end{cases} \tag{E.64}$$

Now for the moments.

$$\vec{M}_{sep} = \sum_{i=0}^{n-1} \vec{r}_i \times \vec{F}_i$$

$$= \sum_{i=0}^{n-1} [l\vec{\imath} + \ h(\vec{\jmath} cos\frac{2\pi i}{n} + \vec{k} sin\frac{2\pi i}{n})] \times \vec{\imath}(F_{base} \tag{E.65}$$

$$+ \ dF \ h \cos\frac{2\pi i}{n}) \, .$$

As in the equal motor forces case, the length drops out.

$$= h \sum_{i=0}^{n-1} \vec{\jmath} \left(sin\frac{2\pi i}{n} \right) (F_{base} + \ dF \ h \cos\frac{2\pi i}{n}) - \vec{k}(cos\frac{2\pi i}{n})(F_{base} \tag{E.66}$$

$$+ \ dF \ h \cos\frac{2\pi i}{n})]$$

$$= h \, F_{base} \sum_{i=0}^{n-1} \left(\vec{\jmath} \sin\left(\frac{2\pi i}{n}\right) - \vec{k} \cos\left(\frac{2\pi i}{n}\right) \right)$$

$$+ h \sum_{i=0}^{n-1} \vec{\jmath} \left(sin\frac{2\pi i}{n} \right) \ (dF \ h \cos\frac{2\pi i}{n}) \tag{E.67}$$

$$- \vec{k}(cos\frac{2\pi i}{n})(dF \ h \cos\frac{2\pi i}{n})] \, .$$

The first sum is zero except the cosine term when $n = 1$, in which case the moment arising from just one motor is $-hF_{base}\vec{k}$, as one would expect. The second sum is more involved.

$$\vec{M}_{sep}(2^{nd}sum) = h^2 dF \left\{\sum_{i=0}^{n-1} \vec{j}\, \cos\frac{2\pi i}{n} \sin\frac{2\pi i}{n} - \vec{k}\cos^2\frac{2\pi i}{n}]\right\}. \tag{E.68}$$

Using the familiar double angle formulae from high school trigonometry,

$$2\cos\theta \sin\theta = \sin 2\theta \tag{E.69}$$

and

$$2\cos^2\theta - 1 = \cos 2\theta \tag{E.70}$$

$$\vec{M}_{sep}(2^{nd}sum) = h^2 dF \left\{\vec{j}\sum_{i=0}^{n-1} \frac{1}{2}\sin\frac{4\pi i}{n} - \vec{k}\sum_{i=0}^{n-1} \frac{1}{2}(1+\cos\frac{4\pi i}{n})\right\} \tag{E.71}$$

$$= h^2 dF \left\{\vec{j}\frac{1}{2}\sum_{i=0}^{n-1} \sin\frac{4\pi i}{n} - \vec{k}\frac{1}{2}n - \vec{k}\frac{1}{2}\sum_{i=0}^{n-1} \cos\frac{4\pi i}{n}\right\}. \tag{E.72}$$

Altogether,

$$\vec{M}_{sep} = \begin{cases} -(h\, F_{base} - h^2 dF)\,\vec{k}, n = 1 \\ -2h^2 dF\vec{k}, n = 2 \\ -\frac{1}{2}h^2 dFn\vec{k}, n \geq 3\,. \end{cases} \tag{E.73}$$

E.3 Pneumatic Pushers

Assume C.M. of both stages is on the centerline (the body/station X axis), both stages are perfectly aligned initially, that is, the stages have initially collinear stage station coordinates.

$$\vec{F}_{s_i} \equiv force\ of\ i^{th} pusher\ in\ stage\ station\ coordinates, spent\ stage$$

$$\vec{r}_{s_i} \equiv position\ of\ i^{th} pusher\ in\ stage\ station\ coordinates, spent\ stage$$

$$\vec{F}_{o_i} \equiv force\ of\ i^{th} pusher\ in\ stage\ station\ coordinates, ongoing\ stage$$

$$\vec{r}_{o_i} \equiv position\ of\ i^{th} pusher\ in\ stage\ station\ coordinates, spent\ stage$$

Initially, assume that all pushers exert the same force. For $\vec{F}_{s_i} = -\vec{F}^{s}_{o_i} = \vec{F} = F_p\vec{p}$, where $F_p \equiv$ $scalar\ value\ of\ common\ per-pusher\ force$ and $\vec{p} \equiv direction\ of\ the\ pusher\ force$, common for all pushers. Note that at the time of separation $t = 0$, the fixed frame axes are parallel to the spent stage body axes, though the origin is different.

$$\vec{F}_{sep_s} = \sum_{i=0}^{n-1} \vec{F} = \sum_{i=0}^{n-1} F_p \vec{p} = nF_p \vec{p} = -\vec{F}^{s}_{sep_o} \tag{E.74}$$

$$\vec{M}_{sep_s} = \sum_{i=0}^{n-1} \vec{r}_{s_i} \times \vec{F}_{s_i} = \sum_{i=0}^{n-1} \vec{r}_{s_i} \times F_p \vec{p} = F_p \sum_{i=0}^{n-1} \vec{r}_{s_i} \times \vec{p}\,. \tag{E.75}$$

If the force is also parallel to spent stage station coordinate X axis, then

$$\vec{p} = \vec{\imath}_s \tag{E.76}$$

$$\vec{F}_{sep_s} = nF_p \vec{\imath}_s = -\vec{F}^{s}_{sep_o} \tag{E.77}$$

$$\vec{M}_{sep_s} = F_p \sum_{i=0}^{n-1} \vec{r}_{s_i} \times \vec{\imath}_s\,. \tag{E.78}$$

If, in addition, all motors are mounted circumferentially about the forward skirt of the spent stage at a common distance from the C.M.,

$$\vec{r}_{i_s} = l_s \vec{\imath}_s + h\left(\vec{\jmath}_s \cos\theta_i + \vec{k}_s \sin\theta_i\right), \tag{E.79}$$

where

$$l_s \equiv distance\ from\ spent\ stage\ C.M.\ to\ plane\ of\ pusher\ ring$$

$$h \equiv radius\ of\ pusher\ ring$$

$$n \equiv number\ of\ motors$$

$$\theta_i \equiv angle\ of\ i^{th} pusher\ from\ the\ Y\ axis.$$

Now

$$\theta_i = \frac{360i}{n}\deg = \frac{2\pi i}{n} rad \tag{E.80}$$

$$\vec{M}_{sep_s} = F_p \sum_{i=0}^{n-1} \left\{ l_s \vec{\imath}_s + h\left(\vec{\jmath}_s \cos\theta_i + \vec{k}_s \sin\theta_i\right)\right\} \times \vec{\imath}_s\,. \tag{E.81}$$

Since $\vec{\imath}_s \times \vec{\imath}_s = \vec{0}$, all l_s terms drop out.

$$\vec{M}_{sep_s} = F_p h \sum_{i=0}^{n-1} \vec{\jmath}_s \sin\frac{2\pi i}{n} - \vec{k}_s \cos\frac{2\pi i}{n} \tag{E.82}$$

$$= F_p h \left\{ \vec{\jmath}_s \sum_{i=0}^{n-1} \sin\frac{2\pi i}{n} - \vec{k}_s \sum_{i=0}^{n-1} \cos\frac{2\pi i}{n} \right\}. \tag{E.83}$$

From Appendix D, the above sum is clearly

$$\vec{M}_{sep_s} = \begin{cases} -hF_p\vec{k}_s, n = 1 \\ 0, n > 1 \, . \end{cases} \tag{E.84}$$

This is the same value calculated for the separation thrusters when all thrusters provide the same separation force. For the practical case of equal pushers (more than one), no moment ever develops, so the stages remain aligned (that is, the stage station coordinate axes are parallel, and the X axes pass through the same points) as separation proceeds.

The force and moments for the ongoing stage are the same in magnitude and opposite in direction, as would be expected for two free bodies exerting forces on one another.

Now, as for the thrusters, a linear variation in pusher force with offset in stage Y coordinates will be considered.

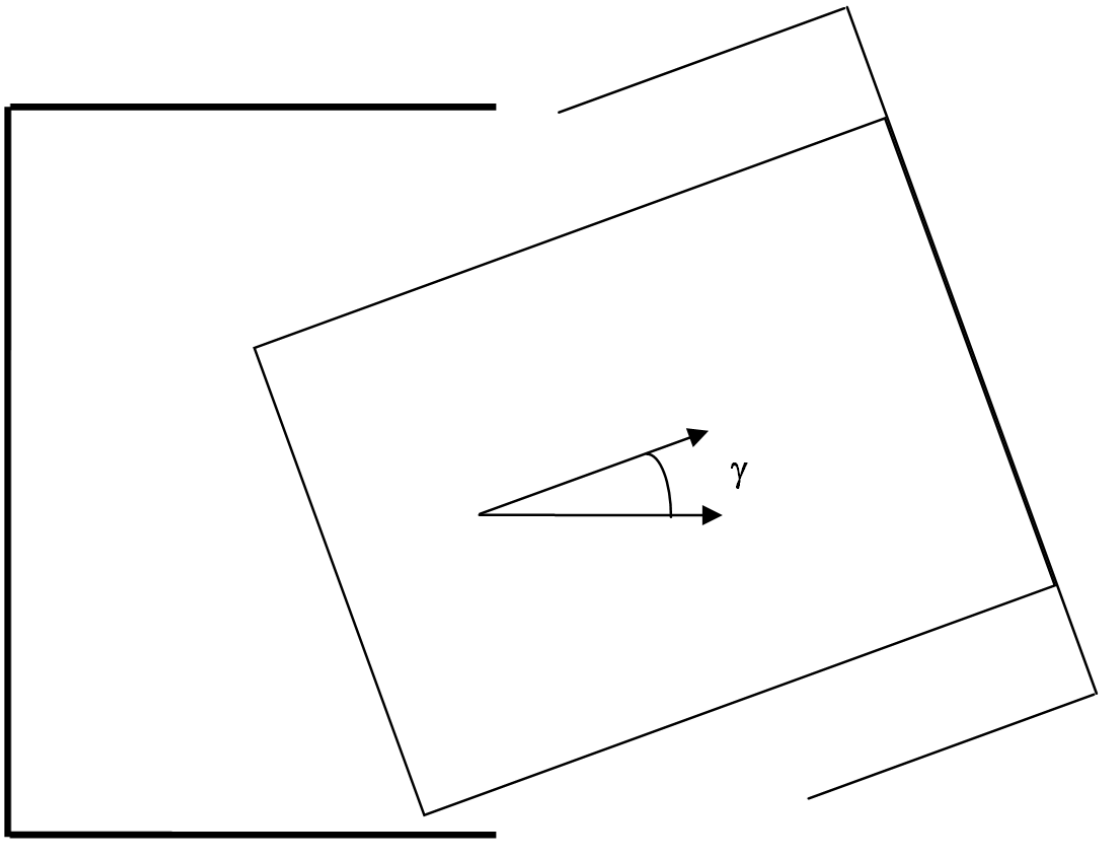

Figure E.1 2D Geometry of re-contact showing stage angle γ

We need to know the pusher extension over time for each pusher. From p.2 of Geometry and Re-contact section, let point A be on the centerline at the base of the ongoing stage.

$$\begin{bmatrix} x_A^S \\ y_A^S \end{bmatrix} = \begin{bmatrix} \cos\gamma & -\sin\gamma \\ \sin\gamma & \cos\gamma \end{bmatrix} \begin{bmatrix} x_A^O \\ y_A^O \end{bmatrix} + \begin{bmatrix} x_{CM_o}^S \\ y_{CM_o}^S \end{bmatrix}. \tag{E.85}$$

Assuming a small angle for γ is justified because (1) the angle $\gamma = 0deg$ at the beginning of separation ($t = 0$), and (2) a large angle would not be of interest, since re-contact would have almost certainly occurred. Most situations of practical interest can be modeled assuming $\gamma < 10deg$. Also, point A always lies along the centerline of the ongoing stage, so that $y_a^o = 0$. Incorporating small angle assumptions,

$$\begin{bmatrix} x_A^S \\ y_A^S \end{bmatrix} = \begin{bmatrix} 1 & -\gamma \\ \gamma & 1 \end{bmatrix} \begin{bmatrix} x_A^O \\ 0 \end{bmatrix} + \begin{bmatrix} x_{CM_o}^S \\ y_{CM_o}^S \end{bmatrix}. \tag{E.86}$$

Or simply

$$x_A^s = x_A^o + x_{CM_o}^s$$
$$y_A^s = \gamma x_a^o + y_{CM_o}^s \,. \tag{E.87}$$

Now, accounting for pusher ring of radius h with pushers at angles $\theta_i$round about,

$$\vec{r}_i^{\,o} = l_o \vec{\imath}_o + h(\overrightarrow{J_o} \cos\theta_i + \vec{k}_o \sin\theta_i) \tag{E.88}$$

$$\vec{F}_i^{\,o} = A^T \vec{F}_i^{\,s} = \begin{bmatrix} 1 & -\gamma \\ \gamma & 1 \end{bmatrix} \begin{bmatrix} F_{x_i}^s \\ F_{y_i}^s \end{bmatrix} \tag{E.89}$$

$$\begin{bmatrix} F_{x_i}^o \\ F_{y_i}^o \end{bmatrix} = \begin{bmatrix} F_{x_i}^s + \gamma F_{y_i}^s \\ F_{y_i}^s - \gamma F_{x_i}^s \end{bmatrix}. \tag{E.90}$$

Each pusher's force exerted on the ongoing stage in the coordinates of the spent stage (to which the pushers are attached) is

$$\vec{F}_i^{\,s} = \vec{\imath}_s (F_{base} + \, dF \; h \cos\frac{2\pi i}{n}) \tag{E.91}$$

$$\begin{aligned} \vec{M}_{sep}^{o} &= \sum_{i=0}^{n-1} \vec{r}_i^{\,o} \times \vec{F}_i^{\,o} \\ &= \sum_{i=0}^{n-1} \{l_o \, \vec{\imath}_o + h \cos\theta_i \, \vec{\jmath}_o + h \sin\theta_i \, \vec{k}_o\} \times (F_i^s \vec{\imath}_o \\ &\quad - \gamma F_i^s \vec{\jmath}_o) \end{aligned} \tag{E.92}$$

$$= \sum_{i=0}^{n-1} \{-l_o \gamma F_i^s \, \vec{k}_o - h F_i^s \cos\theta_i \, \vec{k}_o + h F_i^s \sin\theta_i \, \vec{\jmath}_o + h\gamma F_i^s \sin\theta_i \, \vec{\imath}_o\} \tag{E.93}$$

$$\begin{aligned} &= -l_o \gamma \sum_{i=0}^{n-1} F_i^s \vec{k}_o + \; h \sum_{i=0}^{n-1} \{\gamma F_i^s \sin\theta_i \, \vec{\imath}_o + F_i^s \sin\theta_i \, \vec{\jmath}_o \\ &\quad - F_i^s \cos\theta_i \, \vec{k}_o\} \end{aligned} \tag{E.94}$$

$$\begin{aligned} &= -l_o \gamma \sum_{i=0}^{n-1} (F_{base} + \, dF \; h \cos\frac{2\pi i}{n}) \vec{k}_o \\ &\quad + \; h \sum_{i=0}^{n-1} \{\gamma (F_{base} + \, dF \; h \cos\frac{2\pi i}{n}) \sin\frac{2\pi i}{n} \vec{\imath}_o \\ &\quad + (F_{base} + \, dF \; h \cos\frac{2\pi i}{n}) \sin\frac{2\pi i}{n} \vec{\jmath}_o - (F_{base} \\ &\quad + \, dF \; h \cos\frac{2\pi i}{n}) \cos\frac{2\pi i}{n} \vec{k}_o\} \,. \end{aligned} \tag{E.95}$$

From Appendix D,

$$\sum_{i=0}^{n-1} \sin\frac{2\pi i}{n} = 0; \sum_{i=0}^{n-1} \cos\frac{2\pi i}{n} = \begin{cases} 1, n = 1 \\ 0, n > 1 \end{cases}. \tag{E.97}$$

From here forward, only the non-trivial ($n > 1$) case will be considered. Applying the above sums and using the familiar half-angle formulae,

$$\begin{aligned} \vec{M}_{sep}^{o} = -l_o \gamma n F_{base} \vec{k}_o + h^2 \gamma dF \vec{i}_o \sum_{i=0}^{n-1} \frac{1}{2} \sin\frac{4\pi i}{n} \\ + h^2 dF \vec{j}_o \sum_{i=0}^{n-1} \frac{1}{2} \sin\frac{4\pi i}{n} \\ - \frac{h^2 dF \vec{k}_o}{2} \sum_{i=0}^{n-1} (1 + \cos\frac{4\pi i}{n}) . \end{aligned} \tag{E.98}$$

Again, from Appendix D,

$$\sum_{i=0}^{n-1} \sin\frac{4\pi i}{n} = 0; \sum_{i=0}^{n-1} \cos\frac{4\pi i}{n} = \begin{cases} 1, n = 1 \\ 2, n = 2 \\ 0, n \geq 3 \end{cases}. \tag{E.99}$$

This leaves

$$\vec{M}_{sep}^{o} = -l_o \gamma n F_{base} \vec{k}_o - \frac{1}{2} h^2 dF n \vec{k}_o \tag{E.100}$$

for $n \geq 3$. The first term is the contribution of (growing) misalignment. The second term is the direct result of the non-uniform pushers.

The assumption of small angle in gamma was not particularly important, and may have been detrimental to accuracy. It works against the conservation of momentum, which may be particularly important here. The forces acting on both stages are not the same after the small angle assumption.

E.4 Pusher Extent

Given pusher force F, ongoing stage mass m, and stage extent s, find time to full extent.

$$\frac{F}{m} = a_{rel} \tag{E.137}$$

$$s = \frac{1}{2}at^2 \tag{E.138}$$

$$t_{sep} = \sqrt{2\frac{s}{a}} \tag{E.139}$$

$$t_{sep} = \sqrt{2\frac{sm}{F}} \tag{E.140}$$

$$v_{rel_{sep}} = at_{sep} \tag{E.141}$$

$$= \sqrt{2\frac{sm}{F}}\frac{F}{m} = \sqrt{2\frac{Fs}{m}}, \tag{E.142}$$

where m is the composite mass of both stages given in Equation (5.23), $m = \frac{m_1 m_2}{m_1 + m_2}$.

E.5 Relative Velocity with Pusher

Consider a model of a pusher with a mass on each end (Figure E.2). The pusher provides a constant force out to a maximum extent, and then the force drops to zero. The relative velocity of the masses at the moment of loss of contact, that is, at the moment when the pusher reaches maximum extent, is sought.

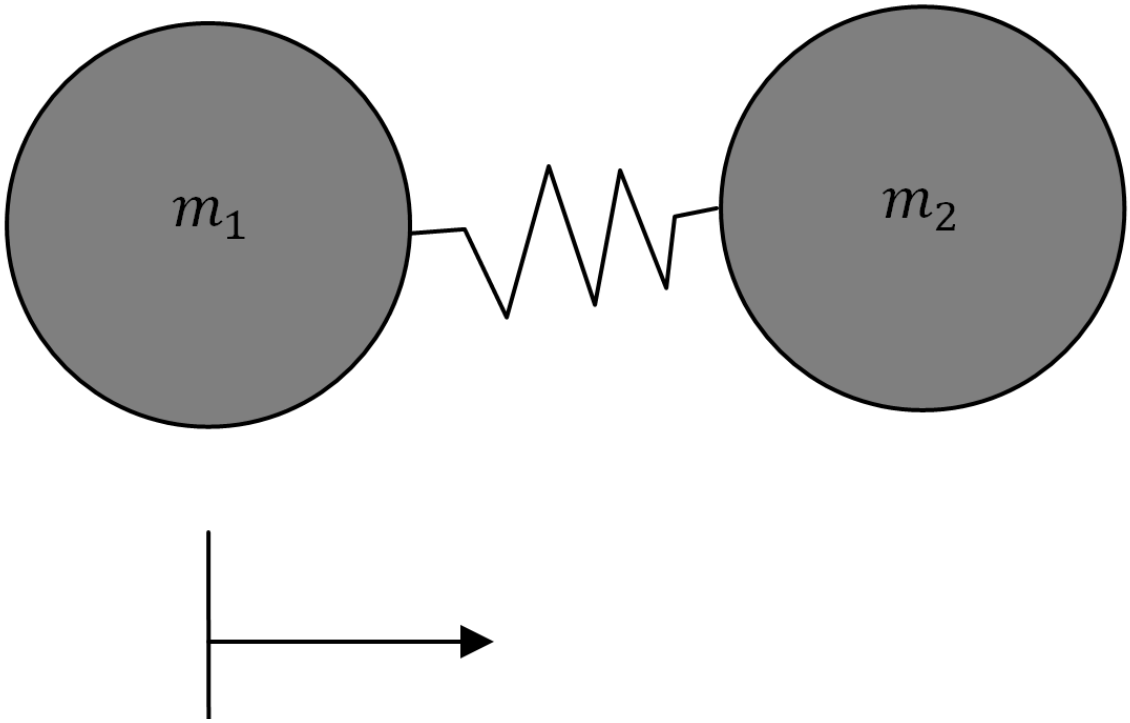

Figure E.2 Simplified two mass pusher model

The initial conditions for velocity and position are

$$\dot{x}_1(0) = x_1(0) = 0 \tag{E.143a}$$

and

$$\dot{x}_2(0) = x_2(0) = 0\,. \tag{E.143b}$$

Newton's Equation for each mass is

$$m_1\ddot{x}_1 = F \tag{E.144}$$

$$m_2\ddot{x}_2 = -F \tag{E.145}$$

$$\ddot{x}_1 = \frac{F}{m_1}\,. \tag{E.146}$$

Integrating,

$$\dot{x}_1 = \frac{F}{m_1}t + \dot{x}_1(0) = \frac{F}{m_1}t\,. \tag{E.147}$$

Integrating again,

$$x_1 = \frac{1}{2}\frac{F}{m_1}t^2 + x_1(0) = \frac{1}{2}\frac{F}{m_1}t^2 . \tag{E.148}$$

Also,

$$x_2 = -\frac{1}{2}\frac{F}{m_2}t^2 . \tag{E.149}$$

If s is the maximum extent,

$$x_{11} = s = x_2 - x_1 \tag{E.150}$$

$$= -\frac{1}{2}Ft^2(\frac{1}{m_2} + \frac{1}{m_1}) \tag{E.151}$$

$$= -\frac{1}{2}Ft^2\frac{m_1 + m_2}{m_1 m_2} \tag{E.152}$$

$$v_{21} = v_2 - v_1 \tag{E.153}$$

$$\dot{x}_{21} = \dot{x}_2 - \dot{x}_1 \tag{E.154}$$

$$= -\frac{F}{m_2}t - \frac{F}{m_1}t = -Ft(\frac{1}{m_1} + \frac{1}{m_2}) \tag{E.155}$$

$$\dot{x}_{21} = -Ft\frac{m_1 + m_2}{m_1 m_2} . \tag{E.156}$$

E.6 Conservation of Angular Momentum

In two dimensions,

$$H = I\omega = Mt , \tag{E.157}$$

where H is the angular momentum, I is the moment of inertia, ω is the angular rate, M is the moment, and t is the time of exertion of the moment. Considering a vehicle of two separating stages with no external moments applied (i.e., pushers and springs are used to separate, but no thrusters), the angular momentum must be conserved. What is lost by one stage must be gained by the other:

$$0 = \ H = I\omega = H_1 + H_2 = I_1\omega_1 + I_2\omega_2 = M_1 t + M_2 t = t(M_1 + M_2) \tag{E.158}$$

$$I_1\omega_1 = -I_2\omega_2 \tag{E.159}$$

$$\omega_1 = -\frac{I_2}{I_1}\omega_2 . \tag{E.160}$$

Let

$$\omega_{rel} = \omega_2 - \omega_1 = \omega_{21} \tag{E.161}$$

$$= \omega_2 + \frac{I_2}{I_1}\omega_2 = -\frac{I_1}{I_2}\omega_1 - \omega_1 \tag{E.162}$$

$$\omega_{rel} = \omega_2\left(1 + \frac{I_2}{I_1}\right) = -\omega_1\left(1 + \frac{I_1}{I_2}\right) \tag{E.163}$$

$$\omega_{rel} = -\frac{M_1 t}{I_1}\left(1 + \frac{I_1}{I_2}\right) = -M_1 t\left(\frac{1}{I_1} + \frac{1}{I_2}\right). \tag{E.164}$$

E.7 Conservation of Linear Momentum

In one dimension,

$$mv = F\,t\,, \tag{E.165}$$

where m is the mass, v is the velocity, F is the force, and t is the exertion time of the force. Without any external forces, like thrusters or drag, acting, linear momentum must be conserved between two separating stages.

$$v = F\,\frac{t}{m} \tag{E.166}$$

$$0 = mv = m_1 v_1 + m_2 v_2 = F_1 t + F_2 t = t(F_1 + F_2) \tag{E.167}$$

$$m_1 v_1 = -m_2 v_2 \tag{E.168}$$

$$v_1 = -v_2\frac{m_2}{m_1}. \tag{E.169}$$

Let

$$v_{rel} = v_2 - v_1 = v_{21} \tag{E.170}$$

$$= v_2 + v_2\frac{m_2}{m_1} = -v_1\frac{m_1}{m_2} - v_1 \tag{E.171}$$

$$v_{rel} = v_2\left(1 + \frac{m_2}{m_1}\right) = -v_1\left(\frac{m_1}{m_2} + 1\right) \tag{E.172}$$

$$v_{rel} = -\frac{F_1 t}{m_1}\left(\frac{m_1}{m_2} + 1\right) = -F_1 t\left(\frac{1}{m_1} + \frac{1}{m_2}\right). \tag{E.173}$$

E.8 Mass Offset

This section assesses the potential of gimbaled engine mass offset to induce an angular rate given that separation devices work perfectly and that the spent stage is otherwise perfect. The principal variables are the mass ratios of the engine and tankage, and the distances of each C.M. from the common C.M. Assume that the spent stage consists of two masses: the engine mass and the larger tankage mass. The engine mass includes all mass gimbaled with the engine. The tankage mass includes all non-gimbaled mass like that of the forward and aft skirts, intertank, and thrust structure. Assume that (1) C.M. of tankage lies on the stage centerline, (2) C.M. of engine lies on the stage centerline when gimbal angle is zero, and all mass offset is simply a result of non-zero gimbal angle moving the engine C.M. off the centerline.

Without loss of generality, the problem reduces to two dimensions, where the mass offset resides in the X-Y plane.

$$x_{t_{CM}} \equiv tankage\ C.M.\ in\ station\ coordinates$$

$$m_t \equiv mass\ of\ tankage$$

$$x_g \equiv gimbal\ location\ in\ station\ coordinates$$

$$m_e \equiv mass\ of\ engine$$

$$\delta \equiv gimbal\ angle\ (only\ one\ in\ 2D), +CCW$$

$$l \equiv engine\ C.M.\ distance\ from\ gimbal$$

$$y_e = l \sin\delta \approx -l\delta$$

$$x_e = l \cos\delta \approx l.$$

Since for almost all boosters $\delta < 5°$, especially near burnout, the small angle approximation is justified.

Now find the C.M. of the spent stage, which is the common C.M. of the engine and tankage together, joined at the gimbal. From introductory statics, for X,

$$X \sum m = \sum x_i m_i \tag{E.174}$$

$$X\,(m_t + m_e) = x_{t_{CM}} m_t - (x_g + l) m_e \tag{E.175}$$

$$X = \frac{x_{t_{CM}} m_t - (x_g + l) m_e}{m_t + m_e}. \tag{E.176}$$

And for Y,

$$Y \sum m \; = \; \sum y_i m_i \tag{E.177}$$

$$Y \; (m_t + \; m_e) = \; y_{t_{CM}} m_t + \; y_e m_e \; . \tag{E.178}$$

Since the tankage C.M. lies on the centerline, $y_{t_{CM}} = 0$, and so

$$Y = -\frac{l \; \delta \; m_e}{m_t + \; m_e} . \tag{E.179}$$

Let $m_{f_e} \equiv the\ engine\ mass\ fraction\ of\ the\ stage$ and let

$m_{f_t} \equiv the\ tankage\ mass\ fraction\ of\ the\ stage$, so that

$$m_{f_e} = \frac{m_e}{m_t + \; m_e}; \; m_{f_t} = \frac{m_t}{m_t + \; m_e} \tag{E.180}$$

$$X = x_{t_{CM}} m_{f_t} - \; \left(x_g + \; l\right) m_{f_e}; Y = -l\delta m_{f_e} \; . \tag{E.181}$$

If the stage is separated with devices generating force $\overrightarrow{F} = \; -F\vec{\imath}_1$ straight down the stage centerline, then the moment about the C.M., which is not on the centerline due to engine mass offset, but is instead at a position Y from the centerline, is

$$\vec{M}_{sep} = - \; Y\vec{\imath}_2 \times \; -F\vec{\imath}_1 = -FY\vec{\imath}_3 \tag{E.182}$$

$$\vec{M}_{sep} = \frac{Fl\delta m_e}{m_t + \; m_e} \vec{\imath}_3 \; . \tag{E.183}$$

Find I before $M_{sep} = I \; \omega_{sep}$.

$$\boldsymbol{I}_e^s = \boldsymbol{R}(\delta) \boldsymbol{I}_e \boldsymbol{R}^T(\delta), \tag{E.184}$$

where for axisymmetric engine and small angle δ, as derived in the following section,

$$\boldsymbol{I}_e^s = \begin{bmatrix} I_{e_{xx}} & (I_{e_{yy}} - \; I_{e_{xx}})\delta & 0 \\ (I_{e_{yy}} - \; I_{e_{xx}})\delta & I_{e_{yy}} & 0 \\ 0 & 0 & I_{e_{yy}} \end{bmatrix} . \tag{E.185}$$

The Huygens-Steiner Theorem (the complete parallel axis theorem in 3 dimensions) is used to move $\boldsymbol{I}_e^s$ to the composite spent stage C.M.

$$I'_{ij} = \; I_{ij} + \; m \left[(l_1^2 + l_2^2 + l_3^2)\boldsymbol{\delta}_{ij} - \; l_i l_j\right], \tag{E.186}$$

where $\boldsymbol{\delta}_{ij}$ represents the Kroenecker delta function in this one instance, I_{ij} is the original inertia tensor, I'_{ij} is the new inertia tensor referred to an origin located by the position vector (l_1, l_2, l_3) relative to the original

tensors origin. For the particular case of the engine and the stage, (l_1, l_2, l_3) is the position vector of the engine C.M. relative to the stage C.M. Expanding to matrix form,

$$I'_{ij} = I_{ij} + m \begin{bmatrix} l_2^2 + l_3^2 & -l_1 l_2 & -l_1 l_3 \\ -l_1 l_2 & l_1^2 + l_3^2 & -l_2 l_3 \\ -l_1 l_3 & -l_2 l_3 & l_1^2 + l_2^2 \end{bmatrix}. \tag{E.187}$$

Now,

$$(l_1, l_2, l_3) = \begin{bmatrix} X + (x_g + x_l) \\ Y - y_e \\ 0 \end{bmatrix} \approx \begin{bmatrix} X + (x_g + l) \\ Y + l\delta \\ 0 \end{bmatrix} \tag{E.188}$$

$$= \begin{bmatrix} x_{t_{CM}} m_{f_t} - (x_g + l) m_{f_e} + (x_g + l) \\ -l\delta m_{f_e} + l\delta \\ 0 \end{bmatrix} \tag{E.189}$$

$$= \begin{bmatrix} x_{t_{CM}} m_{f_t} + (x_g + l)(1 - m_{f_e}) \\ l\delta(1 - m_{f_e}) \\ 0 \end{bmatrix}. \tag{E.190}$$

Since $m_{f_t} + m_{f_e} = 1$, and letting $x_{e_{CM}} = x_g + l$,

$$= \begin{bmatrix} x_{t_{CM}} m_{f_t} + x_{e_{CM}} m_{f_t} \\ l\delta m_{f_t} \\ 0 \end{bmatrix} \tag{E.191}$$

$$= m_{f_t} \begin{bmatrix} x_{t_{CM}} + x_{e_{CM}} \\ l\delta \\ 0 \end{bmatrix}. \tag{E.192}$$

The matrix resulting from the Kroenecker delta functions and l vector in the Huygens-Steiner theorem is then

$$I_{mod} = m_{f_t} \begin{bmatrix} l^2\delta^2 & (x_{t_{CM}} + x_{e_{CM}})(-l\delta) & 0 \\ (x_{t_{CM}} + x_{e_{CM}})(-l\delta) & (x_{t_{CM}} + x_{e_{CM}})^2 & 0 \\ 0 & 0 & l^2\delta^2 + (x_{t_{CM}} + x_{e_{CM}})^2 \end{bmatrix} \tag{E.193}$$

$$\boldsymbol{I}_e^{(s|CM)} = \boldsymbol{I}_e^s + m_e(I_{mod}) \tag{E.195}$$

$$\boldsymbol{I}_e^{(s|CM)} = \begin{bmatrix} I_{e_{xx}} & (I_{e_{yy}} - I_{e_{xx}})\delta & 0 \\ (I_{e_{yy}} - I_{e_{xx}})\delta & I_{e_{yy}} & 0 \\ 0 & 0 & I_{e_{yy}} \end{bmatrix} \tag{E.196}$$

$$+m_e m_{f_t}\begin{bmatrix} l^2\delta^2 & -x_{t_{CM}} l\delta - x_{e_{CM}} l\delta & 0 \\ -x_{t_{CM}} l\delta - x_{e_{CM}} l\delta & x_{t_{CM}}^2 + 2x_{t_{CM}} x_{e_{CM}} + x_{e_{CM}}^2 & 0 \\ 0 & 0 & l^2\delta^2 + x_{t_{CM}}^2 + 2x_{t_{CM}} x_{e_{CM}} + x_{e_{CM}}^2 \end{bmatrix}.$$

Now, $m_e m_{f_t} = \frac{m_e m_t}{m_t + m_e}$. For the nominal case, $\delta = 0$, so that

$$\boldsymbol{I}_e^{(s|CM)}\Big|_{\delta=0} = \begin{bmatrix} I_{e_{xx}} & 0 & 0 \\ 0 & I_{e_{yy}} & 0 \\ 0 & 0 & I_{e_{yy}} \end{bmatrix} \tag{E.197}$$

$$+\frac{m_e m_t}{m_t + m_e}\begin{bmatrix} 0 & 0 & 0 \\ 0 & x_{t_{CM}}^2 - 2x_{t_{CM}} x_{e_{CM}} + x_{e_{CM}}^2 & 0 \\ 0 & 0 & x_{t_{CM}}^2 - 2x_{t_{CM}} x_{e_{CM}} + x_{e_{CM}}^2 \end{bmatrix}.$$

Note that gimbaling's contribution to the moment of inertia in the plain is distinctly second order for small angles. In the $I_{e_{zz}}$ position (bottom row, last column), the only contribution due to gimbaling is $l^2\delta^2$. The remainder of the term is independent of gimbaling. So for analysis in the plane, a constant value of $I_{e_{zz}}$ may be used regardless of the gimbal angle.

Thus far the engine. Now for the tankage, which, because it is aligned symmetrically with respect to the stage centerline, has principal axes parallel to its station axes, so all that is needed is for the tankage inertia tensor $\boldsymbol{I}_t^s$ to be referred to the station C.M. Now,

$$\boldsymbol{I}_t^s = \begin{bmatrix} I_{t_{xx}} & 0 & 0 \\ 0 & I_{t_{yy}} & 0 \\ 0 & 0 & I_{t_{yy}} \end{bmatrix}. \tag{E.198}$$

Note that $\boldsymbol{I}_t^s$ has the same moments of inertia about the Y^s and the Z^s axes, since the tankage is symmetric. To refer $\boldsymbol{I}_t^s$ to the stage C.M.,

$$\boldsymbol{I}_t^{(s|CM)} = \boldsymbol{I}_t^s + m_t \boldsymbol{I}_t^{s'}, \tag{E.199}$$

where

$$\boldsymbol{I}_t^{s'} = \begin{bmatrix} 0 & 0 & 0 \\ 0 & \left(x_{t_{CM}} - X\right)^2 & 0 \\ 0 & 0 & \left(x_{t_{CM}} - X\right)^2 \end{bmatrix}. \tag{E.200}$$

Well,

$$x_{t_{CM}} - X = x_{t_{CM}} - \left(x_{t_{CM}} m_{f_t} - \left(x_g + l\right) m_{f_e}\right) \tag{E.201}$$

$$= x_{t_{CM}}\left(1 - m_{f_t}\right) + x_{e_{CM}} m_{f_e} \tag{E.202}$$

$$= x_{t_{CM}} m_{f_e} + x_{e_{CM}} m_{f_e} \tag{E.203}$$

$$= m_{f_e}\left(x_{t_{CM}} + x_{e_{CM}}\right). \tag{E.204}$$

Substituting in,

$$\boldsymbol{I}_t^{s'} = m_{f_e}\begin{bmatrix} 0 & 0 & 0 \\ 0 & \left(x_{t_{CM}} + x_{e_{CM}}\right)^2 & 0 \\ 0 & 0 & \left(x_{t_{CM}} + x_{e_{CM}}\right)^2 \end{bmatrix}. \tag{E.205}$$

The tankage inertia tensor referred to the C.M. is then

$$\boldsymbol{I}_t^{(s|CM)} = \boldsymbol{I}_t^s + m_t m_{f_e}\begin{bmatrix} 0 & 0 & 0 \\ 0 & \left(x_{t_{CM}} + x_{e_{CM}}\right)^2 & 0 \\ 0 & 0 & \left(x_{t_{CM}} + x_{e_{CM}}\right)^2 \end{bmatrix} \tag{E.206}$$

$$\boldsymbol{I}_t^{(s|CM)} = \boldsymbol{I}_t^s + \frac{m_e m_t}{m_t + m_e}\begin{bmatrix} 0 & 0 & 0 \\ 0 & \left(x_{t_{CM}} + x_{e_{CM}}\right)^2 & 0 \\ 0 & 0 & \left(x_{t_{CM}} + x_{e_{CM}}\right)^2 \end{bmatrix}. \tag{E.207}$$

The entire stage inertia tensor at the C.M. may now be found.

$$\boldsymbol{I}^{(s|CM)} = \boldsymbol{I}_e^{(s|CM)} + \boldsymbol{I}_t^{(s|CM)}. \tag{E.208}$$

E.9 Inertia Tensor Rotated Only in Z

An inertia tensor must be taken to a new set of axes, but the only difference between the new frame and the old frame is a rotation of θabout one of the axes. Without loss of generality, assume that the common axis is the Z axis.

Well,

$$\boldsymbol{I}_{new} = \boldsymbol{C}_{old}^{newT}\boldsymbol{I}_{old}\boldsymbol{C}_{old}^{new} \tag{E.209}$$

$$= \begin{bmatrix} cos\theta & sin\theta & 0 \\ -sin\theta & cos\theta & 0 \\ 0 & 0 & 1 \end{bmatrix}\begin{bmatrix} I_{11} & I_{12} & I_{13} \\ I_{21} & I_{22} & I_{23} \\ I_{31} & I_{32} & I_{33} \end{bmatrix}\begin{bmatrix} cos\theta & -sin\theta & 0 \\ sin\theta & cos\theta & 0 \\ 0 & 0 & 1 \end{bmatrix}. \tag{E.210}$$

Noting that inertia tensors are symmetric, $I_{ij} = I_{ji}$,

$$\boldsymbol{I}_{new}$$

$$= \begin{bmatrix} cos\theta & sin\theta & 0 \\ -sin\theta & cos\theta & 0 \\ 0 & 0 & 1 \end{bmatrix}\begin{bmatrix} I_{11}cos\theta + I_{12}sin\theta & -I_{11}sin\theta + I_{12}cos\theta & I_{13} \\ I_{12}cos\theta + I_{22}sin\theta & -I_{12}sin\theta + I_{22}cos\theta & I_{23} \\ I_{13}cos\theta + I_{23}sin\theta & -I_{13}sin\theta + I_{23}cos\theta & I_{33} \end{bmatrix}. \tag{E.211}$$

Let $c\theta = cos\theta$ and $s\theta = sin\theta$ for compactness.

$$= \begin{bmatrix} I_{11}\,c^2\,\theta + I_{12}c\theta s\theta + I_{12}c\theta s\theta + I_{22}\,s^2\,\theta & -I_{11}c\theta s\theta + I_{12}\,c^2\,\theta - I_{12}\,s^2\,\theta + I_{22}c\theta s\theta & I_{13}c\theta + I_{23}s\theta \\ -I_{11}c\theta s\theta - I_{12}s^2\theta + I_{12}c^2\theta + I_{22}c\theta\, s\theta & -I_{11}s^2\theta - I_{12}c\theta s\theta - I_{12}c\theta s\theta + I_{22}c^2\theta & -I_{13}s\theta + I_{23}c\theta \\ I_{13}c\theta + I_{23}s\theta & -I_{13}s\theta + I_{23}c\theta & I_{33} \end{bmatrix}.$$

For small θ, $sin\theta \approx \theta$ and $cos\theta \approx 1$, so that

$$= \begin{bmatrix} I_{11} + I_{12}\theta + I_{12}\theta + I_{22}\,\theta^2 & -I_{11}\theta + I_{12} - I_{12}\,\theta^2 + I_{22}\theta & I_{13} + I_{23}\theta \\ -I_{11}\theta - I_{12}\theta^2 + I_{12} + I_{22}\theta & -I_{11}\theta^2 - I_{12}\theta - I_{12}\theta + I_{22} & -I_{13}\theta + I_{23} \\ I_{13} + I_{23}\theta & -I_{13}\theta + I_{23} & I_{33} \end{bmatrix}. \quad \text{(E.212)}$$

Eliminating second order terms, where $\theta \gg \theta^2$ because of the small angle assumption,

$$= \begin{bmatrix} I_{11} + 2\,I_{12}\theta & I_{12} + (I_{22} - I_{11})\theta & I_{13} + I_{23}\theta \\ I_{12} + (I_{22} - I_{11})\theta & I_{22} - 2\,I_{12}\theta & I_{23} - I_{13}\theta \\ I_{13} + I_{23}\theta & I_{23} - I_{13}\theta & I_{33} \end{bmatrix}. \quad \text{(E.213)}$$

In the special case where the original inertia tensor I_{old} is already referred to the principal axes of the body, then I_{old} is diagonalized ($I_{ij} = 0, i \neq j$), yielding

$$= \begin{bmatrix} I_{11} & (I_{22} - I_{11})\theta & 0 \\ (I_{22} - I_{11})\theta & I_{22} & 0 \\ 0 & 0 & I_{33} \end{bmatrix}. \quad \text{(E.214)}$$

Additionally, if the body is axisymmetric about the original X axis, then $I_{22} = I_{33}$, and the inertia tensor reduces to

$$\boldsymbol{I}_{new} = \begin{bmatrix} I_{11} & (I_{22} - I_{11})\theta & 0 \\ (I_{22} - I_{11})\theta & I_{22} & 0 \\ 0 & 0 & I_{22} \end{bmatrix}. \quad \text{(E.215)}$$

REFERENCES

[1] Frank J. Regan, Satya M. Anandakrishnan, Dynamics of Atmospheric Re-Entry, AIAA, 1993.

[2] Falcon 1 Demo Flight 2 Review Update, SpaceX, 2007.

[3] "Falcon 1 Flight 3 Mission Summary", SpaceX, http://www.spacex.com/updates_archive.php?page=0802-1007 [accessed August 18, 2011].

[4] "Atlas Agena A", Astronautix, http://www.astronautix.com/lvs/atlgenaa.htm [accessed August 18, 2011].

[5] Atlas Launch System Mission Planner's Guide, International Launch Services, September 2000.

[6] Delta IV Payload Planners Guide, United Launch Alliance, September 2007.

[7] Ariane 5 User's Manual Issue 5 Release 0, Arianespace, July 2008.

[8] Roger R. Bate, Donald D. Mueller, Jerry E. White, Fundamentals of Astrodynamics, Dover, 1971.

[9] John Colbaugh, An Investigation of the Effect of Spring Forces on the Separation of Rocket Motor and Payload, University of Alabama Huntsville, 2009.

[10] Bong Wie, Space Vehicle Dynamics and Control, AIAA, 1998.

[11] Peter H. Zipfel, Modeling and Simulation of Aerospace Vehicle Dynamics, Second Edition, AIAA Education Series, 2007.

[12] Peter C. Hughes, Spacecraft Attitude Dynamics, Dover, 1986.

[13] Erwin Kreyszig, Advanced Engineering Mathematics, Ninth Edition, Wiley, 2006.

[14] John H. Blakelock, Automatic Control of Aircraft and Missiles, Wiley, 1965.

[15] Rodger E. Ziemer, William H. Tranter, D. Ronald Fannin, Signals and Systems, MacMillan, 1983.

[16] Kevin E. Konno, Daniel A. Catalano, Thomas M. Krianek, Evaluation of Separation Mechanism Design for the Orion/Ares Launch Vehicle, Proceedings of the 39th Aerospace Mechanisms Symposium, NASA Marshall Space Flight Center, May 7-9, 2008.

[17] Kenneth R. Britting, Inertial Navigation Systems Analysis, Wiley, 1971.

[18] Christer Ericson, Real-Time Collision Detection, Elsevier, 2005.

[19] Edwin J. Purcell, Calculus with Analytic Geometry, Third Edition, Prentice Hall, 1978.

[20] Ferdinand Beer, Jr., E. Russell Johnston, Vector Mechanics for Engineers: Dynamics, Third Edition, McGraw-Hill, 1977.

[21] John L. Chapman, Atlas: Story of a Missile, Harper and Brothers, 1960.

[22] George P. Sutton, Oscar Biblarz, Rocket Propulsion Elements, Seventh Edition, Wiley-Interscience, 2001.

[23] D. Jeyakumar, B. Nageswara Rao, Dynamics of Satellite Separation System, Journal of Sound and Vibration 297 (2006) 444-455.

[24] Kevin E. Duprey, Erik R. Saucier, Separation Systems Comparison for ARES I Launch Vehicle, 44th AIAA/ASME/SAE/ASEE Joint Propulsion Conference & Exhibit 21-23 July 2008, Hartford, CT.